LOAN DOCUMENT

PHOTOGRAPH THIS SHEET

DTIC ACCESSION NUMBER

LEVEL

INVENTORY 0

AFRL-ML-TY-TR-1999-4558

DOCUMENT IDENTIFICATION

31 Dec 95

DISTRIBUTION STATEMENT A
Approved for Public Release
Distribution Unlimited

DISTRIBUTION STATEMENT

HANDLE WITH CARE

ACCESSION FOR
NTIS GRA&I ☒
DTIC TRAC ☐
UNANNOUNCED ☐
JUSTIFICATION

BY

DISTRIBUTION/

AVAILABILITY CODES

DISTRIBUTION	AVAILABILITY AND/OR SPECIAL	
A-1		

DISTRIBUTION STAMP

DATE ACCESSIONED

DATE RETURNED

20000215 022

DATE RECEIVED IN DTIC

REGISTERED OR CERTIFIED NUMBER

PHOTOGRAPH THIS SHEET AND RETURN TO DTIC-FDAC

DTIC FORM 70A JUN 90 — DOCUMENT PROCESSING SHEET — PREVIOUS EDITIONS MAY BE USED UNTIL STOCK IS EXHAUSTED.

DTIC QUALITY INSPECTED 1

LOAN DOCUMENT

AFRL-ML-TY-TR-1999-4558

LABORATORY STUDIES OF NITROGEN OXIDE REMOVAL BY PULSED STREAMER CORONA

ROBERT R. LOCKE
KALYANA SWAMINATHAN
WRIGHT C. FINNEY

APPLIED RESEARCH ASSOCIATES, INC.
4300 SAN MATEO BLVD. NE, SUITE A220
ALBUQUERQUE NM 87110

AIR FORCE RESEARCH LABORATORY
MATERIALS & MANUFACTURING DIRECTORATE
AIRBASE & ENVIRONMENTAL TECHNOLOGY DIVISION
TYNDALL AFB FL 32403-5323

NOTICES

USING GOVERNMENT DRAWINGS, SPECIFICATIONS, OR OTHER DATA INCLUDED IN THIS DOCUMENT FOR ANY PURPOSE OTHER THAN GOVERNMENT PROCUREMENT DOES NOT IN ANY WAY OBLIGATE THE US GOVERNMENT. THE FACT THAT THE GOVERNMENT FORMULATED OR SUPPLIED THE DRAWINGS, SPECIFICATIONS, OR OTHER DATA DOES NOT LICENSE THE HOLDER OR ANY OTHER PERSON OR CORPORATION; OR CONVEY ANY RIGHTS OR PERMISSION TO MANUFACTURE, USE, OR SELL ANY PATENTED INVENTION THAT MAY RELATE TO THEM.

THIS REPORT IS RELEASABLE TO THE NATIONAL TECHNICAL INFORMATION SERVICE (NTIS). AT NTIS, IT WILL BE AVAILABLE TO THE GENERAL PUBLIC, INCLUDING FOREIGN NATIONS.

THIS TECHNICAL REPORT HAS BEEN REVIEWED AND IS APPROVED FOR PUBLICATION.

JOSEPH D. WANDER, Ph.D
Program Manager

CHRISTINE WAGENER-HULME, Lt Col, USAF, BSC
Chief, Environmental Technology Development Branch

RANDY L. GROSS, Col, USAF, BSC
Chief, Airbase & Environmental Technology Division

REPORT DOCUMENTATION PAGE

Form Approved
OMB No. 0704-0188

1. AGENCY USE ONLY *(Leave blank)*	2. REPORT DATE	3. REPORT TYPE AND DATES COVERED
	31 December 1995	Annual Report 1 Jan 1995 - 31 December 1995

4. TITLE AND SUBTITLE
Laboratory Studies of Nitrogen Oxide Removal by Pulsed Streamer Corona

5. FUNDING NUMBERS
F08635-93-C-0020
JON 1900 A 35 B

6. AUTHORS
Locke, Robert R.; Swaminathan, Kalyana; Finney, Wright C.

7. PERFORMING ORGANIZATION NAME(S) AND ADDRESS(ES)
Applied Research Associates, Inc.
4300 San Mateo Blvd. NE, Suite A220
Albuquerque, NM 87110

8. PERFORMING ORGANIZATION REPORT NUMBER

9. SPONSORING/MONITORING AGENCY NAME(S) AND ADDRESS(ES)
AFRL/MLQE
139 Barnes Drive, Ste 2
Tyndall AFB FL 32403-5323

10. SPONSORING/MONITORING AGENCY REPORT NUMBER
AFRL-ML-TY-TR-1999-4558

11. SUPPLEMENTARY NOTES
Performed by subcontract to Department of Chemical Engineering, FAMU-FSU College of Engineering
Florida State University, Tallahassee, FL 32310-6064

12a. DISTRIBUTION/AVAILABILITY STATEMENT
Approved for Public Release; Distribution Unlimited

12b. DISTRIBUTION CODE
A

13. ABSTRACT *(Maximum 200 words)*

Pulsed streamer corona treatment is an advanced oxidation technology using a nonthermal plasma that produces hydroxyl radicals, hydrogen peroxide, and aqueous electrons, all of which react with water-borne organic contaminants in the removal process. Pulsed streamer corona is an electrical discharge created by applying a continual series of sustainable, short lived, high voltage pulses to a smaller diameter metallic electrode. This discharge creates an electric field between a point-to-plane electrode geometry within a batch reactor containing organic contaminants in deionized water. This process is applied to the removal of nitrogen oxides. This research documents the reactions and reaction products that are produced in the pulsed streamer corona reactor and the optimization of the pulsed streamer corona reactor process for this purpose.

14. SUBJECT TERMS	15. NUMBER OF PAGES
Pulsed streamer corona; nitrogen oxides; plasma; oxidation	134
	16. PRICE CODE

17. SECURITY CLASSIFICATION OF REPORT	18. SECURITY CLASSIFICATION OF THIS PAGE	19. SECURITY CLASSIFICATION OF ABSTRACT	20. LIMITATION OF ABSTRACT
UNCLASSIFIED	UNCLASSIFIED	UNCLASSIFIED	UL

NSN 7540-01-280-5500 Computer Generated STANDARD FORM 298 (Rev 2-89)
Prescribed by ANSI Std 239-18
298-102

CLASSIFIED BY:

DECLASSIFY ON:

ACKNOWLEGEMENTS

We would like to acknowledge Dr. Ronald Clark, FSU Chemistry Department, for assistance with chemical identification using GC/MS; Mr. David Grymonpre', FAMU-FSU Department of Chemical Engineering, for assisting in the setup of the gas distribution system, running of the reactor, and preparing of the report; Mr. Alex Papadopolis, FAMU-FSU Department of Chemical Engineering, for assistance in running some of the corona reactor experiments, Cadet Steve Lucas, United States Air Force Academy, for a summer research project on pulse waveform characterization of the pulsed corona reactor, and Cadet Derrick Lincoln, United States Air Force Academy, for a summer research project on ozone generation in the pulsed corona reactor. Laboratory facilities were provided by the Department of Chemical Engineering at the FAMU-FSU College of Engineering, and some equipment was obtained from the FSU Department of Physics (former laboratory of Professor Robert Davis).

EXECUTIVE SUMMARY

The purpose of this project was to assemble a test gas distribution system and to perform laboratory experiments with an existing gas phase pulsed streamer corona reactor to support the US Air Force's effort to investigate the feasibility of using this technology for removing nitrogen oxides from the combustion exhaust gases of jet engine testing facilities. This contract was performed at the FAMU-FSU College of Engineering through a subcontract between The Florida State University and Applied Research Associates, Inc. (ARA). This subcontract was created from a primary contract between ARA and the United States Air Force. This project is a continuation of Contract FSESCR41580100, Construction of a Pulsed Streamer Corona Reactor, performed at the Department of Chemical Engineering, FAMU-FSU College of Engineering (Locke and Finney, 1995).

A pulsed streamer corona reactor utilizes a high voltage electrical discharge in a non-uniform electrode geometry to initiate chemical reactions that lead to the removal of various pollutants. The physical aspects of a gas phase pulsed discharge in a non-uniform electrical field include the formation of ionization waves (streamers) through the growth of electron avalanches formed by electron impact ionization events in the gas. The streamer is a region of highly ionized gas (a non-then-nal plasma) where a wide range of highly reactive radicals and species are formed through collisions among electrons, molecules, and ions. If nitric oxide (NO) is present in the test gas, it is generally first converted to nitrogen dioxide (NO_2) through a variety of reactions that may include direct reaction with dissociated oxygen or reactions with ozone. N02may be removed through reactions with hydroxyl radicals created from water vapor or possibly by organic species. The N02 is converted to nitric acid aerosols that in turn may be removed by scrubbers, particle filtration devices, or electrostatic precipitators.

The major objectives of the present work were: 1) to run the FSU-constructed pulse streamer corona reactor under a variety of gas feed conditions, including the addition of water and ethylene, 2) to determine the effect of the presence of ethylene on nitrogen oxide removal. 3) to look for byproduct formation from the reactions of ethylene with nitrogen oxides, and 4) to develop a mathematical model of the gas phase pulsed corona reactor that accounts for the major chemical reactions occurring in the process. In addition, basic electrical characterization of the corona reactor was performed in order to determine power usage and energy efficiency for nitrogen oxide removal, and to allow comparison with other data reported in the literature.

The major results of this study are as follows. The presence of 500 ppm ethylene in dry air in the pulsed corona reactor results in significant enhancement of NO removal. Quantitative analysis of treated gas samples by GC/MS indicates that 23% to 26% of the ethylene is decomposed in the corona reactor with an input voltage of 50 kV and a residence time of 0.6 min. The presence of water in the air feed (no ethylene) has a smaller effect than that of ethylene in dry air, and the presence of water and ethylene in air shows a small improvement in NO removal than the case with ethylene only (no water). Ethylene breakdown byproducts were not found by sample analysis with GC/MS. Energy costs for NO

removal for dry air, air with ethylene, air with water, and air with both ethylene and water are in the same general range as those reported in the literature. The mathematical model developed for this work predicts trends similar to those found in the experiments on the effects of water and ethylene on NO removal. The reaction chemistry in the model predicts that some fraction of NO is converted to N_2 and O_2, and that NO_2 levels are reduced in the presence of ethylene.

TABLE OF CONTENTS

LIST OF FIGURES

LIST OF TABLES

1. GENERAL INTRODUCTION AND BACKGROUND

A pulsed streamer corona reactor utilizes a high voltage electrical discharge produced within a non-uniform electrode geometry to initiate chemical reactions that lead to the removal of various pollutants from a gas stream. The physical aspects of a gas phase pulsed discharge in a non-uniform electrical field include the formation of ionization waves (streamers) through the growth of electron avalanches formed by electron impact ionization events in the gas (Nassar, 1971; Gallimberti, 1987; Bastein and Marode, 1979,1995; Morrow, 1985). The streamer is a region of highly ionized gas (a non-therrnal plasma), where a wide range of highly reactive radicals and chemical species are formed through collisions among electrons, molecules, and ions. NO is generally first converted to NO_2 through a variety of reactions that may include direct reaction with dissociated oxygen or reactions with ozone. NO_2 may be removed through reactions with hydroxyl radicals created from water vapor or possibly by organic species. The NO_2 is thus converted to nitric acid aerosols that in turn may be removed by scrubbers, particle filtration devices, or electrostatic precipitators.

The physical and chemical processes involved in gas phase non-thermal plasma processes have been the subject of a number of experimental and theoretical studies. In this section, a brief review of the literature relevant to the application of pulsed streamer corona for the removal of nitrogen oxides from combusti on gases will be presented. The basic chemical reactions expected to occur in the process and a description of the physical process of streamer propagation will be given.

1. 1. Chemical Reactions in Pulsed Corona

The chemical reaction mechanisms for the removal of nitrogen oxides (NO and NO) by gas phase non-thermal plasma reactions have been studied extensively (Creyghton, 1994; Tas, 1995; Alekseev et al., 1993; Wren, 1989; McFarlane and Wren, 1991; Mizuno et al., 1993, Tokanaga and Suzuki, 1984; Matzing 1989). One model of the reaction chemistry that has been extensively used for pulsed corona systems was developed at IVTAN in Moscow (Alekseev et al., 1993), and this code uses over 900 individual chemical reactions. The chemical reactions used in this model were adapted from earlier work on electron beam technology in Germany (Matzing, 1989). The extensive nature of these chemical reactions arises from the many molecular, ionic, and radical species that are formed from an exhaust gas that may include SO_2, NO, NO_2, CO, CO_2, O_2, N_2, and H_2O. Recent work has shown, however, that a system of approximately 50 chemical reactions can describe the overall reaction very well (Creyghton. 1994; Tas, 1995).

Previous modeling and experimental work with pulsed streamer corona reactors and similar non-thermal plasma systems have shown that nitrogen oxide removal is a strong function of the applied electrical field and the composition of the feed gases. The amounts of water vapor and oxygen in the feed, as well as the presence of some organic species, have been found to be very important in affecting the nitrogen oxide removal rates. An essential feature of any method that will improve the operation of the pulsed streamer corona reactor

for nitric oxide removal is the suppression of any back reactions or any radical recombination reactions that lead to the formation of NO.

High energy electrons produced in the pulsed discharge will collide with the major gas phase species, primarily N_2 and O_2 to lead to dissociation of these species by

$$N_2 + e^- \rightarrow 2N + e^- \quad (1)$$

$$O_2 + e^- \rightarrow 2O + e^- \quad (2)$$

These dissociated nitrogen and oxygen radicals can recombine, react together, or react with other species.

The primary reactions that lead to nitrogen oxide *removal* consist first of the oxidation of NO to NO_2 through reactions with O_2, O_3, and O.

$$2NO + O_2 \rightarrow 2NO_2 \quad (3)$$

$$NO + O + M \rightarrow NO_2 + M \quad (4)$$

$$NO + O_3 \rightarrow NO_2 + O_2 \quad (5)$$

In the presence of water vapor, NO can also be oxidized by the hydroperoxy radical through

$$NO + HO_2^{\cdot} \rightarrow NO_2 + OH^{\cdot} \quad (6)$$

and subsequent reactions of NO_2 with hydroxyl radical lead to acid formation

$$NO_2 + OH^{\cdot} \rightarrow HNO_3 \quad (7)$$

The nitric acid thus formed may condense in existing water droplets, it may form acid aerosols through heterogeneous nucleation via existing particles in the gas (Kiang et al., 1973), or it may form acid aerosols via homogeneous nucleation and particle growth (Seinfeld, 1986).

In the presence of water vapor and oxygen, direct electron impact with molecular oxygen

$$e^- + O_2 \rightarrow O + O(^1D), \quad (8)$$

and subsequent reaction of singlet oxygen with water vapor leads to hydroxyl radical production

$$O(^1D) + H_2O \rightarrow 2OH^{\cdot} \quad (9)$$

Hydroperoxy radicals can also be formed though reactions of hydroxyl radicals and carbon monoxide

$$CO + OH^{\cdot} + O_2 \rightarrow CO_2 + HO_2. \quad (10)$$

The oxidation of most hydrocarbons also lead to formaldehyde (Seinfeld, 1986) which can in turn lead to additional hydroperoxy radicals via

$$HCHO + OH^{\cdot} \rightarrow HO_2^{\cdot} + CO + H_2O. \quad (11)$$

Many other reactions may be occurring in the system depending upon the composition of the feed gas (Matzing, 1989; Alekseev et al., 1993; McFarlane and Wren, 1991), and of particular importance are the *recombination and back* reactions that produce additional NO that will tend to reduce the efficiency of the process.

In dielectric barrier discharge reactors (Chang et al., 1992), and in pulsed corona reactors (Masuda and Nakao, 1986; Shimazu and Mizuno, 1993), it has been established that the addition of water vapor will greatly improve the removal rates of NO. This is considered to be primarily due to the enhanced production of hydroxyl radicals. Optimal values of water vapor will depend upon both temperature and electric field conditions. Increasing O_2 content has also shown improvement in NO removal. In dielectric baffier discharges, increases in O_2 content show an optimal removal near 5% (volume/volume) of oxygen at higher applied voltages for dry gas. This is thought to be due to the increased production of hydroxyl radicals through reaction with singlet oxygen as shown above (9); however, at very high oxygen levels generation of NO will occur through *back* reactions such as

$$NO_2 + O \rightarrow NO + O_2, \quad (12)$$

or recombination reactions such as

$$N + O \rightarrow NO, \quad (13)$$

both of which will lead to a reduction in efficiency of NO removal. The above two reactions show that it is desirable to remove NO_2 as soon as it is formed, and that optimal levels of O must be achieved to allow hydroxyl radicals to be formed through reactions of O with water, but to not allow too much NO to be formed. NO can also be formed through such reactions as

$$N_2 + O \rightarrow NO + O \quad (14)$$

$$N + O_2 \rightarrow NO + O \quad (15)$$

$$N + OH^{\cdot} \rightarrow NO + H, \quad (16)$$

which is the well known Zeldovich mechanism (Zeldovich, 1946) developed for thermal combustion devices, and therefore dissociated N as well as O can lead to additional NO formation.

It is also interesting to note that NO_2 can react with N (McFarlane and Wren, 1991) to regenerate N_2 by

$$NO_2 + N \rightarrow N_2 + 2O \quad (17)$$

$$NO_2 + N \rightarrow N_2 + O_2. \quad (18)$$

Due to the somewhat slower rate constants for these reactions, they are generally more important at longer residence times. The enhancement of these reactions is certainly desirable because of the obvious advantages of the final products. Tas (1995) concluded that reduction of NO did not occur in his system because he could not detect N_2 production. He performed experiments in He and N_2 environments, however, it is unlikely that N_2 would be produced in the He environment, and that in the N_2 environment the addition of even several hundred parts per million N_2 would be extremely difficult to detect. The question of how much, if any, N_2 is produced by the above reactions remains open.

The oxidation of NO to NO_2 has been found to occur only after the onset of the corona discharge (Masuda and Nakao, 1990). Increases in peak voltages beyond corona onset were found to maintain total NO_X at a constant until a critical field intensity was reached. This indicates that NO was oxidized to NO_2 without further conversion of NO_2 to acid. Beyond this critical field intensity the NO_2 value rapidly decreased (Masuda and Nakao, 1990). These authors claim that the highest possible peak voltage will result in the most effective removal strategy in order to minimize the amount of NO formed by recombination of NO_2 and O; however the use of water and or ammonia is necessary to scavenge the NO_2 before it can react with oxygen to regenerate NO. One would expect that at very high fields NO will be formed through the recombination of N and O and that there must therefore be an optimal field strength. Indeed, Ohkubo et al. (1994) observed an optimum in NO_X reduction as a function of corona power for certain treatment conditions, and they also observed a general decrease in energy yield of NO removal with corona power. By optimizing the addition of NH_3, CO_2, O_2, and N_2 they were able to show increased NO removal and higher energy yields.

Recent work by the group at Eindhoven Technical University (Tas, 1995; Creyghton. 1994) have considered the effects of water vapor, oxygen content and the addition of solid catalytic particles on NO removal in pulsed corona reactors. They found that increasing the oxygen content from 0% to 9% caused a decrease in efficiency of NO removal in a dry nitrogen feed gas. When water vapor was added, they found the opposite trend; the removal efficiency increased as the water content was varied from 0.0 to 11.7%. They did not find optimal values for O_2 or H_2O as was observed in the work on dielectric discharge reactors. Their corona reactor was run with constant residence time (1 see) and pulsed voltage level (28

kV), constant NO input (1200 ppm), and with variable pulsed voltage frequency (5 - 240 Hz). The power input to the reactor varied from 0.05 to 1.5 watts.

A number of studies have emphasized the importance of the presence of ammonia to enhance the removal of nitrogen oxides via reactions with nitric acid to form ammonium nitrate

$$HNO_3 + NH_3 \rightarrow NH_4NO_3 \qquad (19)$$

which will create a solid aerosol particle that can be removed by electrostatic precipitation or filtration. The advantage of this process is the production of a salable byproduct that can be used as a fertilizer; however the disadvantages are: 1) the need for handling large quantities of highly toxic ammonia gas, and 2) the necessity to remove any unreacted ammonia from the exit gas stream. Since the addition of ammonia is not desired in the present work due to these disadvantages, further analysis of the addition of water vapor and oxygen will be considered. It is also important to note that the work by Masuda and Nakao (1990) did not consider the role of CO which, as shown above, is very important to the formation of hydroperoxy radicals.

It is clear that, depending upon the composition of the feed and the reactor conditions, there are *optimal* levels of such additives as water vapor, oxygen, and possibly hydrocarbons (or CO) that will most effectively promote the removal of nitrogen oxides as acid aerosols. It is also clear that the role of hydrocarbons, through the formation of formaldehyde and carbon monoxide, will enhance the production of hydroperoxy radicals through reactions with hydroxyl radicals. In addition, the electric field conditions in the reactor will also strongly affect the removal of the nitrogen oxides as shown in the work of Masuda and Nakao (1990) and Mukkavilli et al. (1988). It is also clear that in order to enhance the efficiency of the removal of NO it is necessary to suppress the "back" reactions and thus minimize the production of additional undesired NO. This can be accomplished through reactions of NO_2 with hydroxyl radicals, and the use of optimal levels of oxygen. Precise control of water vapor and oxygen input would thus serve as a means to optimize the removal of NO and enhancement of reactions that lead to N and O products is also desirable.

The chemistry of ethylene has been studied in relation to gas phase atmospheric chemistry (Atkenson and Lloyd, 1984; Seinfeld, 1986). The primary reactions of ethylene with hydroxyl radicals, ozone, and dissociated oxygen and the resulting effects on photochemical smog have been determined. To date only one report by Mizuno (Mizuno et al., 1993) has considered the effects of a pulsed corona discharge on hydrocarbon reactions. Some work has been reported on VOC removal with pulsed corona technology (Futamura et al., 1995).

In the natural atmosphere, ethylene is expected to react primarily with hydroxyl radicals since the concentration of singlet oxygen and ozone are generally small. The reaction pathway for ethylene in the presence of oxygen, NO and hydroxyl radicals has been well

studied (Seinfeld, 1986). Hydroxyl radicals directly attack ethylene to produce peroxyl radicals that can further react with oxygen and NO through the following reactions

$$C_2H_4 + OH^{\cdot} \rightarrow HOCH_2CH_2 \quad (20)$$

$$HOCH_2CH_2^{\cdot} + O_2 \rightarrow HOCH_2CH_2O_2^{\cdot} \quad (21)$$

NO is converted to NO_2 through

$$HOCH_2CH_2O_2^{\cdot} + NO \rightarrow NO_2 + HOCH_2CH_2O^{\cdot} \quad (22)$$

Approximately 72% of the ethylene leads to formaldehyde production

$$HOCH_2CH_2O^{\cdot} + O_2 \rightarrow HCHO + CH_2OH^{\cdot} \quad (23)$$

while the remaining 28% leads to

$$HOCH_2CH_2O^{\cdot} + O_2 \rightarrow HOCH_2CHO + HO_2^{\cdot} \quad (24)$$

$$CH_2OH^{\cdot} + O_2 \rightarrow HCHO + HO_2^{\cdot} \quad (25)$$

The formaldehyde produced in the above reactions can further react with hydroxyl radicals to produce hydroperoxy radicals as discussed previously (see Equation 11).

Direct reactions of ethylene with ozone are also known to occur. These reactions lead to the production of formaldehyde, formic acid, carbon dioxide, and carbon monoxide by

$$C_2H_4 + O_3 \rightarrow HCHO + H_2COO \quad (26)$$

$$H_2COO \rightarrow CO_2 + H_2 \quad (27)$$

$$H_2COO \rightarrow CO + H_2O \quad (28)$$

$$H_2COO + 2O_2 \rightarrow CO_2 + 2HO_2^{\cdot}, \quad (29)$$

with a net reaction given by

$$C_2H_4 + O_3 \rightarrow HCHO + 0.4H_2COO + 0.18CO_2 + 0.42CO + 1.2H_2 + 0.42H_2O + 0.12HO_2^{\cdot}. \quad (30)$$

If no water is initially present in the feed, the water formed through the ozone reactions with ethylene may lead to the production of hydroxyl radicals.

Mizuno et al. (1993), performed pulsed corona reactor experiments with dry air containing NO and ethylene. He observed the formation of acetic acid, however, none of the other products considered above were directly observed using Fourier IR Spectroscopy. Additional reactions, normally considered negligible in the atmosphere, include

$$C_2H_4 + O(^3P) \rightarrow CH_3 + HCO \quad (31)$$

$$C_2H_4 + O(^3P) \rightarrow CH_2CHO + H \quad (32)$$

$$C_2H_4 + O(^3P) \rightarrow CH_2CO + H_2 \quad (33)$$

These reactions may be important in the plasma environment of the pulsed corona reactor. According to Atkenson and Lloyd (1984), the reaction pathways of the above reactions gives 55% to the first, 36% to the second, and the remainder to the third reaction. The vinoxy radical at low pressure leads to

$$CH_2CHO + O_2 \rightarrow HCHO + CO + OH \quad (34)$$

1.2. Physical Processes Occurring in Streamer Propagation

The chemical reactions initiated by a pulsed corona discharge that were discussed above are a direct result of a number of physical processes that occur in the non-thermal plasma. The purpose of this section is to provide A brief review of some of the basic physical processes occurring in a pulsed corona reactor. The material is obtained primarily from Nasser (1971) and Creyghton (1994).

Normal air at standard conditions contains approximately 10^3 electrons, positive ions, and negative ions per cm^3. These species arise from UV and cosmic radiation and are generally in a Boltzmann equilibrium. In the presence of a small uniform DC electric field (1 V/cm), small current pulses of less than 10^{-16} A arise. When enough free electrons are present due to external volume ionization and electrode emissions from external radiation, a steady current arises. In this situation, the current flow due to the motion of charged species has a small effect on the Boltzmann equilibrium, and the conductivity depends upon the rate of ion and electron production, recombination, and motion. As the applied electrical field increases, the equilibrium is upset as the number of ions and electrons are neutralized when they reach the electrodes. The rate of increase of current with voltage decreases and a saturation region with current density of approximately 10^{-9} A/cm^2 occurs. This is termed the "dark discharge region", which is a region where the discharge is not self-sustaining because it requires an external source of radiation to provide electrons and ions.

A further increase in voltage causes the current to rise at an increasing rate. Ionization by collision or electron impact ionization occurs through

$$A + e^- \rightarrow A^+ + e^- + e^-, \quad (35)$$

whereby an avalanche is created through a cascade where two electrons are released for every one impact with molecular species A. This is known as the Townsend discharge region and the current is generally greater than 1 μA. This region is followed by an abrupt transition leading to breakdown, where an over exponential increase in current is followed by a collapse in voltage. The current can be increased by reducing the resistors of the outer circuit which will lead to a voltage drop and a glow region. Higher currents will lead to arc formation.

A number of different types of corona discharges can occur in non-uniform electric fields, and these are reviewed in the literature (Nasser, 1971). Of direct interest here is pulsed corona, which is characterized by strong branching and a large region of existence in terms of the applied voltage.

The key aspect to understanding a corona discharge is a proper description of the Townsend avalanche. Yamamoto states "...the Townsend avalanche is a conceptual description of the electron multiplication process. The process begins with a free electron in a strong field. The electron gains enough energy through collisions with gas molecules to ionize one of them. This produces another electron and a positive ion. The two free electrons are able to produce further electrons in a cascade..... The rate of ionization is described by the first Townsend coefficient (X, which is the number of electrons produced per cm' per initial electron." The major factors that limit the growth of avalanches include 1) a rapid decrease in field as the distance from the electrode increases, 2) electron attachment to gas molecules which removes electrons from the avalanche leading to the repulsion of electrons from negative ions, and 3) a buildup of positive ions behind the front of electrons which will lead to a retardation of the rate of electron propagation (Nasser, 1971).

The transition from an avalanche to a "streamer" in a uniform electric field begins at the cathode where the avalanche is initiated. This avalanche propagates to the anode. and near the anode a build-up of positive ions occurs. During the primary avalanche, propagation excitation of gas molecules occurs. Photons are emitted by these excited states and these photons lead to photoionization and the creation of photo electrons. These in turn create secondary avalanches that will also propagate toward the anode and lead to additional photoionization and third generation avalanches. The merging of the secondary avalanches with positive space charge gives rise to the growth of an ionized channel from the anode to the cathode, and the electrons w ill move toward the anode. The propagation of one streamer tip continues and the others stop advancing due to the lack of avalanches feeding them.

Of the mechanisms for ionization, photoionization, given by

$$A + h\nu \rightarrow A + e^- \tag{36}$$

is the most important. The electric field generated by the negative ions allows streamers to propagate into regions of low field. The electron avalanche forms streamers when the electric field created by the electron space charge reaches the magnitude of the geometric field. In the

words of Nasser (1971), "...the streamer discharges are highly localized positive or negative space charge waves which enhance the applied field in front of the wave (active region) and propagate because of electron avalanches in the high field.....photoionization is generally assumed to be the mechanism that supplies secondary seed electrons and triggers avalanches. Along the track of the wave remains a weakly ionized filament plasma (passive region), along which the conduction current flows to the high voltage electrode, and supplies energy for streamer advancement."

The major characteristics of streamers include length, number, speed of propagation, width, number of electrons and ions, time lag, and electric field distribution. Typical values of streamer width are in the range of 25 to 100 Em and the speed of propagation is in the range of 0.7 - 0.9 mm/ns (Creyghton, 1994). The number of electrons and ions varies in space and time in the streamer with an upper range of about $10^{20}/m^3$. The distribution of streamers along a wire electrode has been measured using Schlieren photography to be approximately 7/cm (Creyghton, 1994). The Raether-Meek criterion for streamer onset in a uniform field has been extended for non-uniform fields that are required to produce pulsed streamer corona (Creyghton, 1994). This onset voltage for a non-uniform field in a wire-cylinder geometry according to this criterion is about 17 kV (Creyghton, 1994).

Creyghton (1994) reviews the basic physical models of streamer formation. In general, one dimensional convective/diffusive/reaction equations for positive and negative ions and electrons, coupled with the Poisson equation for the electric field and given electron velocity distributions (obtained experimentally by solution of the Boltzmann equation, or by Monte Carlo simulation) are solved to determine the rate of propagation of the streamer in a uniform or non-uniform electric field. Simulations have been performed coupling streamer models with chemical kinetics (Alekseev et al., 1993, McFarlane and Wren, 1991). Due to a number of uncertainties in the properties of the streamers, no direct model/experimental comparisons have been made without some decree of empirical fitting.

2. EXPERIMENTAL APPARATUS AND PROCEDURES

2.1. Power Supply and Corona Reactor

The reactor and power supply used in the present study was constructed on contract with the United States Air Force and is described in extensive detail by Locke and Finney (1995). The overall experimental system is shown in Figure 1. Feed gas is prepared using a building supply of dry air and gas regulators/cylinders. The gases are metered using mass flow controllers and then are fed into a mixing chamber. Thereafter the feed gas flows into the corona reactor. Downstream from the reactor some gas is vented to a fume hood, some gas flows into a NO_X monitor, and some gas is collected in sampling vessels.

The pulsed power supply, shown schematically in Figures 2 and 3, utilizes a high voltage AC 60 Hz input provided by a Universal Voltronics 130 kV, 28 mA power supply. The AC voltage first flows through a bank of 333 kohm current limiting resistors. A high voltage rectifier, made up of a diode chain, serves to modify the AC voltage waveform by removing the lower half of the sine wave. A capacitor bank located between line voltage and ground charges during the rising portion of each voltage waveform. A mechanical rotating spark gap matched in frequency to the line voltage (60 Hz) serves as the pulse producing device. When the rotating arm and the sphere electrodes are not aligned, the voltage charges the capacitors; the gap discharges the capacitors when the arm and spheres are aligned. The characteristics of the capacitor bank determine the rise time for the pulsed waveform that is ultimately delivered to the reactor. The rise time is approximately 20 - 50 ns, and the pulse duration is on the order of 200 ns. The spark gap is aligned and synchronized to line voltage with a strobe lamp. The unit developed in this work is fundamentally similar to other units developed at Florida State University (Clements et al., 1989; Mizuno and Clements, 1987) as well as to those used in the literature (Creyghton, 1994; Tas, 1995; Mizuno et al., 1993).

The main body of the pulsed corona reactor is shown in Figure 4. The reactor is constructed of a 4" diameter, #316 stainless steel cylinder 18" long from end to end. The active region of the reactor consists of a 12" section of the reactor where a stainless steel wire electrode runs concentrically down the center of the reactor body. Three flow rates were used in the present study: 500 sccm (standard cubic centimeters per minute), 5000 sccm, and 10,000 sccm. The corresponding residence times in the active region of the reactor are 12 min,. 1.2 min, and 0.6 min (36 seconds). Corresponding Reynolds numbers in the reactor are 7, 70, and 140, respectively. This indicates that for all runs the reactor flow is laminar.

2.2. Gas Feed System

The gas feed system consists of: 1) building supply source of dry compressed air, 2) gas cylinders and regulators containing 1% NO in dry N_2 and pure ethylene, 3) gas cylinders and regulators containing a calibration gas of 100 ppm NO in N_2, 4) water tank through which

the air and other gas can be bubbled, 5) flow meters and mass flow controllers, and 6) mixing chamber. MKS, Instruments, Inc., mass flow controllers are used on the bulk air flow, the NO gas feed, and the ethylene gas feed. Bypass loops around the MKS units are available if needed. The mixing chamber contains stainless steel wool to provide a turbulent environment for adequate gas mixing. Figure 5 shows a schematic of the complete gas feed system.

2.3. Analytical Instrumentation

The analysis of the outlet gases from the reactor (Figure 5) include direct measurement of NO, O_3, N_2O, and hydrocarbon breakdown products. Nitrogen oxides are measured using a Thermo-Environmental Instruments, Inc. Model 42 H Chemiluminescence NO Analyzer. Ozone is measured using a PCI Ozone Corporation, Model HC-1 ozone monitor. The gas phase products, including N_2O and hydrocarbon breakdown products, are measured using a Hewlett-Packard GC/MS instrument located in the Department of Chemistry at Florida State University. The pulse waveform characteristics are measured using a Tektronix TDX 460 Four Channel Digitizing Oscilloscope with a P6015A 1000x 3.0 pF, 1000 MΩ voltage probe and a TM502A/AM503B current probe. Graphic devices included a Tektronix HC-100 color plotter for printing oscilloscope waveforms, and a Fisher Recordall Series 5000 chart recorder to monitor NO concentrations from the NO_X monitor.

2.4. Sampling Methods

The outlet gas from the reactor was fed directly into the Thermo-Environmental Instruments NO_X analyzer where NO and NO_2 were measured. Gas samples were collected in 500 ml glass sampling chambers equipped with ports for GC/MS analysis. These samples were taken directly to the Chemistry Department for analysis and were usually measured within several hours of collection. Controls were run to ensure that leakage and degradation within the sampling containers were minimal. The sampling containers were washed with deionized water and dried overnight with clean air.

2.5. Experimental Run Procedures

1. Turn on mass flow controllers and let warm up for at least 30 minutes.

2. Open the valve for the compressed air and adjust the pressure regulator to about 20 psig.

3. Adjust needle valves (2) in the compressed air line to make sure air at atmospheric pressure is going through the NO_X monitor.

4. Turn on the NO_X monitor and let warm up for around 2 hours.

5. Attach the gas calibration standards (NO, NO_2) to the NO_X monitor.

6. Calibrate the NO_X monitor to the concentrations of the calibration gas (100 ppm).

7. Turn on the chart recorder and adjust to necessary paper speed.

8. Once the mass flow controllers stabilize, make sure they are reading zero and adjust as necessary.

9. Clean the electrodes in the rotating spark gap using sandpaper and ethanol.

10. Turn on the rotating spark gap, the strobe lamp, the fan inside the faraday cage, the fan on the diode board, and the fan on the load resistors.

11. Adjust the rotating spark gap and align in a position perpendicular to the discharge position when strobe lamp is in line frequency mode (60 Hz).

12. Check that the valves in the sample gas line are open, and make sure that the gas has an open path through either the rotameters or the mass flow controllers, through the mixing chamber and the reactor, and then to a vent or into an analytical or sampling device.

13. On the gas cylinder that is to be used, open the main valve on the tank.

14. Adjust the pressure regulators and needle valves to desired flow rate.

15. Open sampling vessel and let sample gas pass through for enough time to come to equilibrium.

16. Close the valves on the sampling tube and replace with another sampling tube.

17. Get the baseline reading from NO_X monitor.

18. Turn on the oscilloscope, place the voltage probe at the insulator conductor on the reactor opposite the input of the pulsed power, and place the current probe on the wire grounding the reactor.

19. Ground the reactor body and check all of the gas and electrical connections between the pulse generator and the reactor.

20. Plug in the AC line cord for the power supply.

21. Put all three switches on the front of the power supply in the ON position, press the HV reset button, press the HV ON button, and then turn the dial to the desired voltage.

22. Allow all analytical devices to reach equilibrium for each new condition during experimental run.

23. Adjust waveforms on oscilloscope and save the waveforms in memory.

24. Close the valves on the sampling vessel and remove from the system.

25. Turn off the power to the reactor.

26. Ground the reactor and rotating spark gap with the portable grounding rod.

27. Plug in printer and attach to oscilloscope.

28. Print hardcopy of waveforms.

29. Close the vanes on the gas cylinder.

30. Purge the system with compressed air for several minutes.

31. Turn off the mass flow controllers and the NO_X monitor.

32. Close the compressed air valve and reduce regulator pressure.

3. EXPERIMENTAL RESULTS

3.1. Initial Power Supply Characterization

Preliminary characterization of the pulsed voltage waveform supplied to the corona reactor was carried out by Cadet Steve Lucas from the Department of Chemistry, United States Air Force Academy, while he was working at Florida State University as part of the Cadet Summer Research Program during the time of this project. Additional work including measurement of the power input to the reactor has been performed recently, and all of the major features of the pulsed power supply characterization are reported below.

The initial characterization of the pulsed power supply included calibration of the power supply dial settings, and measurement of the voltage pulse width (decay time), pulse rise time, resonant frequency, and output voltage at several locations in the circuit and for a range of input voltage levels.

Calibration of the power supply dial settings showed that the average peak AC voltage delivered to the pulse-forming network was linear with the dial settings. This is shown in Figure 6 over the range of 5 kV to 30 kV. Above 30 kV the average peak voltage was determined through extrapolation of the linear relationship found for the lower voltages.

The Tektronix high voltage probe with oscilloscope was connected to one of the ceramic insulator conductors in order to measure several pulsed voltage characteristics. For pulsed voltages in the range of 12 to 30 kV, the voltage decay time (one measure of the pulse width) was observed to range from 1.385 to 1.600 ps. A typical voltage waveform is shown in Figure 7, and the plot illustrates the typical "ringing" oscillatory pattern of the voltage decay. The resonance period for these oscillations was found to be 100 ns and this was independent of the applied voltage. These oscillations are typically observed in the literature (Mizuno et al.. 1993; Masuda and Nakao, 1990; Creyghton, 1994).

Pulsed corona onset was found to occur between an input voltage of 13 and 14 kV. The corresponding peak voltages seen on the oscillograms were 1.04 and 23.4 kV, respectively. Below onset, the output voltage reading was very low and had erratic and rapid variations. Once onset occurred, the output voltage rapidly rose to 23.4 kV. Between 23.4 and 41.0 kV peak pulsed voltages the rise time and decay time were seen to vary from 45 to 60 ns and 1.535 to 1.665 ps, respectively. It was found that there was no significant difference between the voltage required to initiate the corona and that required to maintain it, i.e., there was no hysteresis.

Analysis of the voltage waveform at the HV line side of the capacitor during repetitive spark gap closures was performed to determine the voltage loss. It was observed that the frequency of the capacitor discharge matched the frequency of the rectified wave (60 Hz) as expected, and the discharge was very fast, 1.6 ps, compared to the calculated RC capacitor charging time of 5 ms. However, there was a loss of about 1.2 - 2.0 kV once the capacitor

reached its maximum charge. This loss has been attributed to a slow leak to ground in the capacitors. From the waveform, it was observed that the oscillations present in the output voltage waveform are not present at the line side of the capacitor. This suggests that the source of the oscillations is probably due to inductance in the circuit.

Load resistors (R_2 in Figure 2) are present in the circuit since the impedance of the wire-cylinder separation gap is too high to sustain a pulsed discharge in the gas phase reactor. Generally, the value of this resistance is 100 - 200 ohms. The number of load resistors (8 ohms each) were changed to analyze the effect of the total resistance on the output voltage waveform. The decay time was strongly affected by the load resistance. All subsequent NO removal experiments were performed with approximately 150 ohms tail resistance in place.

3.2. Pulse Waveform Characteristics

Figures 7, 8, and 9 show typical pulsed voltage, current, and power characteristics measured at the reactor discharge conductor. Measurements were repeated for input voltage dial settings of 30 kV to 50 kV. The oscilloscope was set to average the waveform over 100 pulses. The amount of oscillation in the voltage waveform was observed to decrease as the voltage was increased. The current pulses are generally shorter than the voltage pulses, and the current waveforms also show a reversal to negative current for a short period following the peak in the pulse. Multiplying a corresponding voltage and current waveform gives a power waveform; the power waveforms follow a trend similar to that of the current pulses, however, they generally had a double peak.

Table I summarizes the data for the power supply characterization. The voltage and current were measured at the reactor HV electrode using the probes connected to the digital storage oscilloscope. The dial setting on the power supply was varied from 30 to 50 kV. The peak pulsed voltages are also shown in this table and generally increase with increasing input power. The pulse width measured at 1/2 maximum for the voltage pulse varied from 450 ns to 694 ns. The peak current was also seen to generally increase with input voltage, although the width of the current pulse at the baseline was seen to be invariant with the applied voltage.

The energy per pulse was calculated by integrating the voltage times the current over a single pulse. The power per pulse varied from 32.1 mJ/pulse to 107 mJ/pulse, for input voltages of 30 kV and 50 kV, respectively. The power delivered to the reactor was determined by multiplying the energy per pulse by the number of pulses per second (60 Hz). The power was found to vary from 1.9 to 6.4 watts, for voltage inputs of 30 to 50 kV. The energy delivered per pulse was somewhat higher than that reported by Tas (1995) (6 - 7 mJ/pulse), however, the total power delivered was slightly higher than that reported by Tas (1995) (0.05 to 1.5 watts). The energy per pulse was similar to that reported by Mizuno et al. (1993) (20 to 56 mJ/pulse), and the power delivered was slightly smaller than the discharge power reported by Mizuno et al. (1993) (5 to 14 watts). Mizuno et al. (1993) measured both the input power and the discharge power and they found that the discharge power was linearly related to the input power; the discharge power was 20 to 30% of the input power. Masuda and Nakao (1986) reported a power output in the range of 0.5 to 6.0 watts.

Tas (1995) varied the frequency of his power generator (5 - 240 Hz) and held the voltage at a constant level (28 kV; 16 kV/cm). Mizuno et al. (1993) fixed the frequency at 250 Hz and varied the voltage from 6.5 to 14 kV (8.5 - 19 kV/cm). Masuda and Nakao (1986) varied their corona input voltage from 0 to 60 kV (0 - 12 kV/cm). In the present study, the frequency was held constant at 60 Hz and the voltage was varied from 30 - 50. Figure 10 shows that the power output of the FSU pulsed power supply was approximately linear with the input voltage.

Table 1. Power Supply Characteristics

Dial Voltage (kV)	AC Input Voltage (kV)	Peak Pulsed Voltage (kV)	Pulse Width ½ Max (ns)	Peak Current (A)	Current Width (ns)	Energy per pulse (mJ)	Power (watts)
30	29.4	43.2	449	10.5	250	32.1	1.90
35	34.2	44.8	616	12.9	250	44.0	2.65
40	39.0	54.0	627	20.1	250	77.0	4.60
45	43.9	51.2	564	26.0	250	88.0	5.30
50	48.8	60.8	694	26.7	250	107.0	6.4

It is important to note that the operating procedures for the experiments reported here required cleaning the stainless steel spark gap electrodes after each run in order to ensure reproducibility of the data. A light sanding with fine sandpaper and wiping with ethanol (see Section 2.5) was performed after each run because the current and voltage characteristics can be affected by buildup of deposits on the electrodes. Future work will consider running the spark gap in an inert or nitrogen gas in order to minimize this buildup on the electrodes and to reduce the production of ozone by the spark gap. It can be noted that Mizuno et al. (1993) used tungsten-coated electrodes.

3.3. Pulsed Corona Reactor Experiments with Dry Air and NO

Figure 11 shows the steady-state NO concentration vs. applied voltage for the three different residence times used in this study (Run #'s 3, 4, 13, 14, 22, 23, 10, 11, 20, 21, 16, 17, 5, 7, 26, 27, 18, 19). The gas composition was dry air, 150 ppm NO, and no H_2O or ethylene. It is clear from this figure that at 30 kV the removal of NO is very low at the short residence times. There is also a sharp transition between 30 kV and 40 kV at these short residence times and this behavior is consistent with that observed by Mizuno et al. (1993) and Masuda and Nakao (1990). At a residence time of 0.6 minutes, the maximum NO removal (@ 50 kV) was 75%.

Table 2. Summary of Experimental Results

Run #	Dial Volt (kV)	Power (W)	Flow (sccm)	Residence time (min)	NO-in	NO-out	Fraction Removed	eV/mole NO	NO_2-in	NO_2-out	Ethylene	Water	NO_2 formed
1	40	4.6	500	12	233	113	0.515	1070.260	0	0			0
2	40	4.6	500	12	237	123	0.418	1128.695	0	0			0
3	40	4.6	500	12	137	0	1.000	939.206	220	2.2			-217.8
4	40	4.6	500	12	121	0	1.000	1063.398	80	4.6			-75.4
5	30	1.9	500	12	135	42	0.689	571.471	94	141			47
6	30	1.9	500	12	121	67	0.446	984.200	78	124			46
7	30	1.9	500	12	114	50	0.561	830.419	75	91			16
8	40	sample	for	GC/MS	analysis	for	N_2O						
9	20	no	readings	taken									
10	50	6.4	500	12	125	0	1.000	1432.166	78	2.3			-75.7
11	50	6.4	500	12	120	0	1.000	1491.840	77	4.2			-72.8
12	40	4.6	1000	6	143	0	1.000	449.899	69	9.6			-59.4
13	40	4.6	10000	0.6	146	73	0.500	88.131	18	73			55
14	40	4.6	10000	0.6	141	68	0.518	88.131	18	73			55
15	50	no	readings	taken									
16	50	6.4	10000	0.6	147	43	0.707	86.068	21	97			76
17	50	6.4	10000	0.6	147	20	0.864	70.481	29	120			91
18	30	1.9	10000	0.6	145	142	0.021	885.780	24	24			0
19	30	1.9	10000	0.6	146	142	0.027	664.335	20	22			2
20	50	6.4	5000	1.2	150	1.1	0.993	120.229	34	101			67
21	50	6.4	5000	1.2	153	8.9	0.942	124.234	42	134			92
22	40	4.6	5000	1.2	126	26	0.794	128.671	24	98			74

Table 2. Summary of Experimental Results (Continued)

Run #	Dial Volt (kV)	Power (W)	Flow (sccm)	Residence time (min)	NO-in	NO-out	Fraction Removed	eV/mole NO	NO_2-in	NO_2-out	Ethylene	Water	NO_2 formed
23	40	4.6	5000	1.2	126	25	0.802	127.397	26	100			74
24	35	2.65	5000	1.2	123	63	0.488	123.543	29	71			42
25	35	2.65	5000	1.2	125	74	0.408	145.345	27	65			38
26	30	1.9	5000	102	124	119	0.040	1062.936	26	26			0
27	30	1.9	5000	1.2	122	118	0.033	1328.670	23	24			1
28	35	2.65	10000	0.6	143	108	0.245	105.894	25	49			24
29	35	2.65	10000	0.6	137	92	0.328	82.362	23	57			34
30	35	2.65	5000	1.2	119	36	0.697	89.308	14	71	500		57
31	35	2.65	5000	1.2	119	53	0.555	112.312	16	70	500		54
32	no corona	sample	for	GC/MS	analysis	for	background	gases					
33	35	2.65	10000	0.6	155	129	0.168	142.550	20	38	500		18
34	40	4.6	10000	0.6	148	118	0.203	214.452	20	44	500		24
35	no corona	sample	for	GC/MS	analysis	for	background	gases					
36	50	6.4	10000	0.6	165	13	0.921	58.888	24	125	500		101
37	50	6.4	10000	0.6	152	15	0.901	65.336	30	127	500		97
38	no corona	sample	for	GC/MS	analysis	for	background	gases					
39	50	6.4	10000	0.6	179	59	0.670	74.592	35	110	0		81
40	50	6.4	10000	0.6	159	35	0.780	72.186	35	128	0		93
41	50	6.4	10000	0.6	166	1	0.994	54.249	26	81	500	pres	55
42	50	6.4	10000	0.6	152	0.5	0.997	59.083	24	52	500	pres	28
43	50	6.4	10000	0.6	148	0.6	0.996	60.726	25	59	500	pres	34
44	no corona	sample	for	GC/MS	analysis	for	background	gases					
45	50	6.4	10000	0.6	166	9.3	0.944	57.122	-17	64	500	pres	81

Table 2. Summary of Experimental Results (Concluded)

Run #	Dial Volt (kV)	Power (W)	Flow (sccm)	Residence time (min)	NO-in	NO-out	Fraction Removed	eV/mole NO	NO_2-in	NO_2-out	Ethylene	Water	NO_2 formed
46	no corona	sample	for	GC/MS	analysis	for	background	gases					
47	50	6.4	10000	0.6	175	38	0.783	65.336	-16	55	0	pres	71
48	50	6.4	10000	0.6	159	25	0.843	66.799	-16	51	0	pres	67
49	50	6.4	10000	0.6	174	4.4	0.975	52.777	57	106	500		49
50	50	6.4	10000	0.6	176	4.3	0.976	52.132	92	131	500		39
51	30	1.9	10000	0.6	174	164	0.057	265.734	28.4	33.5	500		5.1
52	30	1.9	10000	0.6	186	174	0.065	221.445	33	45	500		12
53	35	2.65	10000	0.6	178	97	0.455	45.757	30	85	500		55
54	35	2.65	10000	0.6	175	101	0.423	50.085	33	86	500		53
55	40	4.6	10000	0.6	176	46.5	0.736	49.680	34.3	118	500		83.7
56	40	4.6	10000	0.6	175	28	0.84	43.766	37	119	500		82
57	no corona	sample	for	GC/MS	analysis	for	background	gases					
58	45	5.3	10000	0.6	194	51	0.737	51.836	42.3	126	500		83.7
59	45	5.3	10000	0.6	188	47	0.750	52.571	46.4	128	500		81.6
60	50	6.4	10000	0.6	196	24	0.878	52.041	51.4	158.4	500		107

Figure 12 shows the NO concentration vs. residence time in the reactor for various voltage dial settings (Run #'s 3, 4, 13, 14, 22, 23, 10, 11, 20, 21, 16, 17, 5, 7, 26, 27, 18, 19). The gas composition was the same as described above. It is again clear that at the low voltage, i.e., 30 kV, the removal of NO at short residence times is very small as mentioned above. At the higher voltages the removal is much greater. At the long residence time of 12 min. virtually 100% of the NO was removed for the two higher voltages of 43.9 and 48.8 kV. It is important to note that at this long residence time the NO_2 also decreased. As the flow rate is increased and the residence time is decreased, a corresponding drop in the amount of NO removed is observed. It is also important to note that the efficiency of NO removal is improved at the higher flow rate as shown in Table 2. Here the amount of energy to remove one mole of NO is approximately 100 eV for the higher voltages (42 to 60 kV) at 10,000 sccm. This number can be compared to that obtained by Tas (1995). For dry nitrogen with 6% oxygen and 1200 ppm NO, Tas obtained an energy of approximately 850 eV/mole of NO removed. He did not report data at the higher oxygen content used in the present study, however he did observe an increase in energy per NO as oxygen content increased from 0 to 6%.

Figure 12 also shows an approximately linear decrease in NO concentration with residence time for the lower voltage condition (30 kV, Run #'s 5, 7, 26, 27, 18, 19). This is consistent with an approximate relationship derived by Tas (1995). At higher power input, with low NO input, Tas (1995) found a first order decay in NO concentration, and this trend is also seen approximately in the data of Figure 12 for the higher voltages (40 and 50 kV).

Analysis of the effluent from the reactor using GC/MS indicated that about 15 ppm N_2O was produced in all the cases with NO feed in dry air. This approximate amount of N_2O appears to be formed in the system regardless of the presence of other species, i.e., water or ethylene. The independence of N20production on feed composition is consistent with observations reported by Mizuno et al. (I 993).

3.4 Pulsed Corona Reactor Experiments with Dry Air, NO, and Ethylene

Figure 13 shows the NO concentration at the reactor outlet as a function of the applied voltage for the case with 500 ppm ethylene and for the case without any ethylene (Run #'s 18, 19, 28, 29, 13, 14, 16, 17, 33, 34, 36, 37, 49, 50, 51, 52, 53, 54, 55, 56, 57, 58, 59, 60). It can be seen that at lower voltages (30 kV) the difference between the two cases is small. The largest difference is seen at 40 kV where the presence of ethylene causes the NO removal to decrease from approximately 50% to approximately 80%. At the highest voltage, 50 kV, the presence of ethylene causes the NO removal to go from about 80% to about 90%.

Energy consumption calculations in the present report use the relationship (Tas, 1995)

$$1 \text{ eV / molecule NO} = 96.4 \text{ kJ / mole NO removed.} \quad (37)$$

The energy consumption per NO removed at 35, 40, 45, and 50 kV was approximately 50 eV/NO, and at 30 kV it was approximately 250 eV/NO. Mizuno et al. (1993) found the

energy consumption to vary from 80 to 151 eV/NO removed when ethylene was added to the reactor for a dry gas with 10% oxygen and 200 to 800 ppm NO. The lower value of 80 EVNO compares well to the value of 50 eV/NO obtained in the present study.

Analysis by GC/MS of the effluent from the reactor with ethylene in the gas feed indicates that at 45 kV, 23% of the ethylene has reacted to products and that at 50 kV, 26% of the ethylene has reacted. This observation is based on a decrease in the ethylene peak area measured by the GC/MS. Since the feed gas contains 500 ppm ethylene this indicates that about 115 to 130 ppm ethylene is decomposed by the pulsed corona. These measurements were made for the reactor run with a 0.6 min residence time and with 170 to 200 ppm NO (Run #s 58, 59, 60). The corresponding amounts of NO removed from the reactor under these conditions were 140 and 170 ppm. Therefore, a slightly larger amount of NO was removed than would be expected if the reaction had a 1:1 stoichiometry. No other reaction products were detected with the GC/MS, although additional experimentation with other sampling techniques and analysis may be necessary to validate this observation.

3.5. Pulsed Corona Reactor Experiments with Humid Air, NO, and Ethylene

Table 3 compares the NO removal for the four cases of NO only, NO with ethylene, NO with water, and NO with water and ethylene. All runs were made at 10,000 sccm and 50 kV voltage dial setting. The concentration of NO in the feed was in the range of 140 to 180 ppm. The gas was at room temperature (approximately 25^{o} C), and the water content was no higher than 1 - 2% by weight (saturation at room temperature, or 3 mole percent). Without additives the NO removal was about 75% (average of Run #'s 16, 17, 39, 40). The effect of 500 ppm ethylene was more dramatic than the effect of water, i.e., 93% removal (average of Run #s 36, 37, 49, 50, 60) vs. 81% removal (average of Run #'s 47, 48). In addition, the case with water and ethylene showed only a relatively small percentage improvement over the case with ethylene only, i.e., 98% removal (average of Run #'s 41, 42, 43, 45) vs. 93% removal.

Table 3 also shows the energy costs for removing one molecule of NO for each of the four conditions reported. The NO only case required 76 eV/NO to remove 73% of the input NO. In dry nitrogen containing 10% oxygen the data of Mizuno et al. (1993) indicate 290 to 370 eV/NO, and in dry nitrogen containing 0 to 6% oxygen the data of Tas (1995) indicate 210 to 850 eV/NO. With the addition of ethylene the present study suggests 56 eV/NO while the data of Mizuno et al. (1993) for 10% oxygen in nitrogen gives 80 to 150 eV/NO. For the case of 10% oxygen in nitrogen with either 4.5 or 9.9% water, Mizuno's data gives 46 to 74 eV/NO, independent of water content. These latter values are in the general range of those given in Table 3.

Table 3. Effect of Water on NO Removal (50 kV, 10,000 sccm air)

NO only	NO + ethylene	NO + water	NO + ethylene + water
75%	93%	81%	98%
76 eV/NO	56 eV/NO	66 eV/NO	58 eV/NO

For all experiments run with the feed air bubbled through a water-filled chamber, it was observed that a slight film was formed on the inside of the glass sampling tubes when gas samples were taken. This film was dissolved in water and the pH of the resulting solution was measured. No decrease in pH was found, although again further validation of this finding needs to be made. Further work needs to be performed to identify the composition of this material and to detect other reaction products from the corona reactor.

In order to compare data obtained under a variety of conditions in our experiments to data from several literature sources, Figures 14 and 15 show "percentage NO removal" for low initial concentration cases and "ppm NO removed" for high concentration cases, respectively, as functions of a factor defined as "the power per volume (energy input divided by flow rate) divided by the square root of the residence time". This type of plot was suggested by Masuda and Nakao (1986), where they were able to compress data from a range of power and residence time experiments onto a single plot. No theoretical justification for this plot is available at present, however it serves as a convenient means to compare data obtained under a variety of conditions.

Figure 14 shows that the data from the present study for dry air falls along a single smooth curve. There is one outlier point not shown in the figure that arises at low voltage (30 kV) and short residence time; this may be due to the low voltage being insufficient to initiate the expected chemical reactions. Data from Masuda and Nakao (1986) and Ohkubo et al. (1994), as well as data from the present study for the cases with ethylene present and water present are shown for comparison. Masuda and Nakao (1986) considered the case of dry air with 180 ppm NO and 180 ppm NH3. The percentage NO removal for this case with ammonia is higher than that of our data for dry air. Our data for the cases of ethylene and water compare well to the data of Masuda and Nakao (1986) at 1.8 $Wh/m^3\text{-}s^{1/2}$. The data of Ohkubo et al. (1994) for cases of 20% O_2 in nitrogen fall somewhat below our data and their data for the case with ammonia does not show much of an effect of ammonia on NO removal. It can be concluded from this figure that the general range of performance of the reactor developed in this project is similar to other reactors reported in the literature. Because of the wide range of gas feed conditions and possibly variation in methods of determining power output, precise comparison between different studies is difficult.

Figure 15 shows data from Tas (1995) and Mizuno et al. (1993) for much higher levels of initial NO concentration. The data obtained by Mizuno et al. (1993) for 10% O^2 with 4.5% or 9.9% H_2O in nitrogen is seen in this figure to be very close to that obtained by Tas (1995)

for 5% O_2 with 11% H_2O in nitrogen. It is interesting to note that the data of Mizuno et al. (1993) shows no effect on reactor performance of water content in the range of 4.5 % to 9.9%. The data of Mizuno et al. (1993) also shows a large effect of ethylene on NO removal from nitrogen gas with 10% O_2. Ethylene removal data (Mizuno et al., 1993) shows a significantly larger energy consumption than the work reported here. It is not clear why that shady differs from the present work, although there are differences in the gas feed composition (oxygen content) that warrant further investigation. The "no ethylene" data of Mizuno et al. (1993) also show significantly higher energy costs than that of the present study.

4. MODELING RESULTS

Although prediction of the performance of pulsed streamer corona reactors through mathematical modeling has been pursued by a number of investigators, no theoretical model has been tested and quantitatively compared with actual experimentally measured output from a pulsed corona reactor. Empirical models developed by Masuda and Nakao (1990) describe the removal efficiency as a function of the input power, but do not explicitly account for the complex chemistry occurring in the system. Many other theoretical models have been applied to corona systems, however, only qualitative trends have been predicted due to the nature of the assumptions made concerning the details of the streamer structure. A range of approaches have been made to modeling NO_X/SO_2 removal (Wren, 1989; Alekseev, 1993; Civitano et al., 1988; Creyghton, 1994; Dinelli et al., 1990; McFarlane and Wren, 1991; Mizuno et al., 1993; Tokunaga and Suzuki, 1990; Gallimberti, 1988; Masuda and Wu, 1987; Masuda et al., 1987; Masuda et al., 1991) and ozone synthesis (Peyrous et al., 1989).

Models of pulsed streamer corona can be classified into those that consider a) streamer propagation through species continuity equations for electrons and ions, and b) batch chemical reaction kinetic models. The analysis of streamer propagation is generally performed with one dimensional convective/diffusion/reaction models that consider electron propagation in a non-uniform electrical field (see Creyghton, 1994, for good introductory review). One of the objectives of these models is to determine the minimum voltage required for streamer inception. Batch chemical kinetics models usually consider a large number of reacting species, including electrons, ions, radicals, and molecular species; however, the electron concentration is input either as a) an empirically determined function (as in measured current pulses), or b) through solution of the Boltzmann equation for electron distribution as a function of the applied electrical field. Coupling the streamer models to the batch kinetic models has been attempted, however, the approaches that have been used require severe limiting assumptions on the nature of the streamer structure (i.e., ideal uniform disk structures). It is therefore clear that it is necessary to further develop the streamer/chemistry models in order to have solid quantitative comparison of experimentally measured reactor output with predictive models.

The modeling results in the present study have focused on the use of a basic set of chemical reactions shown in Table 4. The reaction rate constants for all of these reactions, except the first two electron reactions with N_2 and O_2, were taken from the literature (McFarlane and Wren, 1991). The reaction rate constants for these two reactions were varied to compare with the experimental data. These reactions are expected to be highly dependent upon the electric field strength. Figures 16 and 17 show the NO and NO_2 as a function of residence time for various values of this initiation reaction constant. It can be seen in Figure 16 that at the lower values of the reaction rate constant the decrease in NO with residence time is much slower than that at the higher values. The data from the experiments reported in the present work showed a NO removal at 36 seconds of about 74%. This would fall between the profiles computed with $k_1 = 2 \times 10^{12}$ cm^3/mole-s and $k_1 = 5 \times 10^{12}$ cm^3 /mole-s as shown in this figure. Figure 17 shows the corresponding NO_2 profiles. It is very interesting to note that at

Table 4. Reactions Used to Compute the Different Concentration Profiles

ELEMENTS H E O N C END
SPECIES H2 H O2 O O* OH HO2 H2O2 H2O N N2 NO O3 HNO2 HNO3 E NO2 NO3 N2O
N2O4 C2H4 HCHO HCOOH CO CO2 C2H3O HOC2H4 HOC2H4O2 HOC2H4O CH2OH HOCH2CHO
O2CH2OH OCH2OH HCO END

REACTION	REACTION RATE CONSTANT
N2 + E => 2N + E	0.5E+13
O2 + E => O + O* + E	0.5E+13
H2O + E => H + OH + E	0.5E+13
N + N => N2	6.384E+10
N + O => NO	1.445E+11
N + O2 => NO + O	53604700
N + NO => N2 + O	2.047E+13
N + NO2 => 2NO	1.8069E+12
N + NO2 => N2 + O2	1.0841E+13
N + NO2 => N2 + 2O	1.385E+12
N + OH => NO + H	1.445E+13
N + NO2 => N2O + O	1.8069E+12
O* => O	6.95E+8
O* + O3 => 2O2	7.2276E+13
O* + O3 => 2O + O2	7.2276E+13
O* + N2O => N2 + O2	2.9513E+13
O* + N2O => 2NO	4.0354E+13
O* + H2 => H + OH	6.023E+13
O* + H2O => 2OH	1.3251E+14
O + O => O2	1.0239E+11
O + H => OH	1.08414E+12
O + O2 => O3	7.8299E+9
O + O3 => 2O2	4.8184E+9
O + H2O => OH + O2	3.433E+13
O + OH => O2 + H	1.987E+13
OH + H2 => H2O + H	4.035E+9
OH + OH => H2O + O	1.0841E+12
OH + OH => H2O2	9.937E+12
OH + HO2 => H2O + O2	6.6253E+13
OH + H2O2 => H2O + HO2	1.0239E+12
OH + H => H2O	1.4452E+13
H + O2 => HO2	8.492E+11
H + O3 => OH + O2	1.6864E+13
H + HO2 => H2 + O2	3.372E+12
H + HO2 => 2OH	4.3365E+13
H + HO2 => H2O + O	1.44552E+12
H + H2O2 => H2O + OH	6.023E+10
HO2 + HO2 => H2O2 + O2	1.0239E+12

NO + OH => HNO2	9.0345E+12
NO + O3 => NO2 + O2	8.4322E+9
NO + O => N + O2	2.77058E+9
NO + O => NO2	1.3973E+12
NO + NO3 => 2NO2	1.7466E+13
NO2 + OH => HNO3	1.4455E+13
NO2 + O3 => NO3 + O2	19273600
NO2 + O => NO + O2	5.8423E+12
NO2 + OH => HO2 + NO	1.38529E+13
HNO2 + OH => NO2 + H2O	2.951E+12
HNO3 + OH => H2O + NO3	9.034E+10
N2O4 + M => 2NO2 + M	2.0639E+9
2NO3 => 2NO2 + O2	1.9177E+8
NO3 + O => NO2 + O2	1.0239E+13
NO + NO3 => 2NO + O2	1.8352E+11
O3 + N => NO + O2	6.023E+7
2NO2 + M => N2O4 + M	3.0553E+14
NO2 + NO3 => NO2 + NO + O2	6.4529E+8
OH + H => H2 + O	1.964E+7
H2O + O => 2OH	1.1249E+12
H2O2 + H => HO2 + H2	3.1219E+9
H2O2 + O => OH + HO2	1.0262E+9
O3 + HO2 => OH + 2O2	1.1068E+9
O3 + OH => HO2 + O2	3.3618E+10
HNO2 + O => NO2 + OH	1.8069E+9
HNO3 + HNO2 => 2NO2 + H2O	9.6368E+6
HNO3 + O => NO3 + OH	1.8069E+9
HNO3 + H => HNO2 + OH	6.023E+10
NO3 + H => NO2 + OH	6.6253E+13
NO3 + OH => NO2 + HO2	1.3853E+13
NO3 + HO2 => HNO3 + O2	7.6277E+11
NO3 + HO2 => NO2 + OH + O2	3.0511E+12
N + HO2 => NO + OH	1.3251E+13
O + C2H4 => C2H3O + H	1.6262E+11
C2H3O + O2 => HCHO + CO + OH	6.023E+10
C2H4 + OH => HOC2H4	4.8786E+12
HOC2H4 + O2 => HOC2H4O2	1E+20
HOC2H4O2 + NO => HOC2H4O + NO2	4.2161E12
HOC2H4O => HCHO + CH2OH	6
HOC2H4O + O2 => HOCH2CHO + HO2	4.2161E+9
CH2OH + O2 => HCHO + HO2	1.2046E+12
HO2 + HCHO => O2CH2OH	4.5173E+10
O2CH2OH + NO => OCH2OH + NO2	4.5173E+12
OCH2OH + O2 => HCOOH + HO2	2.1081E+10
HCHO + OH => HCO + H2O	6.6253E+12
HCO + O2 => HO2 + CO	1E+20
END	

the highest k, there is a maximum in NO_2 concentration, and that at longer residence times the NO_2 decreases. This maximum in NO_2 is observed in the data of Masuda and Nakao (1990) with 600 ppm of ammonia present.

For the highest value of k_1 used in Figures 16 and 17 (k, = 5 x 1012 cm3/mole-s), Figure 18 shows the NO, NO_2, and N_2O profiles. This figure indicates that the increase in N_2O is very small until the residence time is long, and that all of the removal of NO cannot be accounted for in the formation of NO_2 and N_2O; i.e., the sum of NO_2, N_2O and all nitrogen oxide species does not equal the initial NO gas feed to the reactor. This indicates that the conversion of some N02 to N2ando2may account for the nitrogen balance.

Figures 19, 20, and 21 show the corresponding profiles (NO, NO_2, and HNO_3) for the cases with 1% water present and the same variation in rate constants as used in the previous "no water" results. The trends are similar to those shown in the previous figures, however, the formation of HNO_3 can now be observed. Comparison of Figure 16 with Figure 19 shows that the presence of 1% water vapor significantly enhances the NO removal. For example, the case of $k_1 = 5 \times 10^{11}$ shows a 22% removal for the dry case and a 36% removal for the wet case. Comparison of Figure 17 with Figure 20 shows a shift in the time where the NO maximum occurs. For example, in the case of $k_1 = 5 \times 10^{12}$, the NO maximum occurs at about 30 seconds in the dry system and the maximum occurs at about 18 seconds, Figure 20, in the wet system. From comparison of Figure 17 and Figure 22, it is also obvious that the concentration of NO_2 is much lower in the wet system. Figure 23 shows the increase in HNO_3 and again, the quantitative amount of products formed as the NO decomposes also indicates that some nitrogen from NO may be converted to N_2.

The presence of 500 ppm ethylene in the dry system (Figure 24) gives about 99% removal of NO at about 50 seconds residence time. This can be compared to the greater than 60 second residence time required in the no additive case shown in Figure 18. The shape of the N_2O and O_3 curves in Figure 25 are also slightly different than those for the no additive case. Figure 26 shows that 500 ppm ethylene strongly enhances the production of ozone.

Figure 27 summarizes the four cases of dry air, air with ethylene, air with water, and air with ethylene and water. With the rate constants used in the simulation, all four cases appear to reduce NO from initial concentrations by over 99% in 60 seconds. At 36 seconds the dry air case showed a 90% reduction in NO, the air with ethylene case showed a 95% reduction in NO, the air with water case showed a 98% reduction in NO, and the air with water and ethylene case showed a 100% reduction in NO. The slowest rate of reduction is that for the dry air alone, as observed in the experimental results, although the experimental data still indicated about a 74% drop in NO with this residence time. The next slowest case shown in the model is for the case of air with ethylene. This does not correspond to the experimental results where the air with water case showed a slower rate of NO removal than the air with ethylene case -- 81% verses 93%, respectively, at a 36 second residence time. This discrepancy may be due to differences in the rate constants used in the model vs. those in the experimental system, or to possible differences in the amount of water used in the

experimental study. A further problem with the model is that the reaction of ethylene with ozone (according to the literature) is five orders of magnitude slower than that of ethylene with hydroxyl radicals or singlet oxygen. In addition, the exact rate constants for all of the individual steps in the ozone reaction mechanism are not known. The computer simulation therefore does not include the ozone reaction with ethylene. The simulation shows that the case of air with water and ethylene has an initially slower slope than the case with water alone, however, these curves cross at about 30 seconds, and the case of air with water and ethylene drops to zero at a shorter residence time than the case of air with water.

Figure 28 shows that the addition of water dramatically affects the ethylene concentration, and that without water very little ethylene is removed. The experimental results show that ethylene is removed significantly (approximately 25%), even without water present in the system. This again may be due to our neglecting the ozone-ethylene reactions as discussed above. Figures 29 and 30 show two of the hydrocarbon byproducts produced from ethylene decomposition in the pulsed corona discharge for the cases of air with and without water. The production of formaldehyde and glycolaldehyde are both strongly enhanced by the addition of water.

5. CONCLUSIONS

The major conclusions from this study include:

1. The addition of ethylene to dry air in the pulsed corona reactor results in significant enhancement of NO removal. With a residence time of 0.6 min and a power input of 6.4 watts, 74% of the NO was removed from dry air at a cost of 76 eV/NO. Upon the addition of 500 ppm ethylene under the same reactor conditions, 93% of the NO was removed at a cost of 56 eV/NO. The qualitative effect of ethylene confirms data reported in the literature (Mizuno et al., 1993). The data of Mizuno et al. (1993), however, indicate an energy cost of between 80 and 150 eV/NO with the presence of 500 ppm ethylene. The upper number corresponds to 200 ppm NO removed and the lower number corresponds to 800 ppm ethylene removed. Quantitative analysis by GC/MS indicates that roughly equivalent amounts of ethylene are decomposed for NO removal. This result has not been previously reported since the, only reported work on the effects of ethylene (that of Mizuno et al. 1993) did not quantify the amount of ethylene decomposed. It may however, be inferred from the data of Mizuno et al. (1993) that a 1:1 correspondence is not to be expected since they were able to remove about 800 ppm NO with an addition of 500 ppm ethylene.

2. The presence of water in air containing ethylene results in a small increase in NO conversion efficiency. About 93% of the NO was removed at a cost of 56 eV/NO for the ethylene only case, as mentioned above. Upon the combination of water and ethylene, 98% of the NO was removed at a cost of 58 eV/NO. Water presence in air containing NO only (no ethylene) gives an NO removal of 81% at a cost of 66 eV/NO. The combined effects of ethylene and water vapor have not been previously reported in the literature. Analysis by GC/MS was not able to detect other ethylene reaction products that would be expected based upon known chemistry. Mizuno et al. (1993) detected acetic acid reaction products using FTIR spectroscopy. The reaction pathways of known atmospheric chemistry do not appear to directly favor the production of acetic acid as shown in the model simulation results and the basic chemistry obtained from atmospheric chemistry literature; this work tends to show more formic acid and formaldehyde produced. Further work is recommended to search for formaldehyde (GC/MS) and acetic and formic acids (HPLC). The model results indicate that water strongly enhances the formation of acetic acid and glycolaldehyde.

3. The removal of NO from dry air shows a sharp transition above 30 kV for the shorter residence times reported in this work. This sharp transition in removal efficiency has been reported by Mizuno et al. (1994), however the quantitative value of the power input in the present system differs from that reported by Mizuno et al. (1995).

4. Results of the present study show good comparison with those obtained by several other investigators. For low NO removal (0 to 200 ppm), the data in the present study show a similar order of magnitude in energy costs to that of Masuda and Nakao (1986) and Ohkubo et al. (1994). For high NO removal (200 to 1000 ppm), the data of Mizuno et al. (1993) show somewhat higher energy costs for the case of ethylene present in comparison to our data. At

the high NO removal range, the data of Mizuno et al. (1993) compares well to the data of Tas (1995) for the case of water present.

5. *Mathematical simulation of the chemical reactions occurring for NO removal indicates that NO_2 initially goes up at the shorter residence times, reaches a maximum at an intermediate residence time, and thereafter drops at the long residence times.* The experimental data in this work reflects this conclusion because at the long residence time of 12 minutes, NO_2 was found to decrease to very low levels in comparison to the levels found at 0.6 and 1.2 minutes. The model also indicates that ethylene reduces the magnitude of the NO_2 peak, however, it does not appear to shift the residence time where the peak occurs. The stoichiometry of the reaction products from the model simulation indicates that a small amount of NO goes to produce N_2O, however, at long residence times a significant quantity of NO may react to form N_2. GC/MS data confirms the presence of N_2O in the trace quantities (< 15 ppm) predicted by the model. The model also indicates that some fraction of the NO is converted to N_2 even in the cases with water and ethylene present.

6. *The effect of water and ethylene on NO removal in the model simulations show similar trends to those found in the experimental studies.* The model shouts that NO is least effectively removed in air alone, and that NO is most effectively removed in air with 1% water and 500 ppm ethylene. The model also shows, however a more pronounced effect of water (at 1%) than of ethylene on NO removal, while the experimental study shows a greater effect on NO removal from the presence of ethylene than of water. The experiments indicate that air with water showed a NO removal of 81% and that air with ethylene showed an increased NO removal of 93%. The model simulations indicate that 1% water increases the removal to 98% and that 500 ppm ethylene increases the NO removal to 95%. The water content of the experimental study is not precisely known, although it can be no larger than about 3% mole fraction and may be somewhat less. A humidity detector that has been ordered but not yet received can be used to measure water content of the gas more accurately. The magnitude of the model predictions for the water results does not correspond exactly to the experiments due to uncertainties in the electron initiation reaction rates, possible uncertainties in the amount of water added during the experimental studies, and/or possible differences in reaction rate constants from those reported in the atmospheric chemistry literature.

7. *GC/MS analysis shows that about 15 ppm N_2O is produced under all gas feed conditions of this study.* The mathematical simulation shows a small variation in N_2O production (5 - 10 ppm) for the cases of air with ethylene, air with water, or air with ethylene and water, however, this variation may be within experimental error of the GC/MS analysis.

6. RECOMMENDATIONS FOR FUTURE WORK

The major recommendations for further investigation of the results presented in this study are:

1. Perform further parametric analysis of the gas feed components including water, CO, and CO_2. Due to time and equipment delivery constraints the present study was unable to perform experiments with these added gases. CO is expected to be especially important in light of reactions known from atmospheric chemistry.

2. Perform more extensive analysis of byproducts formed in the system. GC/MS analysis combined with HPLC should be performed to search for quantitative amounts of such reaction products as acetic acid, formaldehyde, and formic acid. Sampling methods can be improved using liquid nitrogen or acid bath traps to collect larger quantities of sample. Efforts should be made to try to determine how much, if any, NO is converted to nitrogen through reactions in the model simulation. Quantification of HN03production should also be performed.

3. Comparison of the model predictions with experimental results for direct measurements of NO_2, O_3, CO, and other reaction products. The present study did not provide quantitative information on NO_2 due to problems with NO_2 calibration gases. Further work with NO_2 is thus essential. The production of O_3 was not studied in detail due to problems with the ozone monitor, however, further work to test the model predictions should be performed.

4. Measure electron-N_2 reaction rate constants using experiments with only NO in N_2. Compare these rate constants to those from the model and to those used in the present study. Measure electron-O_2 reaction rate constants for ozone production in experiments containing only O_2. Compare these reaction rate constants with those from the model.

5. Improve reactor power calculations by determining the difference between delivered power and output power, i.e., determine amount of power lost in the circuit following the approach of Mizuno et al. (1993), or that of Tas (1995).

Additional recommendations for consideration include:

1. Install temperature control apparatus to allow reactor operation under a variety of temperatures.

2. Develop optimization methods to find optimal operating conditions for the reactor in terms of gas feed composition and power variation.

3. Install equipment to analyze the formation of aerosol particles in the outlet of the reactor.

7. REFERENCES

1. Alekseev, G.Y., A.L. Leuchenko, and V.A. Bityurin, "Flue Gas Cleaning of the Electrostatic Corona, Part II, Chemical Kinetics and Heat and Mass Transfer in NO/SO_2 Removal", Research Report IVTAN-ANRA #93/2, Moscow, 1993.

2. Atkinson, R., and A.C. Lloyd, "Evaluation of Kinetic and Mechanistic Data for Modeling of Photochemical Smog", J. Phys. Chem. Ref. Data, 13(2), 1984, 315.

3. Bastein F., and E. Marode, "The Determination of Basic Quantities during Glow-to-Arc Transition in a Positive Point-to-Plane Discharge", J. Phys. D: Appi. Phys., 12 (1979), 249-263.

4. Bastein F. and E. Marode, "Breakdown Simulation of Electronegative Gases in Non-Uniform Field", J. Ethos. D: Appl. Phys., 18 (1995), 377-393.

5. Bedjai, G., H.K. Orbach, and F.C. Riesenfeld, "Reaction of Nitric Oxide with Activated Carbon and Hydrogen", Industrial and Engineering Chemistry, 50 (1958), 1165.

6. Chang, M.B., M.J. Kushner and M.J. Rood, "Gas Phase Removal of NO from Gas Streams via Dielectric Barrier Discharges", Envir. Sci. Technol., 26 (1990), 777-781.

7. Civitano, L., G. Dinelli, I. Gallimberti, M. Rea, and Z. Turri, "Free Radical Production by Corona Discharges in a $DeNO_X$ - $DeSO_X$ Reaction", IX International Conference on Gas Discharges and their Applications, Venice, Benetton, Padova, Italy, 1988, 603-603.

8. Creyghton, Y.L.M., "Pulsed Positive Corona Discharges, Fundamental Study and Application to Flue Gas Treatment", CIP-DATA Koninkijke Biblitheck, Den Haag, Netherlands, 1994.

9. Dinelli, G., L. Civitano, and M. Rea, "Industrial Experiments on Pulse Corona Simultaneous Removal of NO_X and SO_2 from Flue Gas", IEEE Trans. on Ind. Appl., 26 (1990).

10. Futumura, S., T. Yamamoto, and P.A. Lawless, "Towards Understanding of VOC Decomposition Mechanisms using Nonthermal Plasmas", Transactions of IEEE-Industry Applications Society, (1995), 1453.

11. Gallimberti, I., "Breakdown Mechanisms in Electronegative Gases", V International Symposium on Gaseous Dielectrics, Pergamon, Oxford, UK 61-79, 1987.

12. Gallimberti, I., "Impulse Corona Simulation for Flue Gas Treatment", Pure Appl. Chem., 60 (1988), 663.

13. Gullett, B.K., M.L. Lin, P.W. Groff, and J.M. Chen, "NO_X Removal with Combined Selective Catalytic Reduction and Selective Noncatalytic Reduction: Pilot-Scale Test Results", J. Air & Waste Management Association, 44 (1994), 1188.

14. Jogan, K., A. Mizuno, T. Yamamoto, and J.S. Chang, "Reduction of CO_2 from Combustion Flue Gases by an AC Ferroelectric Packed Bed Reactor", Inst. Phys. Conf Ser. No. 118: Section 3, 1991, 129.

15. Ku, B.J., J. K. Lee, D. Park, and H-K Rhee, "Treatment of Activated Carbon to Enhance Catalytic Activity for Reduction of Nitric Oxide with Ammonia", Ind. Eng. Chem. Res., 33 (1994), 2868-2874.

16. Kiang, C.S., D. Stauffer, V.A. Mohnen, J. Bricard, and D. Vigla, "Heteromolecular Nucleation Theory Applied to Gas-to-Particle Conversion", Atmospheric Environment, 7 (1973), 1279-1283.

17. Locke, B.R. and W.C. Finney, "Construction of a Pulsed Streamer Corona Reactor", Final Report. contract F5ESCR41580100, prepared for the United States Air Force, 325 Contracting Squadron, Tyndall AFB, Florida, June 5, 1995.

18. Masuda, S., Y. Wu, T. Urabe, and Y. Ono, "Pulse Corona-Induced Plasma Chemical Process for $DeNO_X$, $DeSO_X$, and Mercury Vapour Control of Combustion Gas", 3rd Int. Conf. on Electrostatic Precipitation, Padova, Italy, 667-676, 1987.

19. Masuda, S., and Y. Wu, "Removal of NO_X by Corona Discharge Induced by Sharp Rising Nanosecond Pulsed Voltage", Inst. Phys. Conf. Ser. (Electrostatics '87), IOP Pub. Ltd., U.K., 1987, 249-254.

20. Masuda, S. and H. Nakao, "Control of NO_X by Positive and Negative Pulsed Corona Discharges", IEEE-IAS Trans., 26 (1990), 374-383.

21. Masuda, S., X.L. Tu, K. Sakakibara, S. Kitoh, and S. Saito, "Destruction of Gaseous Pollutants by Surface Induced Plasma Chemical Process - SPCP", IEEE-IAS Annual Conf. (1991), 770-746.

22. McFarlane, J. and J.C. Wren, "Modeling Electric Discharge Chemistry", AECL-10374, Atomic Energy of Canada Limited, Whiteshell Laboratories, 1991.

23. Matzing, H., "Chemical Kinetics of Flue Gas Cleaning by Electron Beam", Tech. Report KfK 4494, February 1989, Kemforshungszentran, Karlsruhe, 1989.

24. Mehandrjiev and Bekyarova, "Catalytic Neutralization of NO on a Carbon-supported Cobalt Oxide Catalyst", J. Colloid Interface Sci., 166 (1994), 476-480.

25. Mizuno, A., J.S. Clements, and R.H. Davis, "A Method for the Removal of Sulfur Dioxide for Exhaust Gas Utilizing Pulsed Streamer for Electron Energization", IEEE Transactions on Industry Applications, IA-22 (1986), 516-522.

26. Mizuno, A., K. Simizu, A. Chakrabarti, L. Dascalescu, and S. Furuta, "NO_X Removal Process Using Pulsed Discharge Plasma", IEEE-Industry Applications Society, 1993, 1977.

27. Morrow, R., "Theory of Negative Corona in Oxygen", Physical Review A, 32 (1985), 1799-1809.

28. Mukkavilli, S., C.K. Lee, K. Varghese, and L.L. Tavlarides, "Modeling of the Electrostatic Corona Discharge Reactor", IEEE Trans Plasma Sci., 16 (1988), 656-660.

29. Nasser, E., "Fundamentals of Gaseous Ionization and Plasma Electronics", Wiley-Interscience, New York, 197 1.

30. Ohkubo. T., S. Kanazawa, Y. Nomoto, J.S. Chant. and T. Adachi, "NO_X Removal by a Pipe with Nozzle-Plate Electrode Corona Discharge System", IEEE Trans. Ind. Appl., 30 (1994), 856-860.

31. Peyrous, R., P. Pignolet, and B. Held, "Kinetic Simulation of Gaseous Species created by an Electrical Discharge in Dry or Humid Oxygen", J. Phys. D.: Appl. Phys. 22 (1989), 1658-1667.

32. Seinfeld, J.H., "Atmospheric Chemistry and Physics of Air Pollution", John Wiley and Sons, New York, 1986.

33. Tas, M.A., "Plasma-Induced Catalysis, A Feasibility Study and Fundamentals", Thesis Technische Universiteit Eindhoven, Netherlands, CIP-DATA Koninklijke Bibliotheek, Den Haag. 1995.

34. Tokunga, O., and Suzuki, N., "Radiation Chemical Reactions in NO_X and SO_2 Removal from Flue Gas", Radiat. Phys. Chem., 24, 145-165.

35. Wren, J.C., "Boltzman Calculations for Electrical Gas Discharge Systems I. Theory and Principles of the Boltzman Equation and Calculations Results for N_2", RC-248-1, Atomic Energy of Canada Limited, Whitehead Laboratories, 1989.

36. Zeldovich, Y.B., Acta Physiochem URSS, 21 (1946), 656.

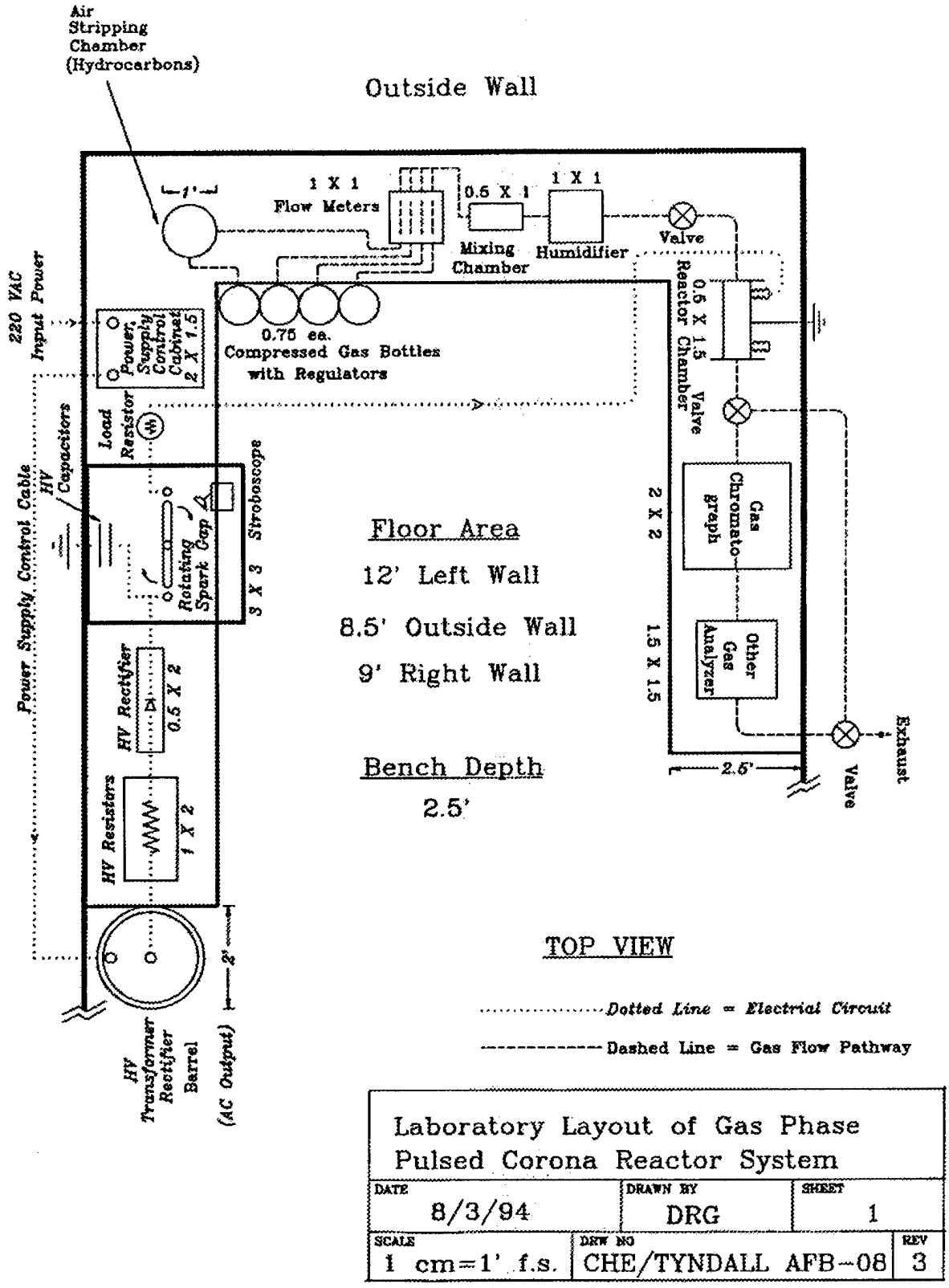

Figure 1. Laboratory Layout of Gas-Phase Pulsed Corona Reactor System

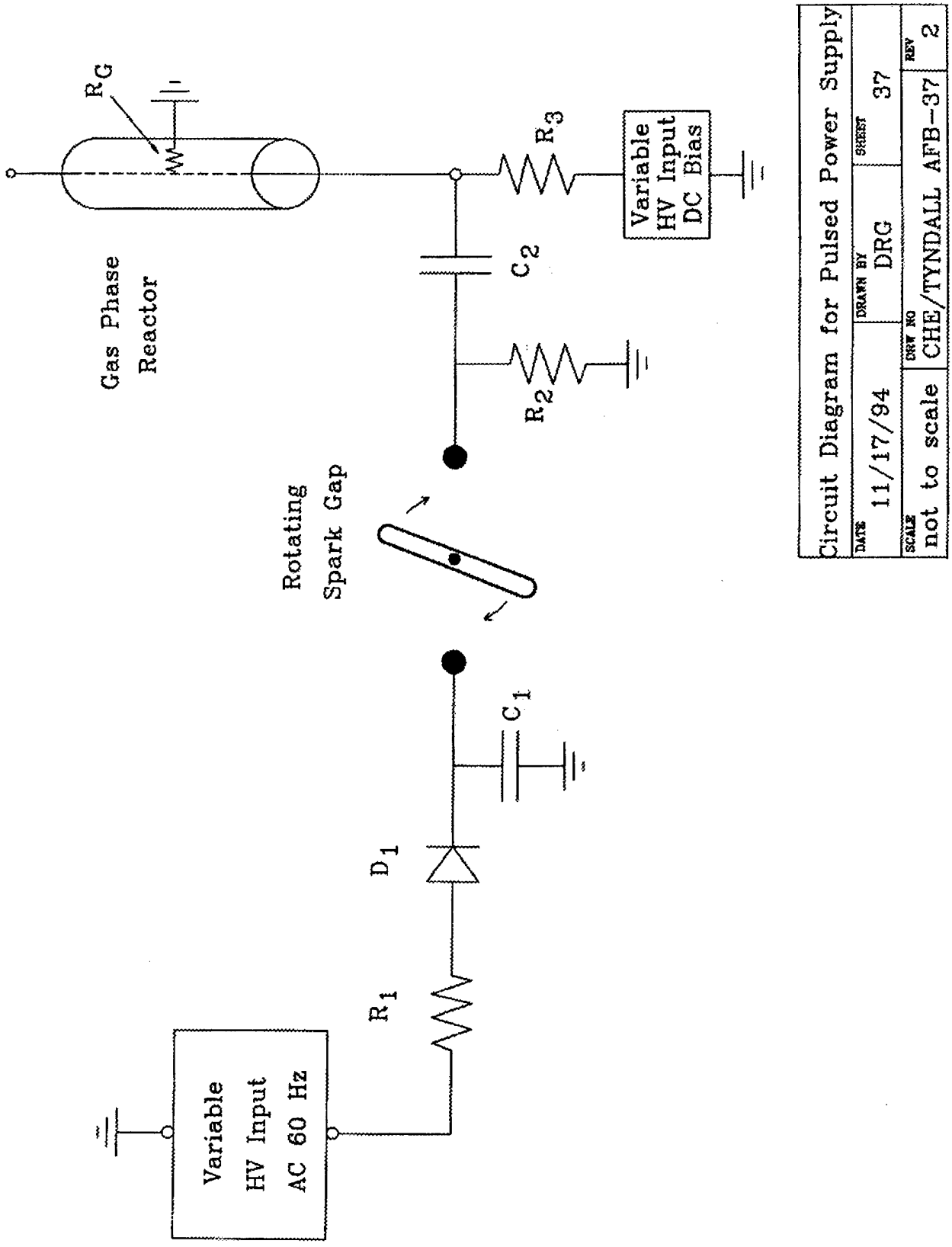

Figure 2. Circuit Diagram for Pulsed Power Supply

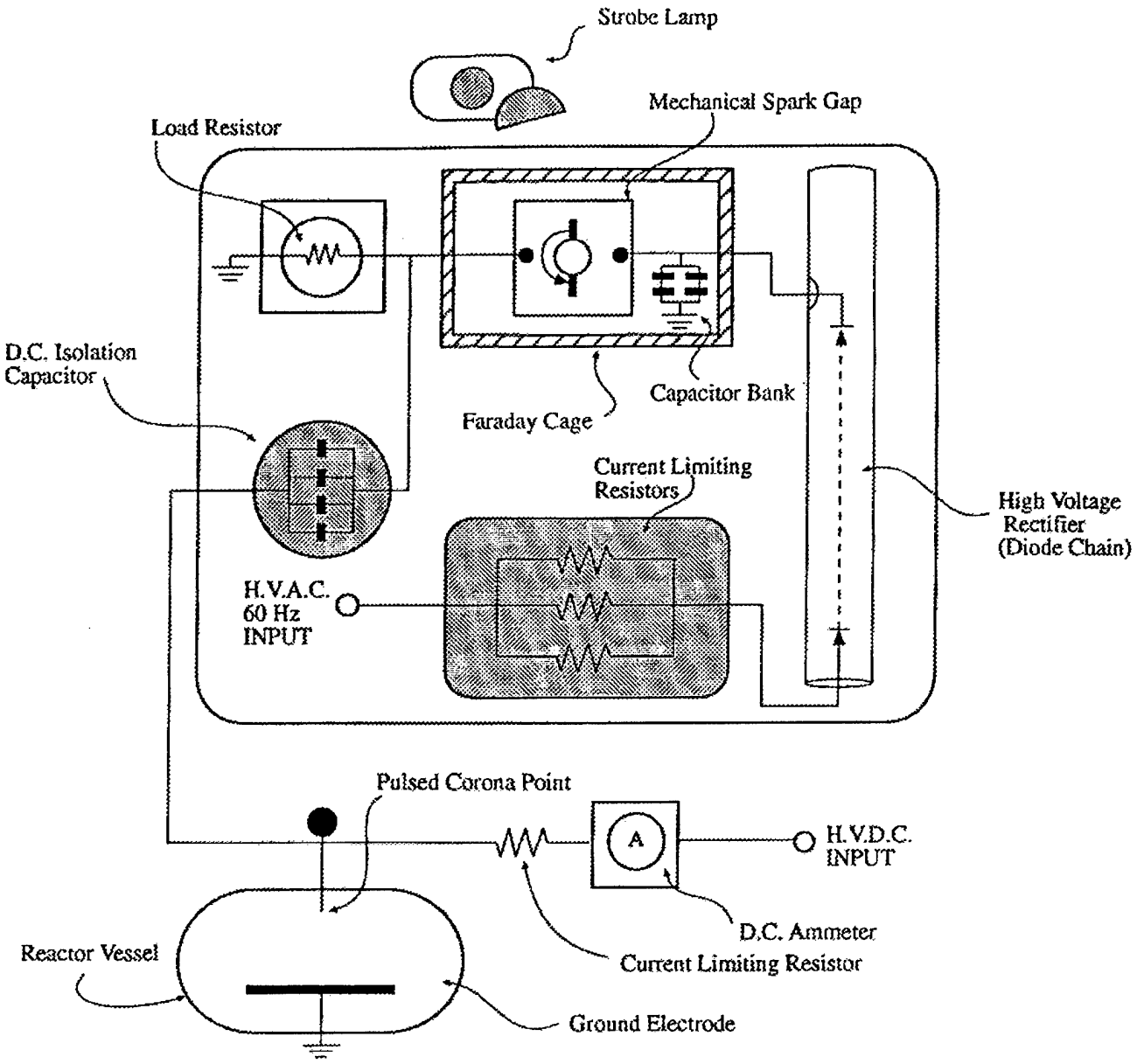

Figure 3. Pulsed Power Supply Schematic

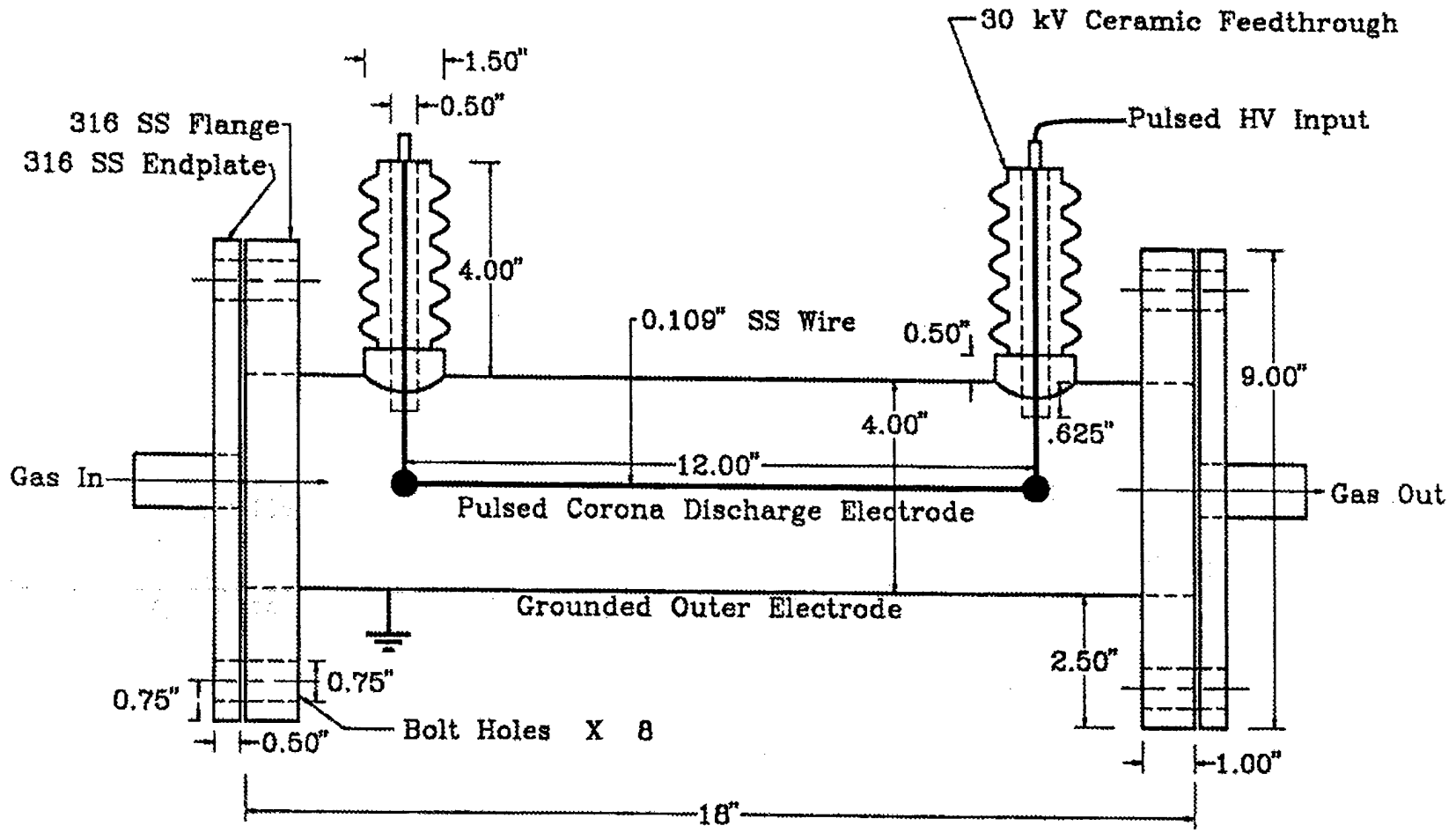

SIDE VIEW

GAS-PHASE PULSED CORONA REACTOR			
DATE 7/5/94	DRAWN BY DRG	SHEET 2	
SCALE 3/8" = 1" f.s	DRW NO CHE/TYNDALL AFB-02	REV 6	

Figure 4. Gas-Phase Pulsed Corona Reactor

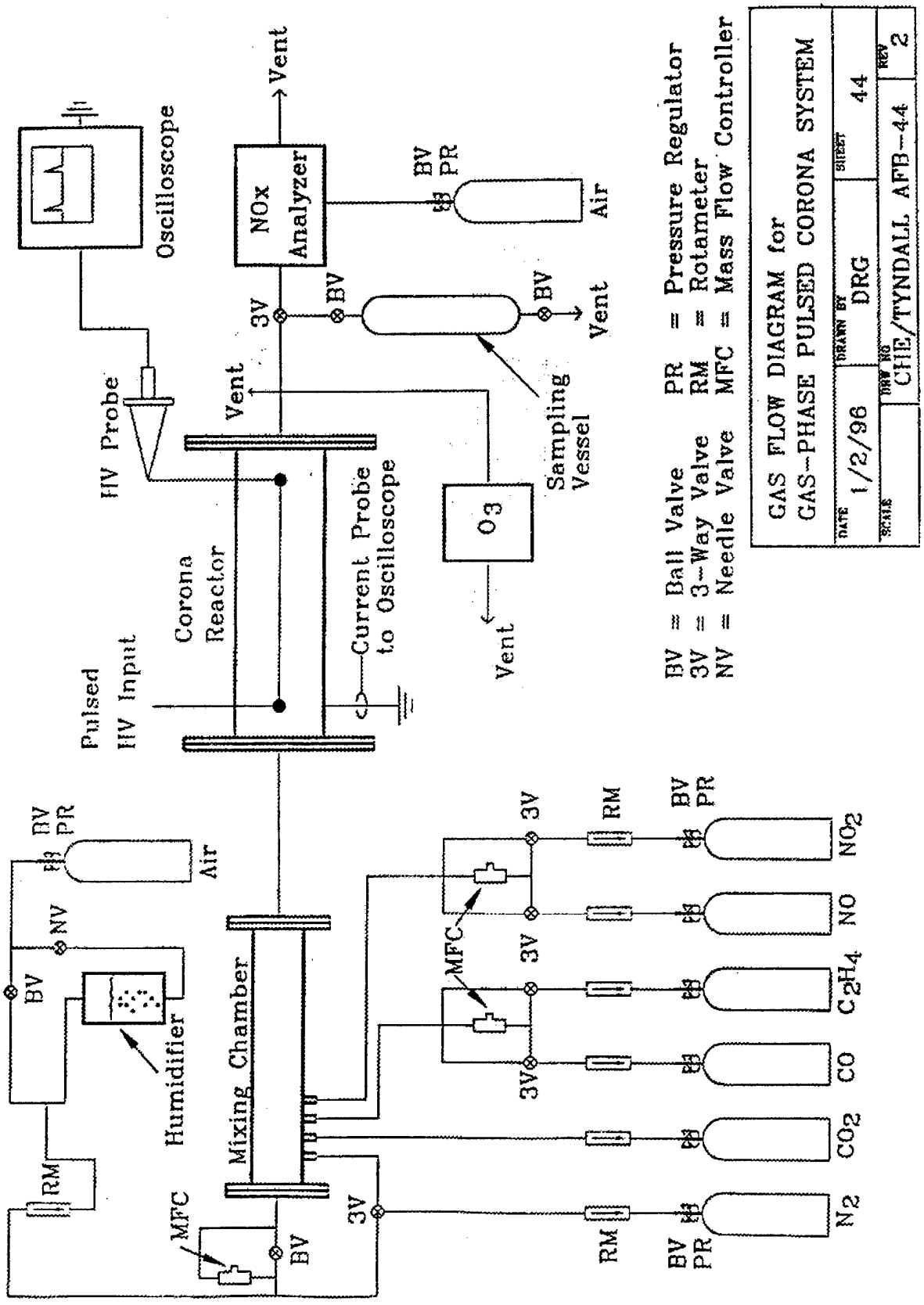

Figure 5. Gas Flow Diagram

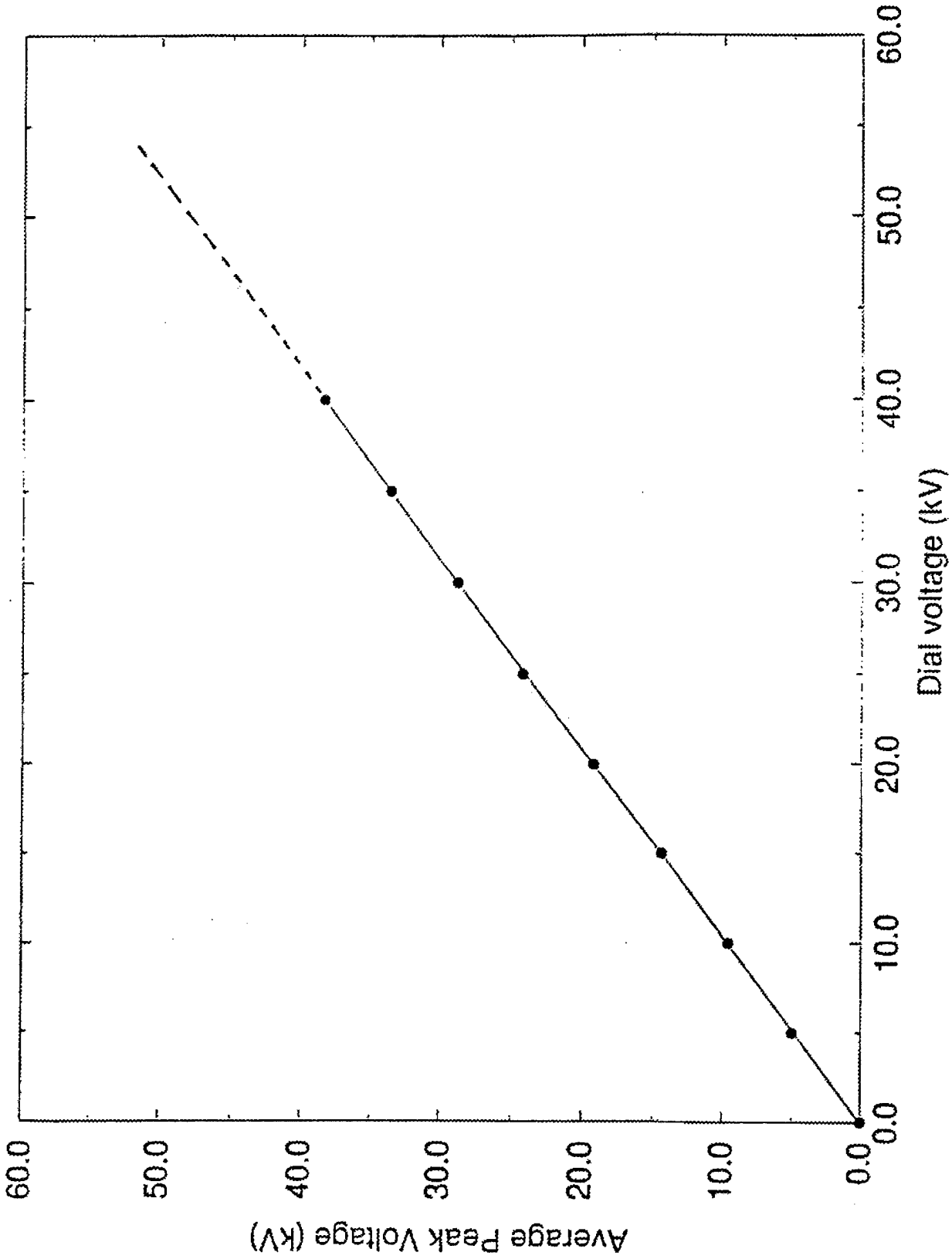

Figure 6. Power Supply Calibration

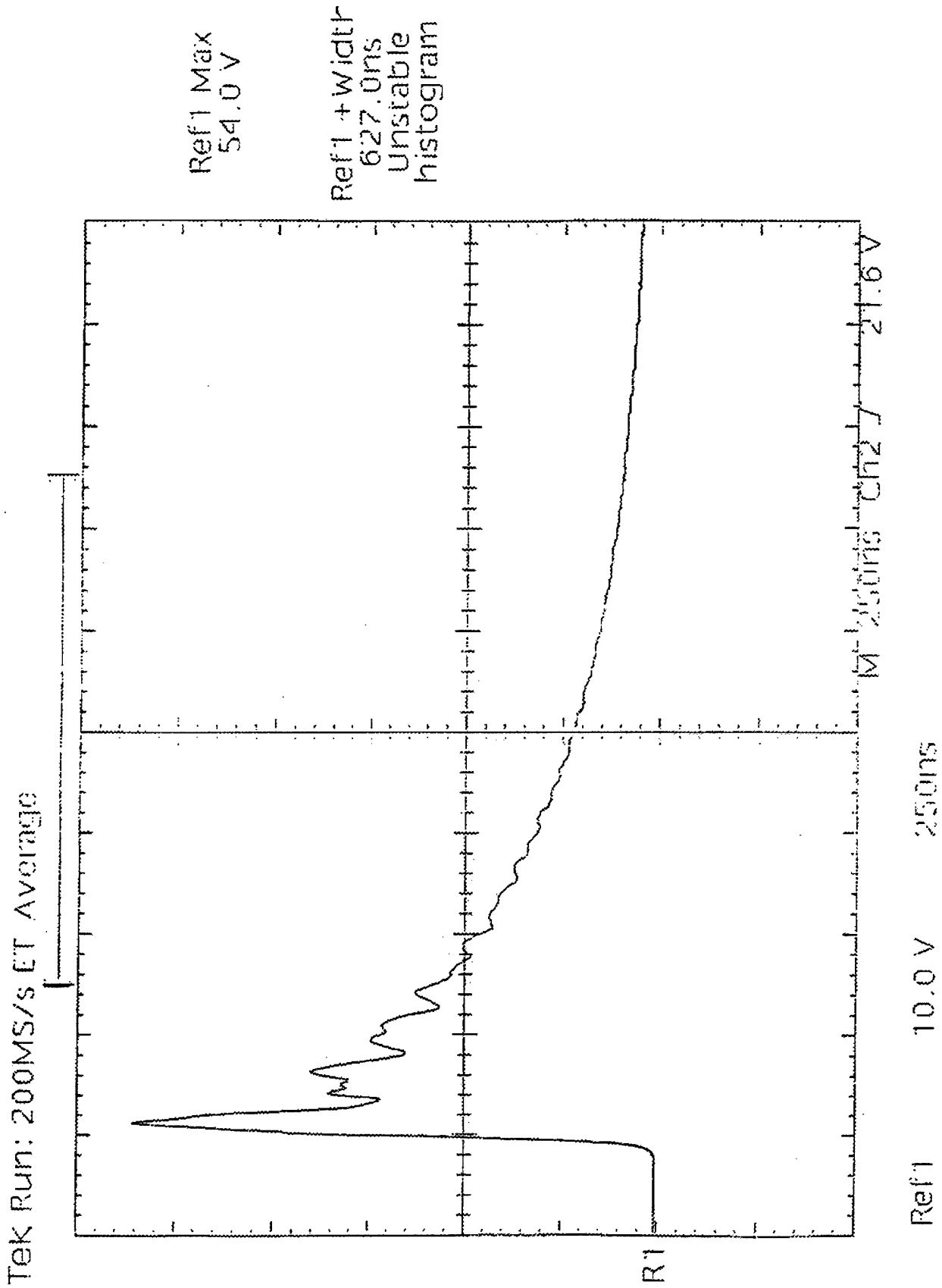

Figure 7. Voltage Waveform for 40 kV Dial at Reactor Outlet

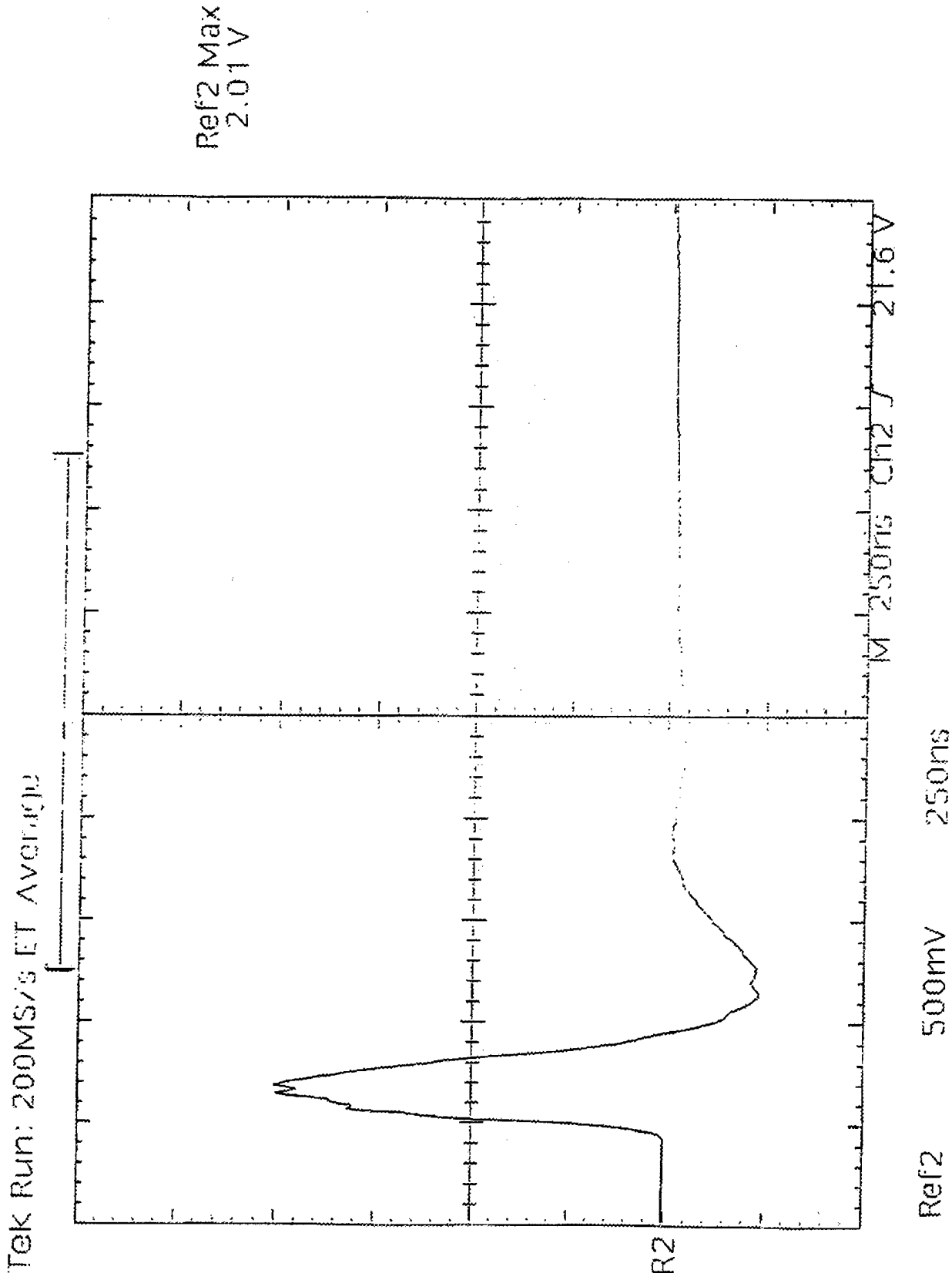

Figure 8. Current Waveform for 40 kV Dial at Reactor Outlet

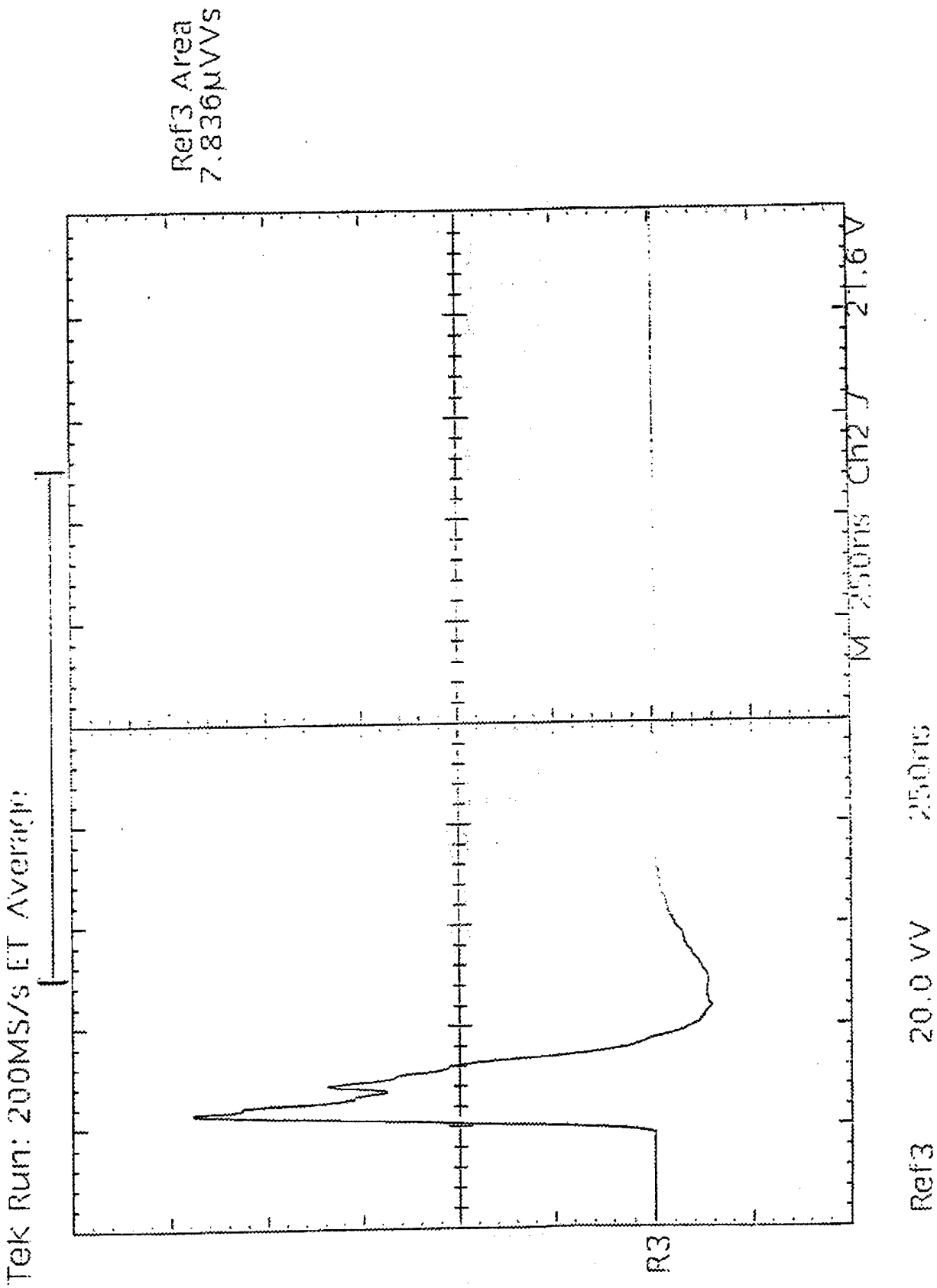

Figure 9. Integrated Power for 40 kV Dial at Reactor Outlet

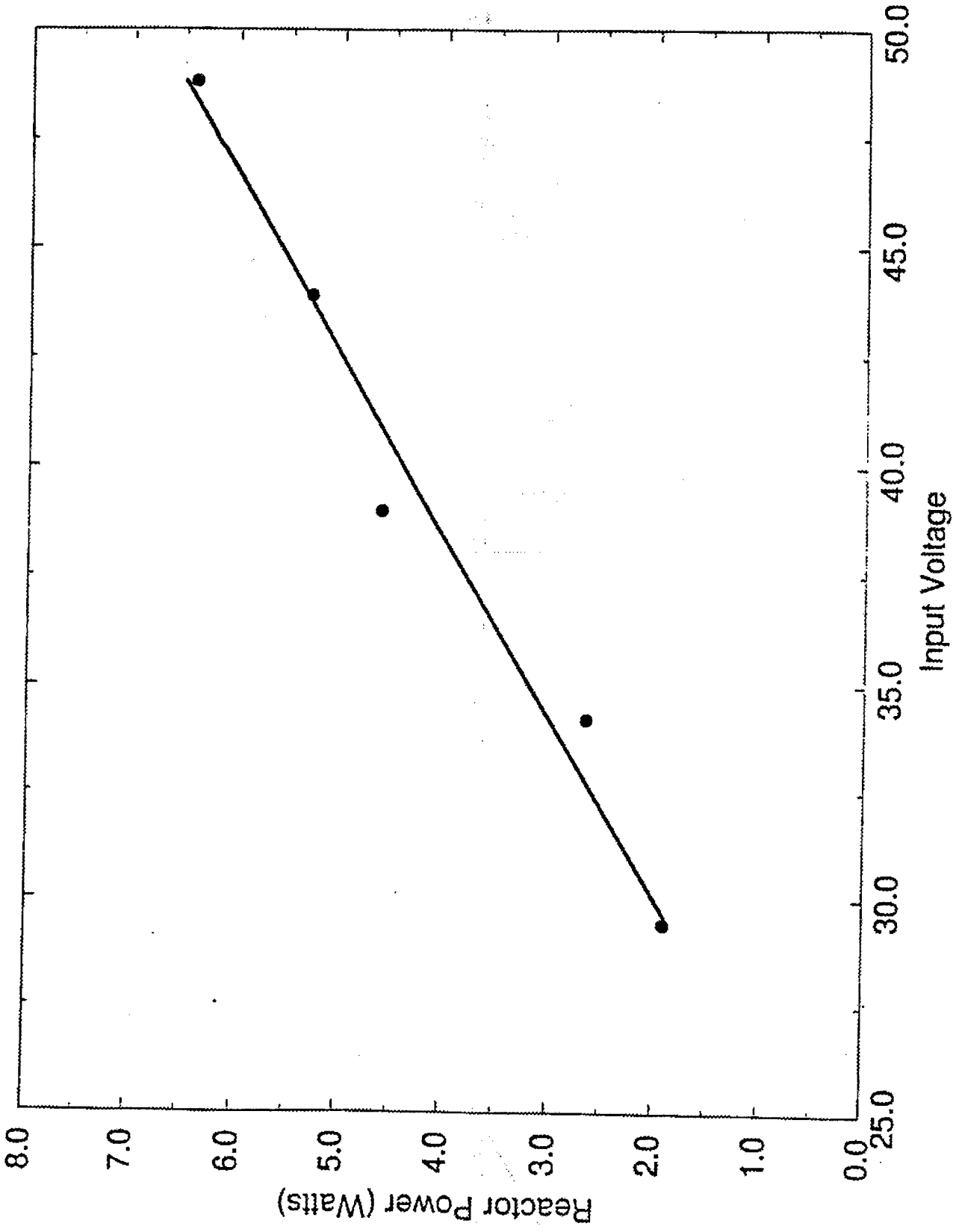

Figure 10. Reactor Power verses Input Voltage

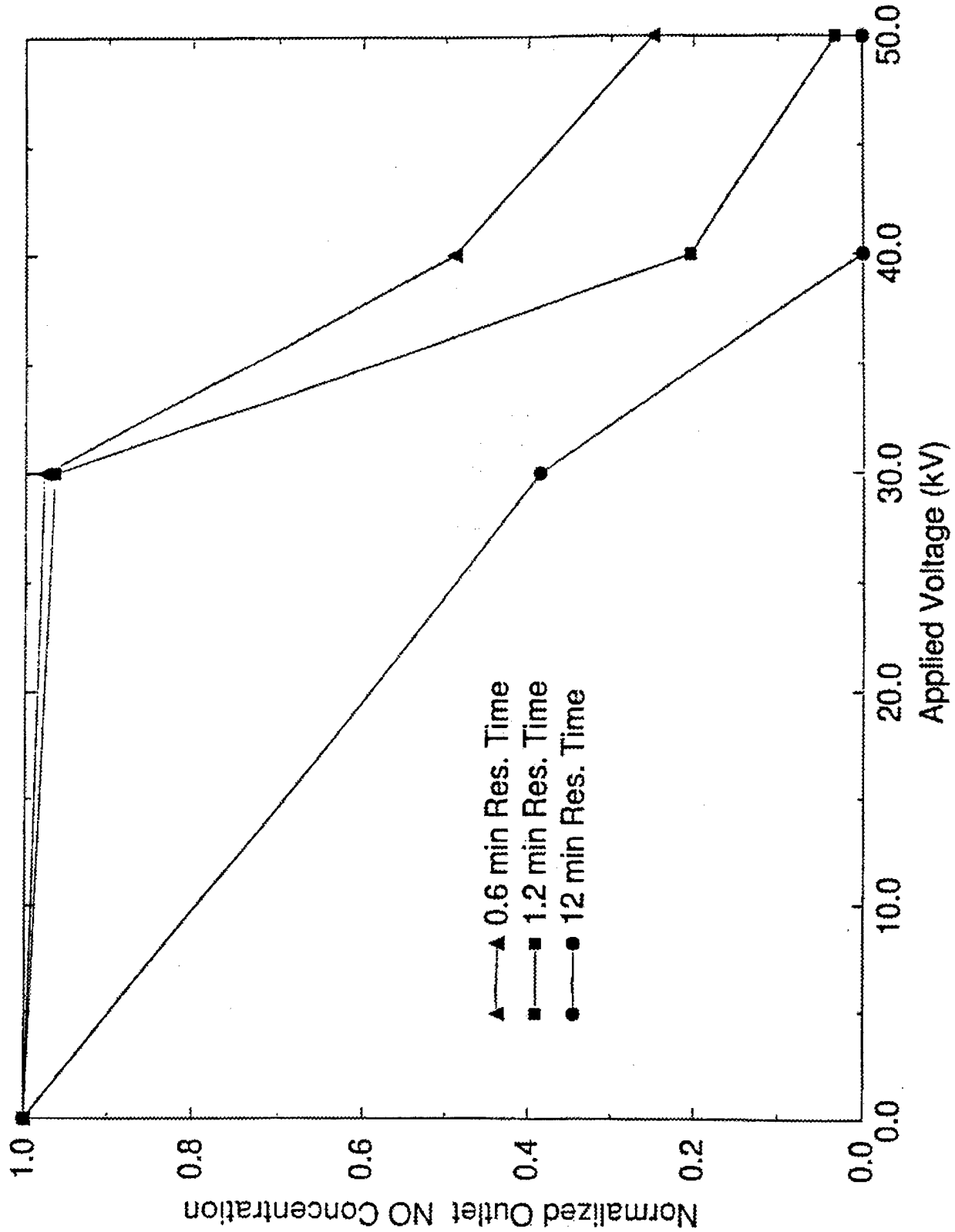

Figure 11. Effect of Voltage on NO Removal from Dry Air
(Initial Concentration of NO 150 ppm, H_2O Absent, Ethylene Absent)

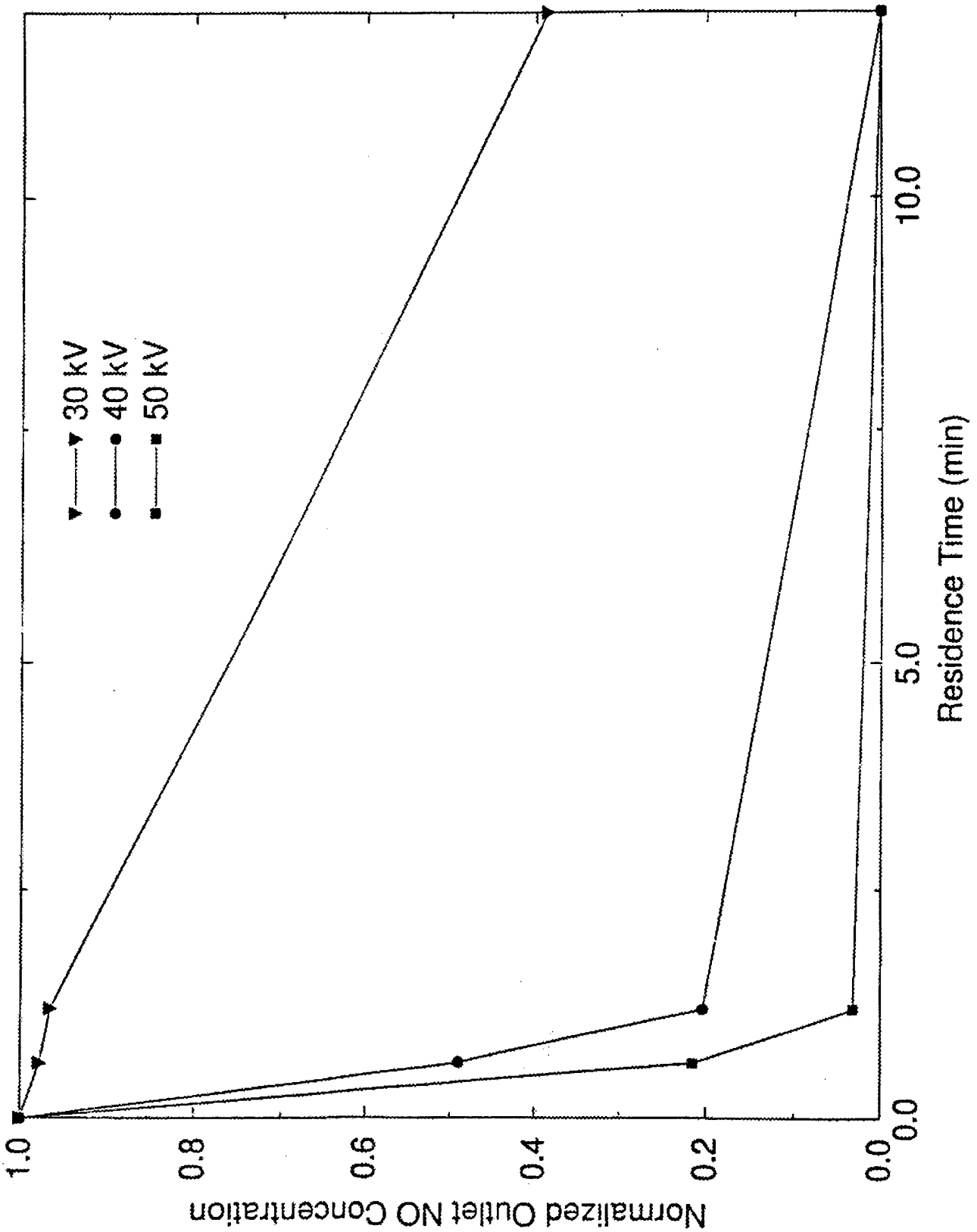

Figure 12. Effect of Residence Time on NO Removal from Dry Air
(Initial Concentration of NO 150 ppm, H_2O Absent, Ethylene Absent)

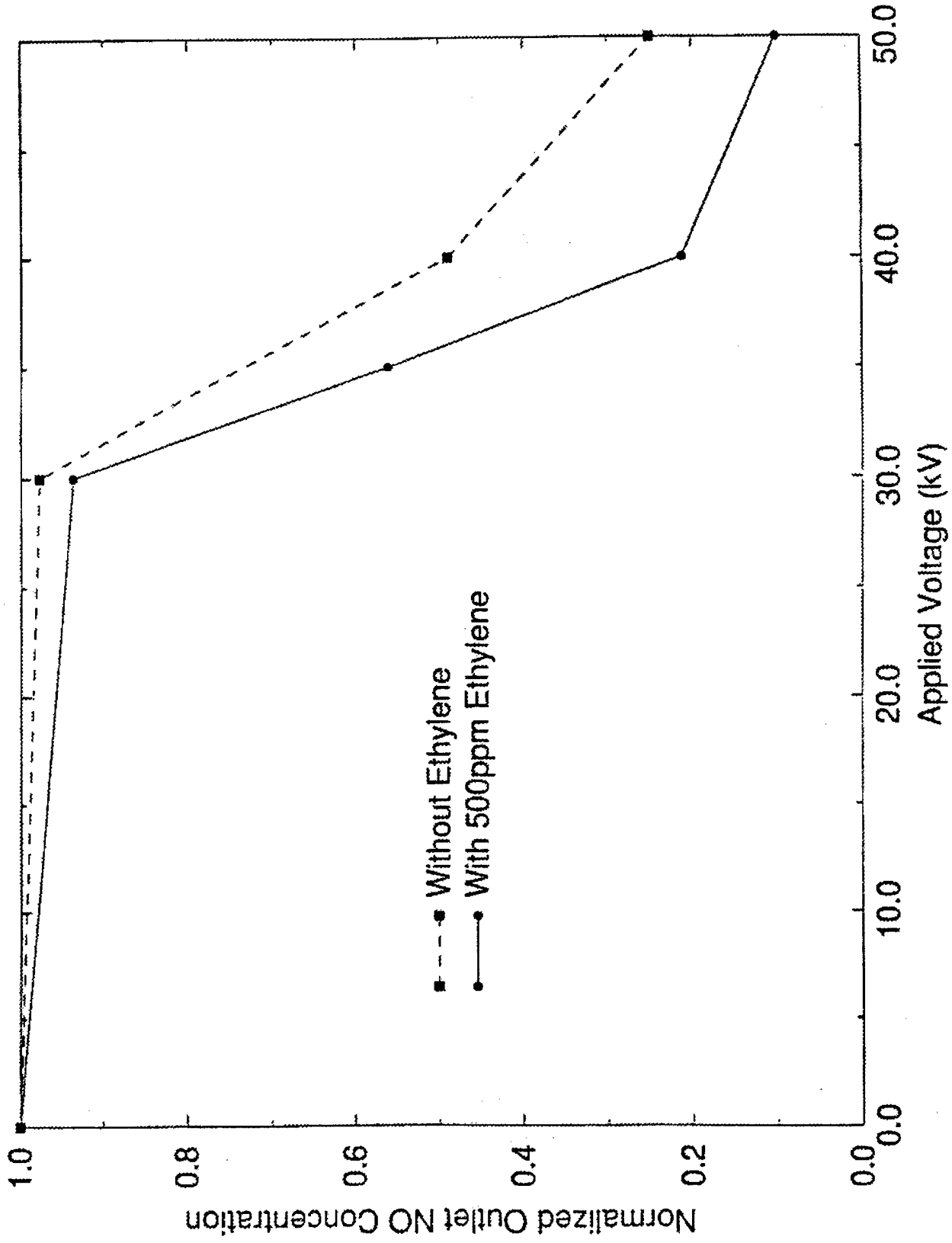

Figure 13. Effect of Voltage on NO Removal With and Without Ethylene
(Flow Rate 10,000 SCCM, NO Conc. 170 ppm, Water Absent, Ethylene Absent)

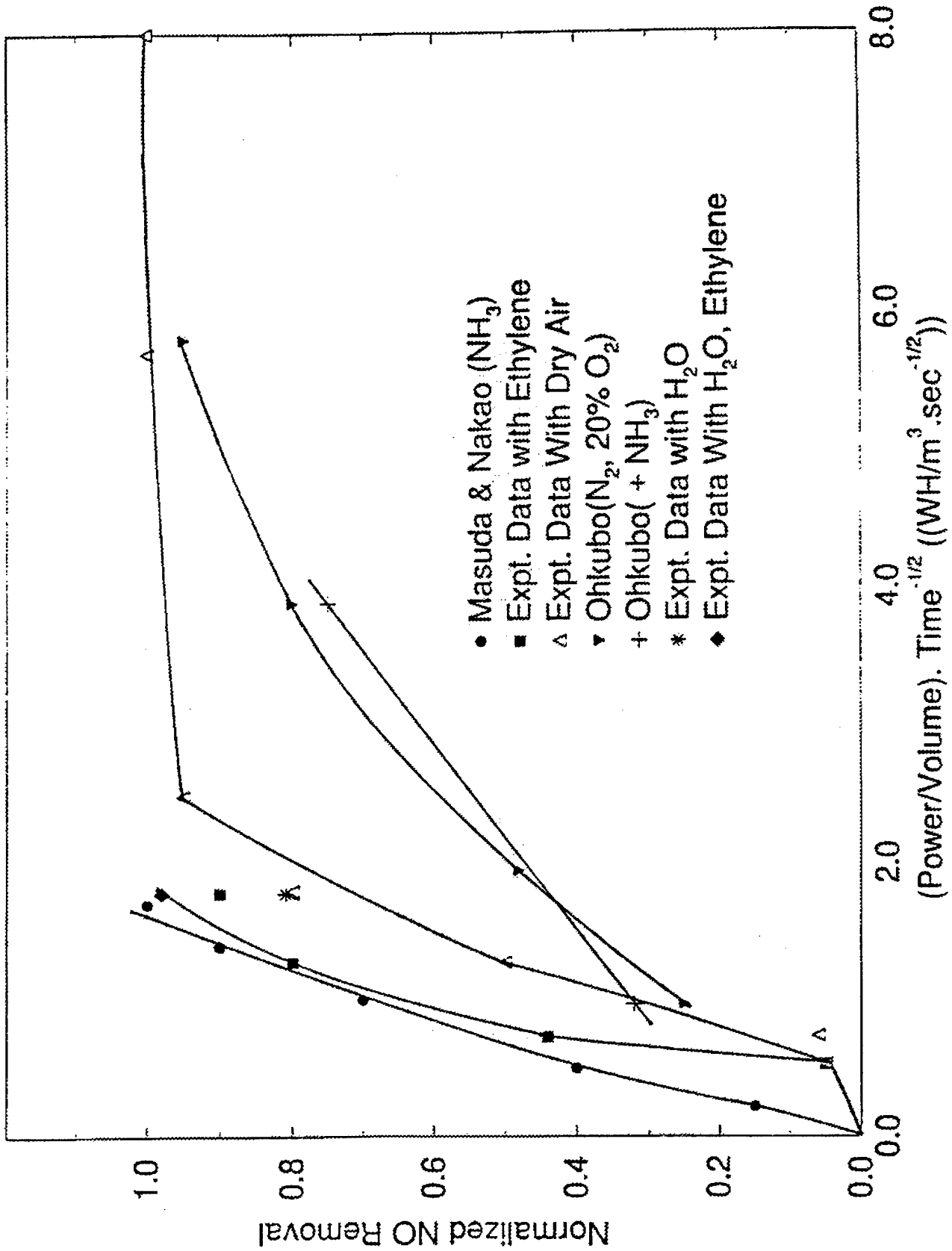

Figure 14. Summary of NO Removal for Low Concentration Data

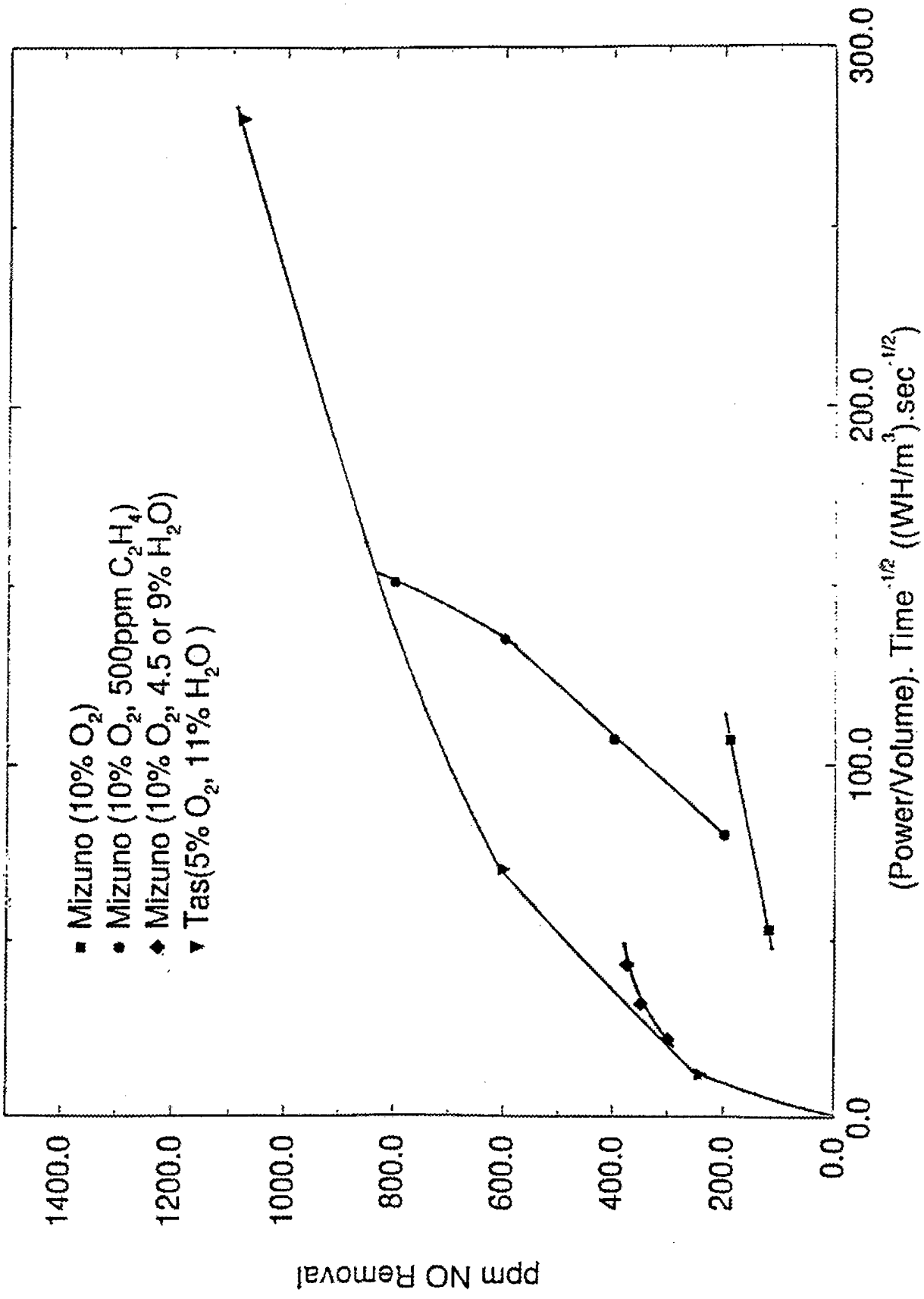

Figure 15. Summary of NO Removal for High Concentration Data

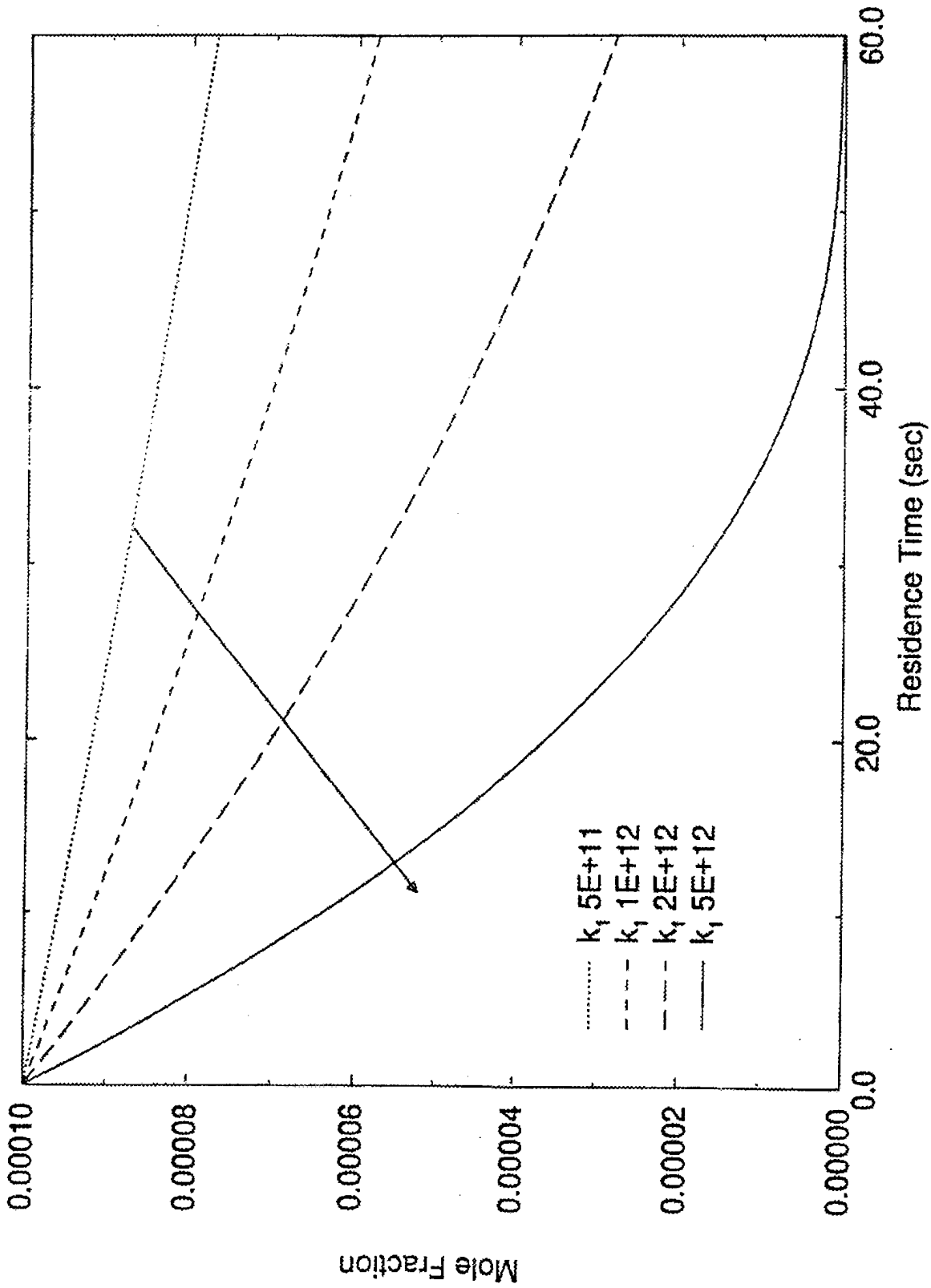

Figure 16. Effect of Electron-N_2 Reaction Rate Constant on Model Results for NO Removal in Dry Air (Dry System, Different Kinetic Constants, No Ethylene)

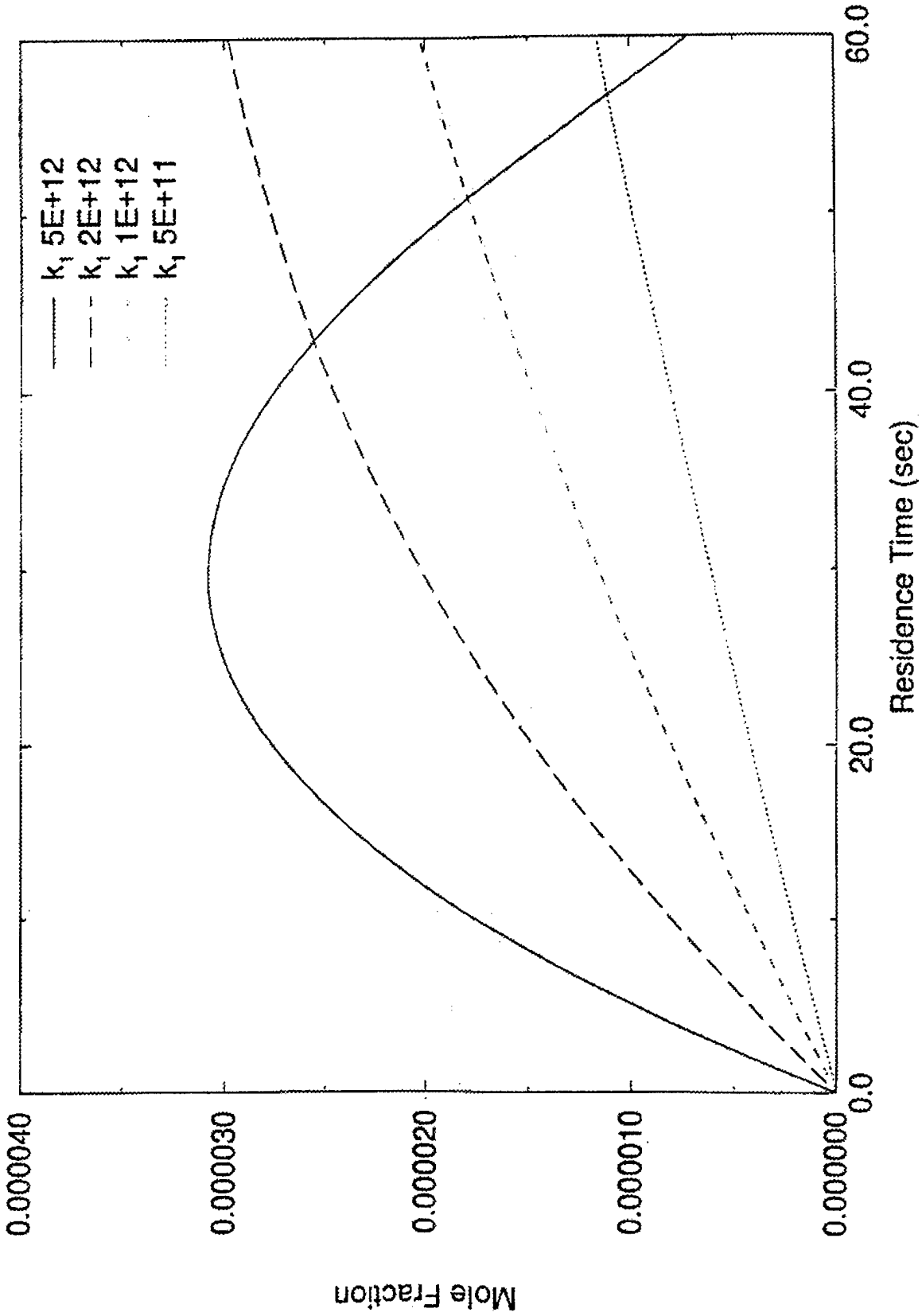

Figure 17. Effect of Electron-N_2 Reaction Rate Constants on the Model Results for NO_2 Removal in Dry Air (No Ethylene)

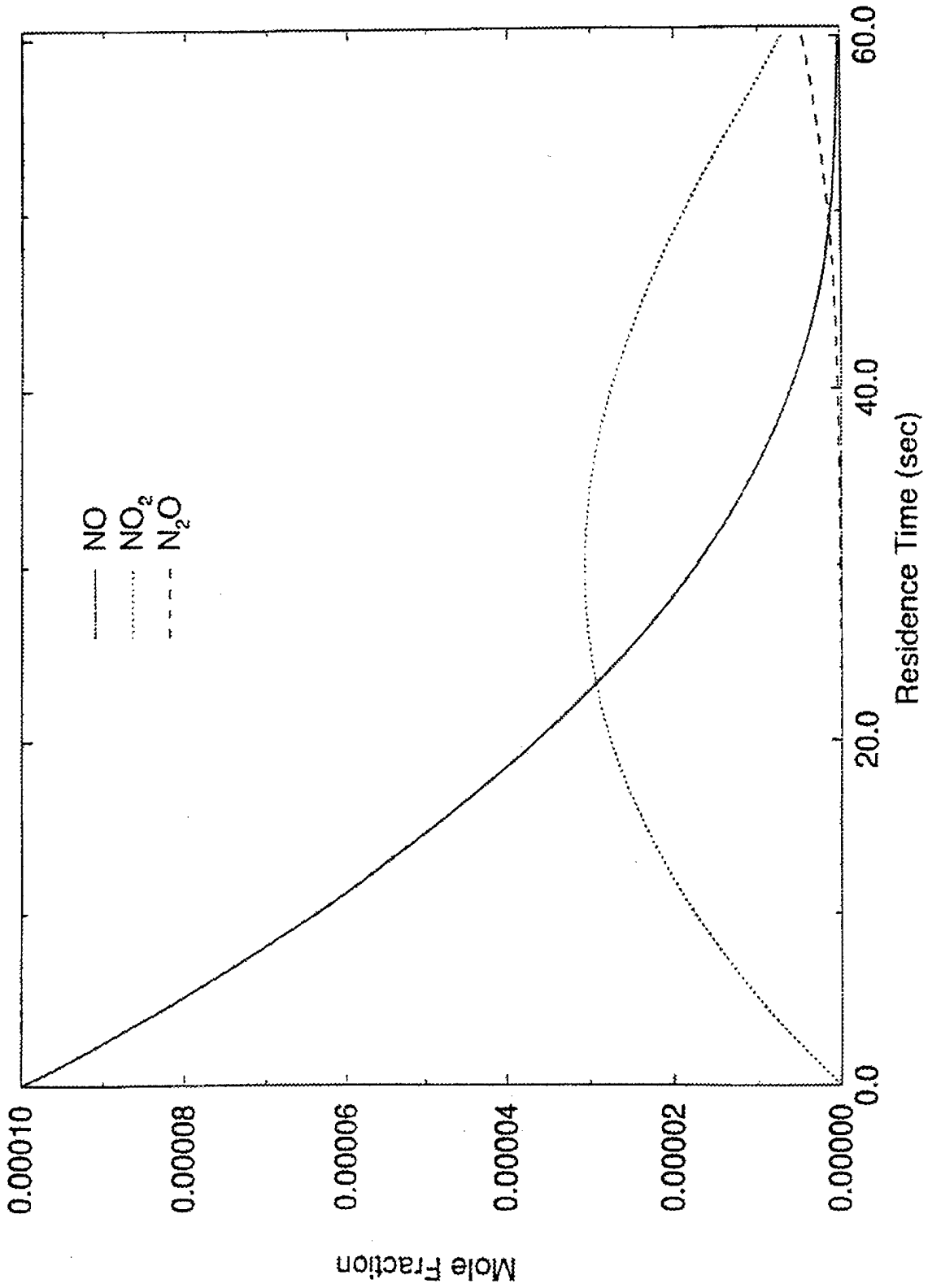

Figure 18. Concentration Profiles for NO Removal, NO_2 Production, and N_2O Production in Dry Air (k_1 = 5E+12)

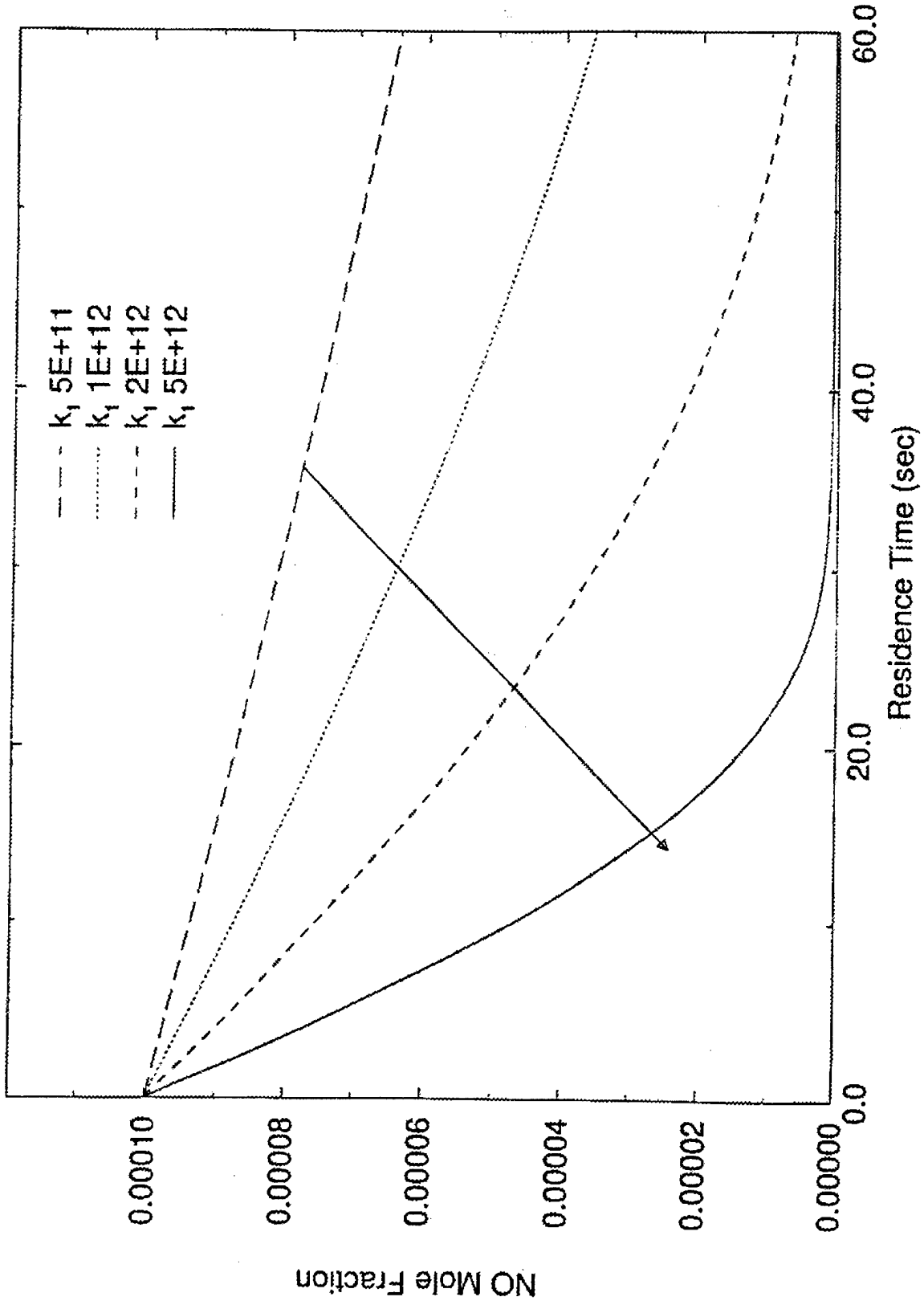

Figure 19. Concentration Profiles for NO Removal for Various Electron-N_2 Reaction Rate Constants (1% Water)

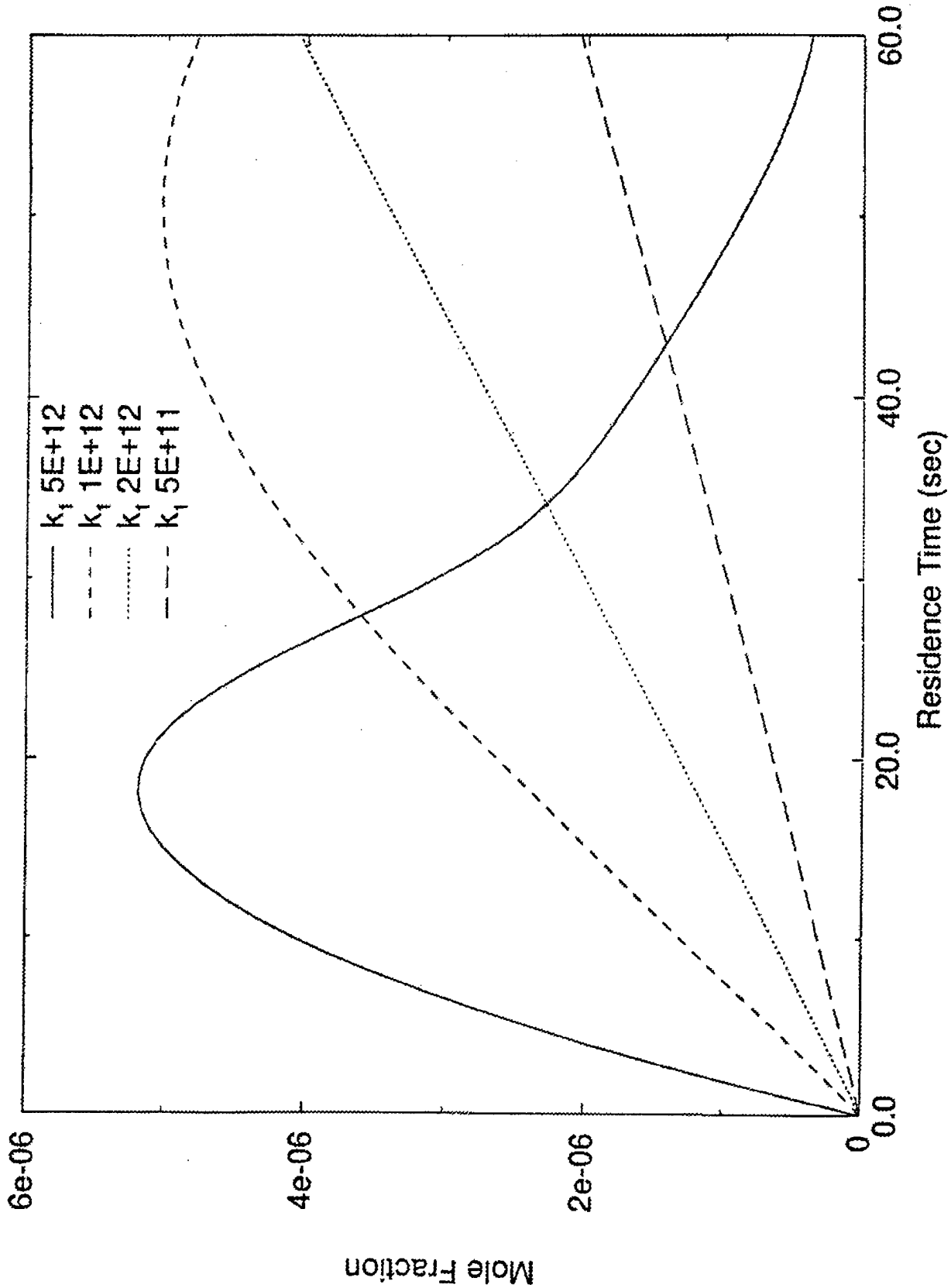

Figure 20. Concentration Profiles for NO_2 in Humid Air for Various Reaction Rate Constants (1% Water)

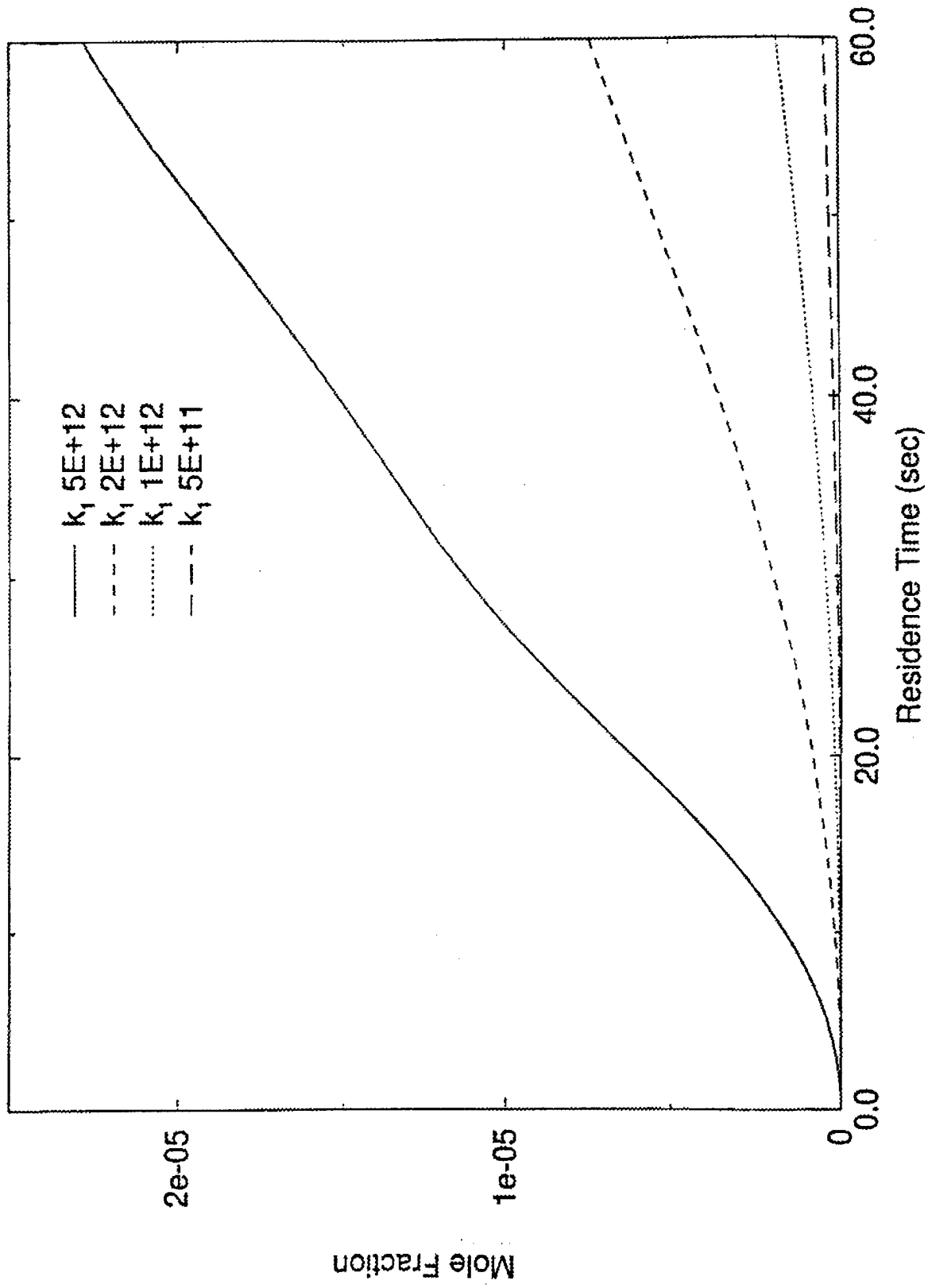

Figure 21. Concentration Profiles for HNO_3 in Humid Air for Various Reaction Rate Constants (1% Water)

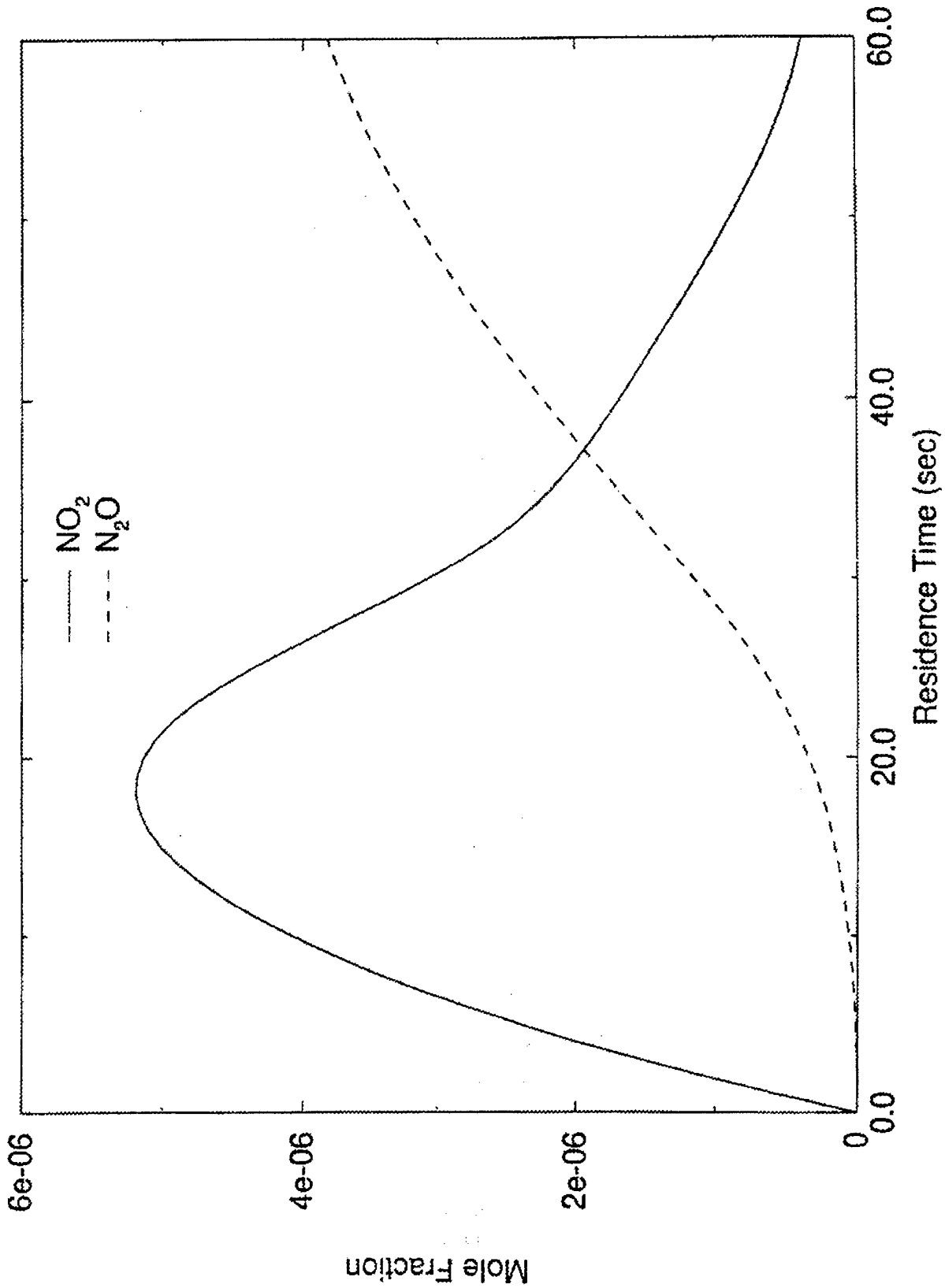

Figure 22. Concentration Profiles for NO_2 and N_2O in Humid Air
(1% Water, k_1 = 5E+12, No Ethylene)

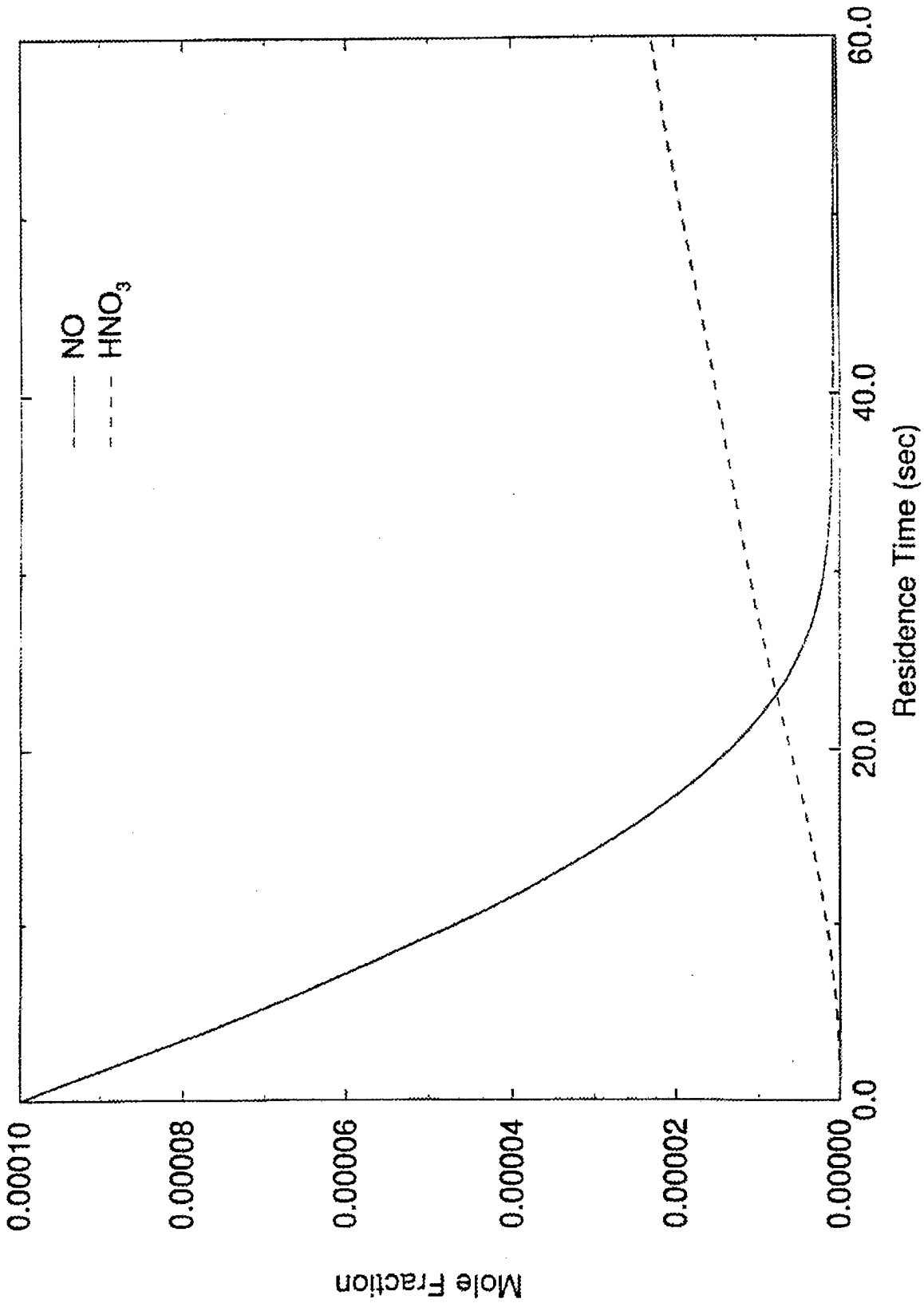

Figure 23. Concentration Profiles of NO and HNO_3 in Humid Air
(1% Water, k1 = 5E+12, No Ethylene)

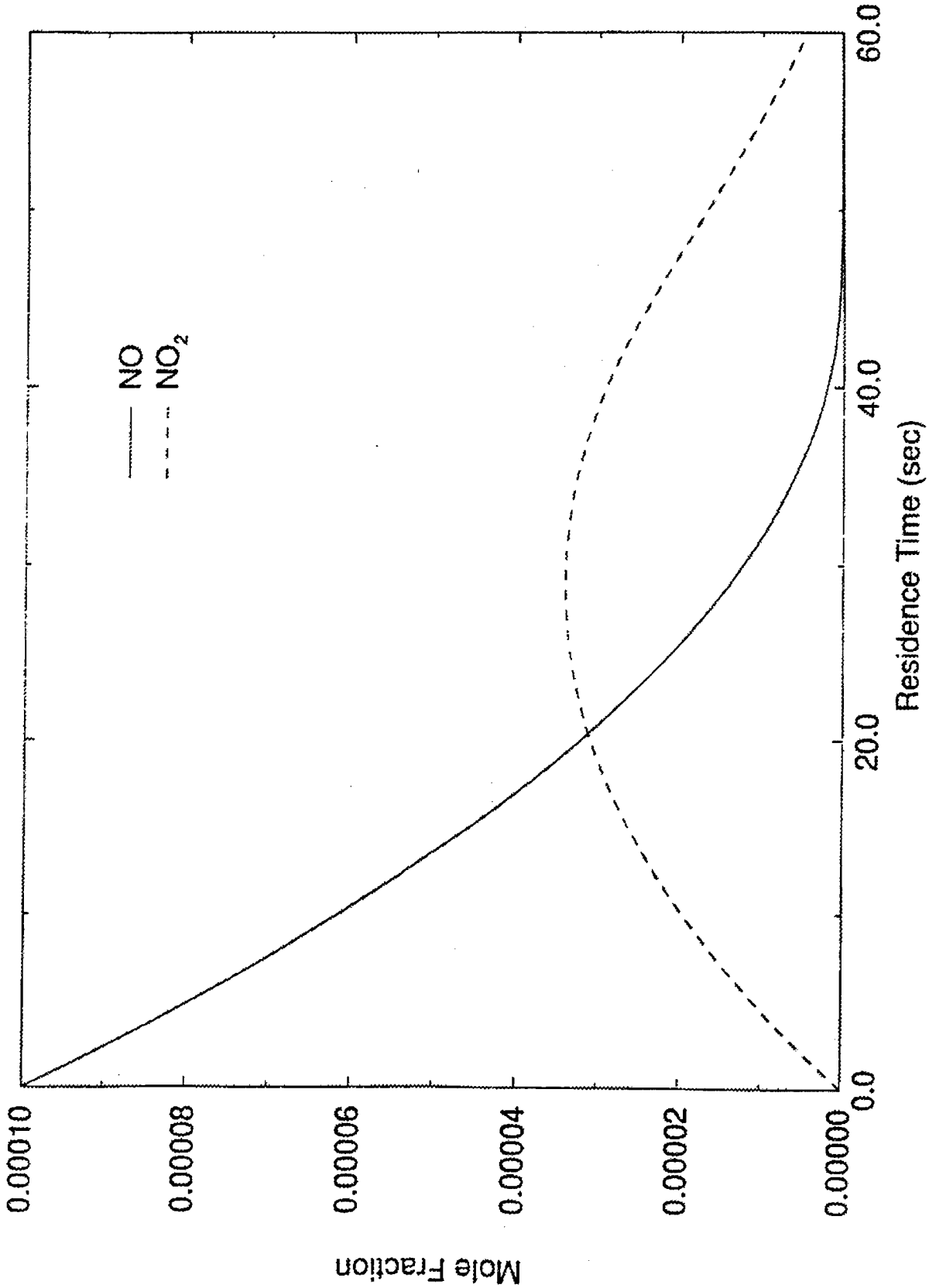

Figure 24. Concentration Profile of NO and NO_2 in Dry Air With Ethylene (500 ppm Ethylene, $k_1 = 5E+12$)

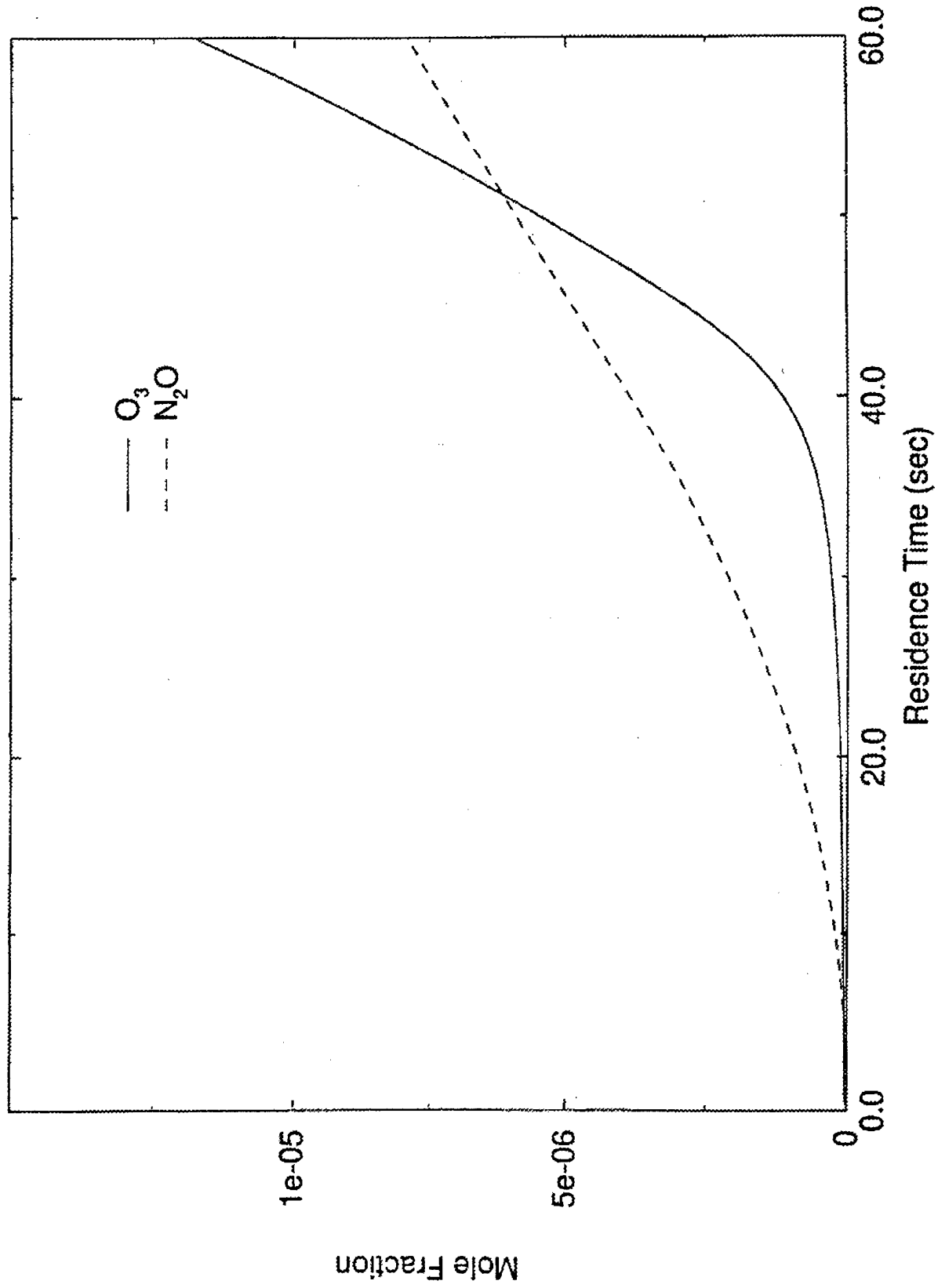

Figure 25. Concentration Profiles of O_3 and N_2O in Dry Air With Ethylene
(500 ppm Ethylene, k_1 = 5E+12)

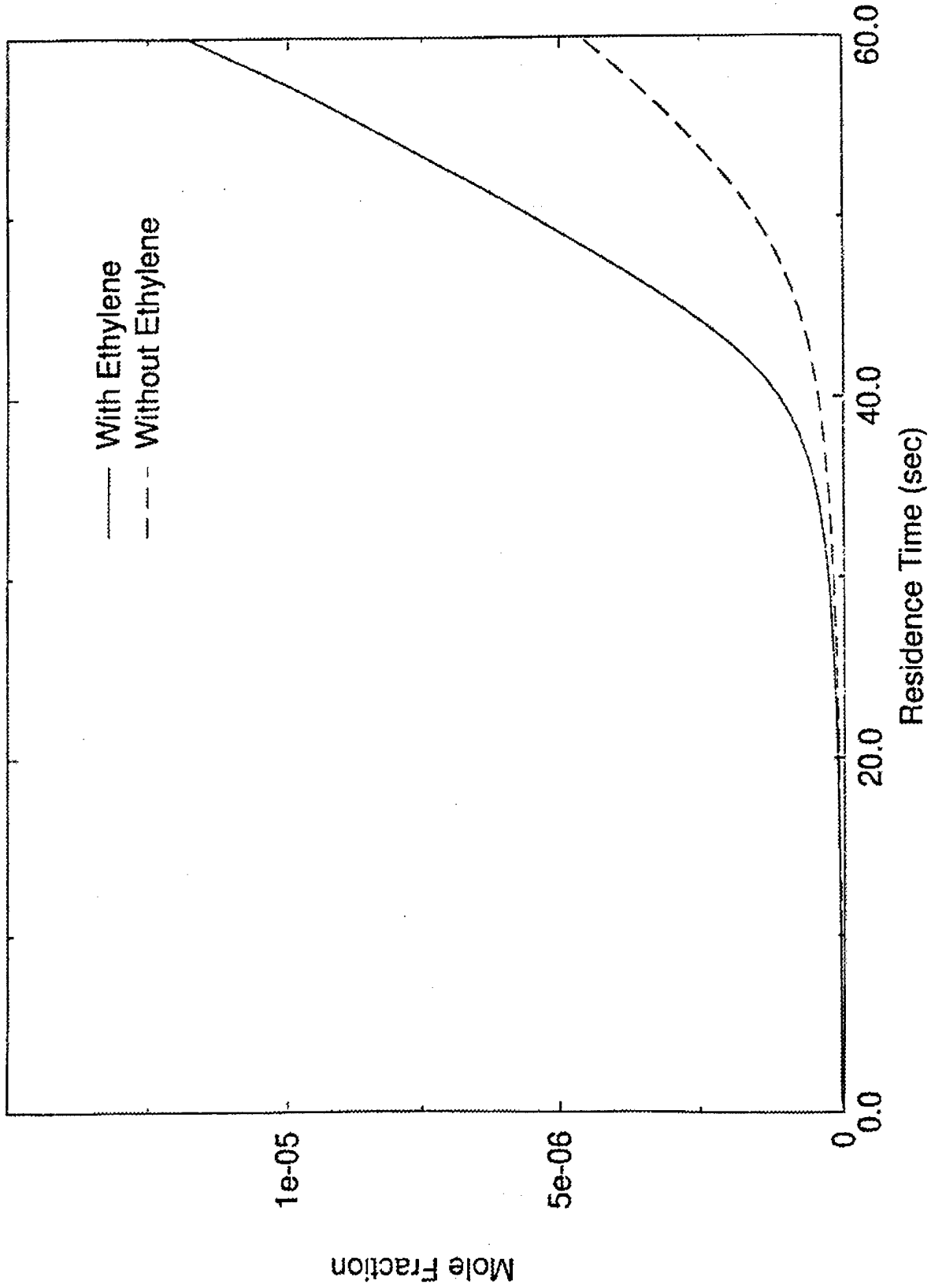

Figure 26. Production of O_3 in Dry Air With and Without Ethylene (k_1 = 5E+12)

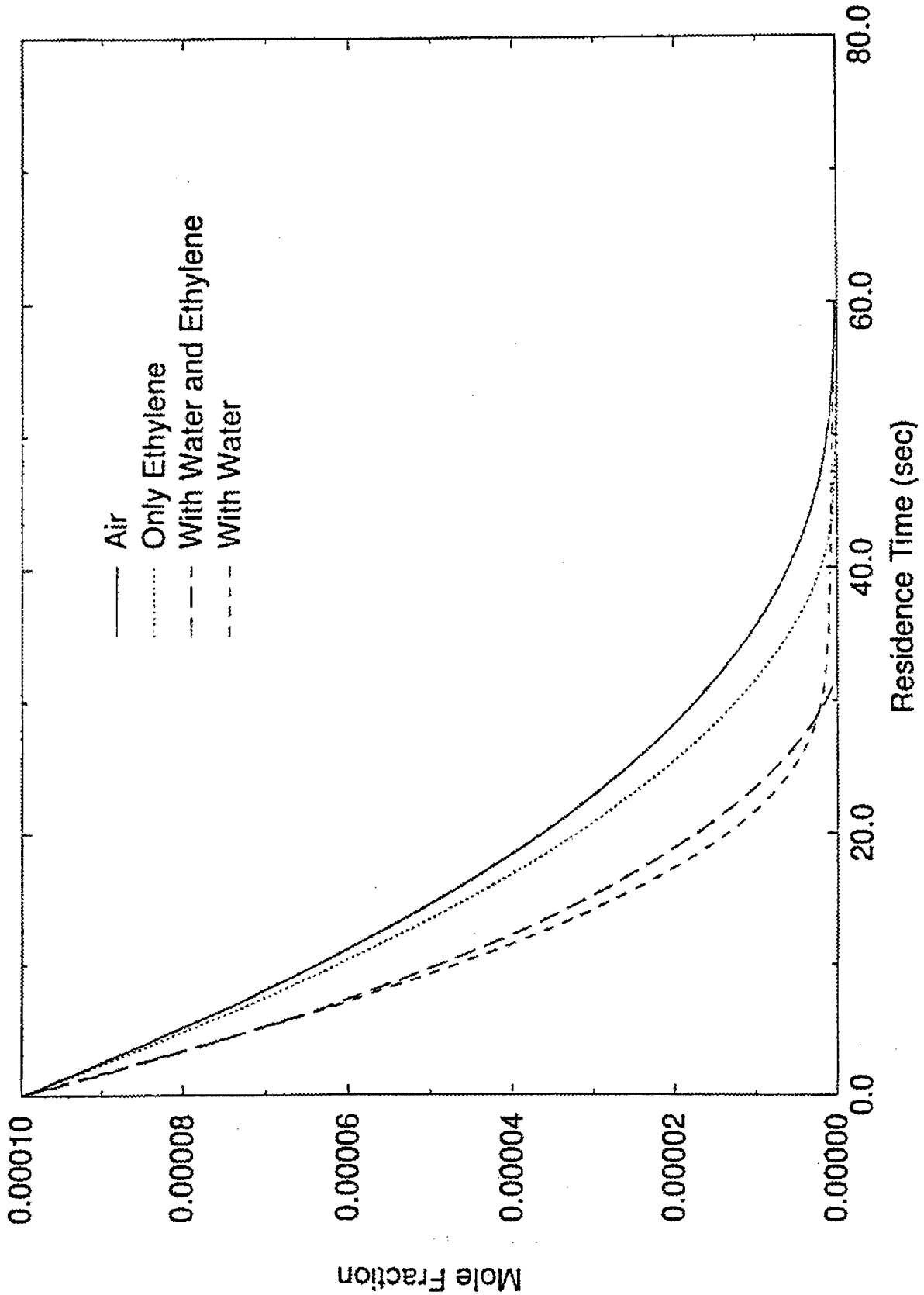

Figure 27. Summary of NO Removal for Dry Air, Dry Air with Ethylene, Wet Air and Wet Air with Ethylene (k_1 = 5E+12)

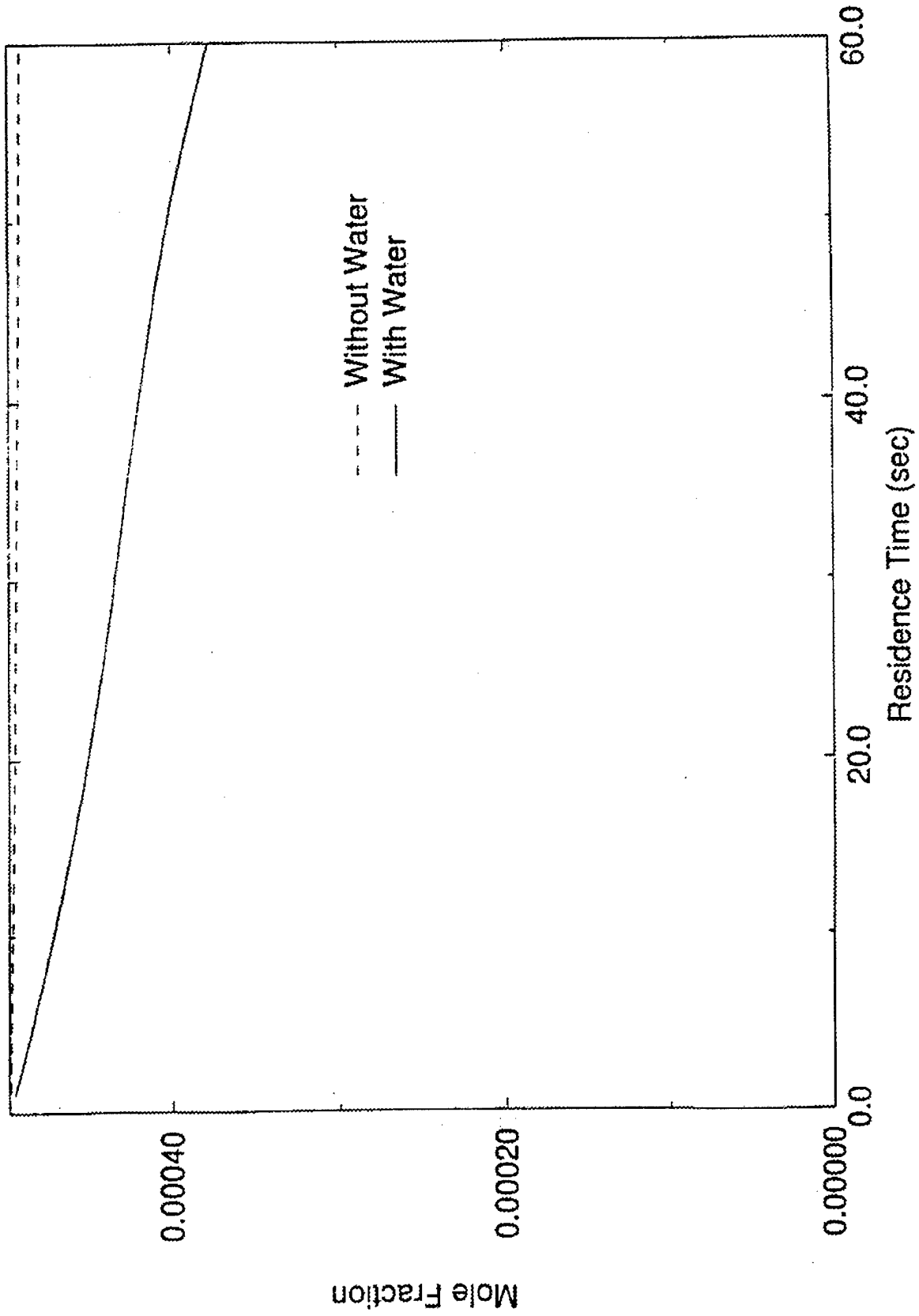

Figure 28. Ethylene Concentration Profiles in Wet and Dry Air
(k_1 = 5E+12)

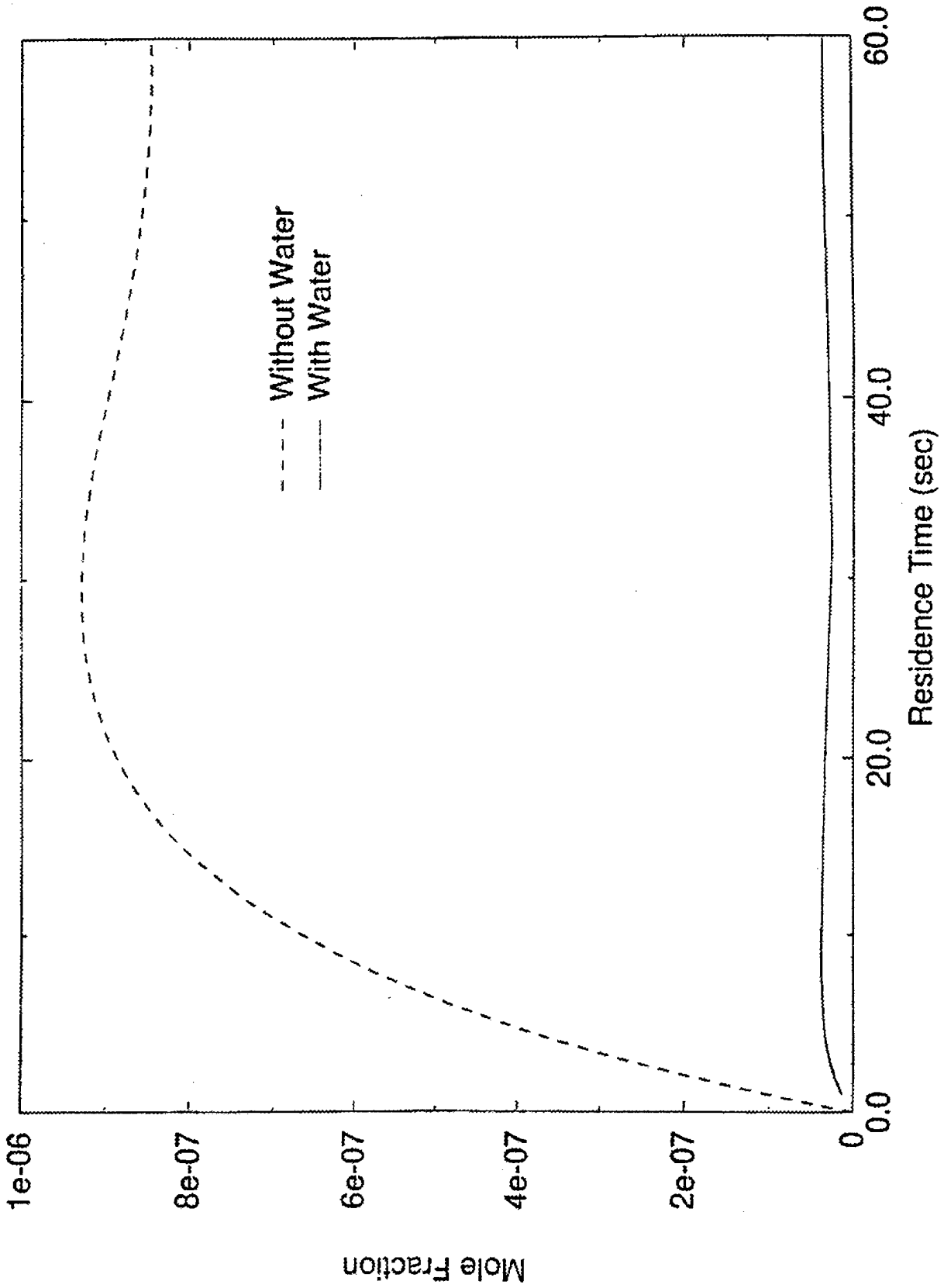

Figure 29. Formaldehyde Concentration Profiles
(k_1 = 5E+12)

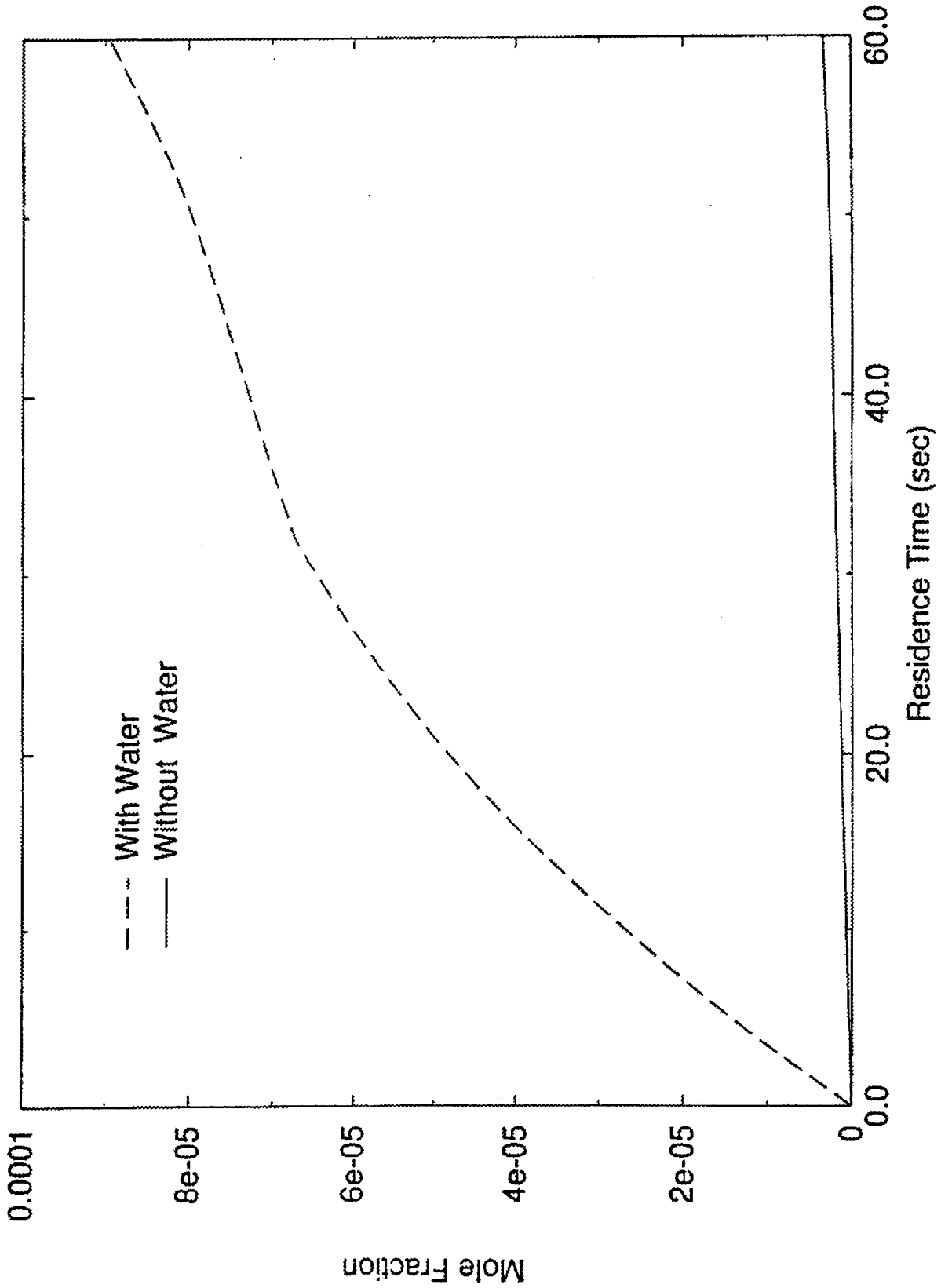

Figure 30. Glycolaldehyde Concentration Profiles
(k_t = 5E+12)

```
C This Program is used to call the ODE Solver and uses the conp.inp file,
C chem.inp files as input files.

C This program is for the mole fractions as its input ..
      PROGRAM COMP
C
C     Integration of adiabatic, constant pressure kinetics problems
C
C     VERSION 1.2:
C     1. Implement new VODE solver
C
C*****precision > double
      IMPLICIT DOUBLE PRECISION (A-H,O-Z), INTEGER(I-N)
C*****END precision > double
C*****precision > single
C     IMPLICIT REAL (A-H,O-Z), INTEGER (I-N)
C*****END precision > single
C
      PARAMETER (LENIWK=4000, LENRWK=4600, LENCWK=500, NK=5, NLMAX=55,
     1        LIN=5, LOUT=6, LINKCK=25, KMAX=50, ITOL=1, IOPT=0,
     2        RTOL=1.OE-6, ITASK=1, ATOL=1.OE-15)
C
      DIMENSION IWORK(LENIWK), RWORK(LENRWK), X(KMAX), Z(KMAX)
      CHARACTER CWORK(LENCWK)*16, KSYM(KMAX)*16, LINE*80
      LOGICAL KERR, IERR
      EXTERNAL FUN
C
      COMMON /RCONS/ P, RU
      COMMON /ICONS/ KK, NWT, NH, NWDOT
C
      DATA KERR/.FALSE./, X/KMAX*0.O/, KSYM/KMAX*' '/
C
C     WRITE (LOUT, 15)
C  15 FORMAT (
C    1/' CONP:  CHEMKIN-II Version 1.2, Aug. 1992',
C*****precision > double

C    2/'           DOUBLE PRECISION')
C*****END precision > double
C*****precision > single
C    2/'           SINGLE PRECISION')
C*****END precision > single
C
C     Initialize CHEMKIN
        OPEN(19, FILE="Conp.dat",STATUS="UNKNOWN")
        OPEN (22,FILE="CONP.DAT1",STATUS="UNKNOWN")
      OPEN (LINKCK, FORM='UNFORMATTED', STATUS='UNKNOWN',
     1              FILE='chem.bin')
      CALL CKLEN (LINKCK, LOUT, LENI, LENR, LENC)
      CALL CKINIT (LENIWK, LENRWK, LENCWK, LINKCK, LOUT, IWORK,
     1 RWORK, CWORK)
      CLOSE (LINKCK)
      CALL CKINDX (IWORK, RWORK, MM, KK, II, NFIT)
```

```
C
      NEQ     = KK + 1
      LRW     = 22 + 9*NEQ + 2*NEQ**2
      NVODE   = LENR + 1
      NWT     = NVODE + LRW
      NH      = NWT + KK
      NWDOT   = NH + KK
      NTOT    = NWDOT+ KK - 1
C
      LIW     = 30 + NEQ
      IVODE   = LENI + 1
      ITOT    = IVODE + LIW - 1
C
      IF (KK .GT. KMAX) THEN
         WRITE (LOUT, *)
     1    ' Error...KMAX too small...must be at least ',KK
         KERR = .TRUE.
      ENDIF
C
      IF (LENRWK .LT. NTOT) THEN
         KERR = .TRUE.
         WRITE (LOUT, *)
     1    ' Error...LENRWK too small...must be at least', NTOT
      ENDIF
C
      IF (LENIWK .LT. ITOT) THEN
        KERR = .TRUE.
        WRITE (LOUT, *)
     1 ' Error...LENIWK too small...must be at least', ITOT
      ENDIF
C
      IF (KERR) STOP
C

      CALL CKSYMS (CWORK, LOUT, KSYM, IERR)
      IF (IERR) KERR = .TRUE.
      CALL CKWT   (IWORK, RWORK, RWORK(NWT))
      CALL CKRP   (IWORK, RWORK, RU, RUC, PATM)
C
C     Pressure and temperature
C
C      WRITE (LOUT, '(/A)') ' ADIABATIC FIXED PRESSURE PROBLEM'
C      WRITE (LOUT, '(/A)') ' INPUT PRESSURE(ATM) AND TEMPERATURE(K)'
      READ (LIN,     *) PA, T
C      WRITE (LOUT,7105) PA, T
      WRITE (19,*) PA, T
      P = PA*PATM
C
C     Initial non-zero moles
C
   40 CONTINUE
      LINE = ' '
C      WRITE (LOUT, '(/A)') ' INPUT MOLES OF NEXT SPECIES'
      READ  (LIN, '(A)', END=45)    LINE
C      WRITE (LOUT, '(1X,A)') LINE
      ILEN = INDEX (LINE, '!')
```

```
         IF (ILEN .EQ. 1) GO TO 40
C
         ILEN = ILEN - 1
         IF (ILEN .LE. 0) ILEN = LEN(LINE)
         IF (INDEX(LINE(:ILEN), 'END') .EQ. 0) THEN
            IF (LINE(:ILEN) .NE. ' ') THEN
                     CALL CKSNUM (LINE(:ILEN), 1, LOUT, KSYM, KK, KNUM,
     1                                NVAL, VAL, IERR)
            IF (IERR) THEN
                     WRITE (LOUT,*) ' Error reading moles...'
                     KERR = .TRUE.
            ELSE
                     X(KNUM) = VAL
            ENDIF
         ENDIF
         GO TO 40
       ENDIF
C
   45 CONTINUE
C
C      Final time and print interval
C
C       WRITE (LOUT, '(/A)') ' INPUT FINAL TIME AND DT'
       READ  (LIN,     *) TT1,T2, DT, III
C       WRITE (LOUT,7105) T2, DT, III
C
         WRITE (22,7100) (KSYM(K), K=1,KK)
       IF (KERR) STOP
C
C      Normalize the mole fractions
C
C      XTOT = 0.00
C      DO 50 K = 1, KK
C         XTOT = XTOT + X(K)
C   50 CONTINUE
C      DO 55 K = 1, KK
C         X(K) = X(K) / XTOT
C   55 CONTINUE
C      WRITE(19,*) XTOT
C      Initial conditions and mass fractions
C
C       TT1 = 0.0
       Z(1) = T
       CALL CKXTY (X, IWORK, RWORK, Z(2))
C
C      Integration control parameters for VODE
C
       TT2      = TT1
       MF = 22
       ISTATE= 1
       NLINES=NLMAX + 1
C
C      Integration loop
C
  250 CONTINUE
C       IF (NLINES .GE. NLMAX) THEN
```

```
C
C        Print page heading
C
C         WRITE (LOUT, 7003)
C         WRITE (LOUT, 7100) (KYSM(K), K=1,KK)
C         NLINES = 1
C
C         DO 200 K1 = NK+1, KK, NK
C             WRITE (LOUT, 7110) (KSYM(K)(:10), K=K1, MIN(K1+NK-1, KK))
C             NLINES = NLINES + 1
C 200     CONTINUE
C       ENDIF
C
C     Print the solution
C
      T = Z(1)
      CALL CKYTX (Z(2). IWORK, RWORK, X)

C
       WRITE (LOUT, 7105) TT1, T, (X(K), K=1,KK)
C      NLINES = NLINES + 1
C
C      DO 300 K1 = NK+1, KK, NK
C         WRITE (LOUT, 7115) (X(K), K=K1, MIN(K1+NK-1,KK))
C         NLINES = NLINES + 1
C   300 CONTINUE
C
      IF (TT2 .GE. T2) THEN
      WRITE(19,7012)(KSYM(K),X(K), K=1,KK)
      WRITE(19,*)'END'
      JJJ=III/2
      QQQ=JJJ*2

        IF(QQQ.EQ.III) THEN
        XINT=1E-6
        T4=TT2
        TT1=T2
        T2=T2+XINT
        T3=XINT/10
        IF (MOD(III,120).EQ.0) THEN
        WRITE(25,7105) TT2,T,(X(K), K= 1,KK)
        ENDIF
        ELSE
        XINT=16.667E-3
        TT1=T2
        T2=T2+XINT
        T3=XINT/10
        ENDIF
        III=III+1
        WRITE(19,*) TT1, T2,T3, III
       STOP
       ELSE
      TT2 = MIN(TT2 + DT, T2)
      ENDIF
C
C     Call the differential equation solver
```

```
C
  350 CONTINUE
C*****precision > single
C      CALL SVODE
C*****END precision > single
C*****precision > double
      CALL DVODE
C*****END precision > double
     *              (FUN, NEQ, Z, TT1, TT2, ITOL, RTOL, ATOL, ITASK,
     1               ISTATE, IOPT, RWORK(NVODE), LRW, IWORK(IVODE),
     2               LIW, JAC, MF, RWORK, IWORK)
C
      IF (ISTATE .LE. -2) THEN
         IF (ISTATE .EQ. -1) THEN
              ISTATE = 2
              GO TO 350
         ELSE
              WRITE (LOUT,*) ' ISTATE=',ISTATE
              STOP
         ENDIF
      ENDIF
      GO TO 250
C
C        FORMATS

 7003 FORMAT (1H1)
 7100 FORMAT (3X, 'T(SEC)', 9X, 'TMP(K)', 9X, 20(4X,A10))
 7105 FORMAT (36E16.8)
 7110 FORMAT (26X, 5(1X,A10))
 7115 FORMAT (22X, 10E11.3)
 7012 FORMAT ((1X,A10),4X,1E14.8)
      END
C
      SUBROUTINE FUN (N. TIME, Z, ZP, RPAR, IPAR)
C
C*****precision > double
      IMPLICIT DOUBLE PRECISION(A-H,O-Z), INTEGER(I-N)
C*****END precision > double
C*****precision > single
C IMPLICIT REAL (A-H,O-Z), INTEGER(I-N)
C*****END precision > single
C
      COMMON /RCONS/ P, RU
      COMMON /ICONS/ KK, NWT, NH, NWDOT
      DIMENSION Z(*), ZP(*), RPAR(*), IPAR(*)
C
C     Variables in Z are: Z(1) = T
C                         Z(K+1) = Y(K)
C
C     Call CHEMKIN subroutines
C
      CALL CKRHOY (P, Z(1), Z(2), IPAR, RPAR, RHO)
      CALL CKCPBS (Z(1), Z(2), IPAR, RPAR, CPB)
      CALL CKWYP (P, Z(1), Z(2), IPAR, RPAR, RPAR(NWDOT))
      CALL CKHMS (Z(1), IPAR, RPAR, RPAR(NH))
C
```

```
C     Form governing equation
C
      SUM = 0.0
      DO 100 K = 1, KK
         H    = RPAR(NH + K - 1)
         WDOT = RPAR(NWDOT + K - 1)
         WT   = RPAR(NWT + K - 1)
         ZP(K+1) = WDOT * WT / RHO
C         SUM = SUM + H * WDOT * WT
 100  CONTINUE
C      ZP(1) = -SUM / (RHO*CPB)
C
      RETURN
      END
```

```
# This program executes the Pulse-on or Pulse off duration of the Program
#!/bin/sh
# to execute: sh conp.sh logname &
sh 1> ${1}.log 2>&1 << ENDSH

set -x
#cd /scr/$LOGNAME              #go to user's scratch directory
#mkdir "${1}$$"                #make subdirectory /myrun##
#cd "${1}$$"                   #go to /myrun##

cat << EOF > makefile

include chemmake.h

OBJS = conp.o cklib.o vode.o math.o
INPS = therm.dat chem.inp conp.inp
OUTS = chem.out chem.bin conp.out
EXES = chem.exe conp.exe

chem.exe: ckinterp.o
          $(LINK) chem.exe ckinterp.o

conp.exe: $(OBJS)
          $(LINK) conp.exe $(OBJS)
EOF


touch makefile; make chem.exe conp.exe
chem.exe; conp.exe < conp.inp > conp.out
cat fort.25 >> yy2.out &
rm fort.25
mv Conp.dat conp.inp
mv chem.inp temp.inp
mv tchem.inp chem.inp
mv temp.inp tchem.inp
#cat conp.out >> yy.out &
mv conp.out temp.out &
#f77 -o average average.f
#average
cat temp1.out >> temp2.out &
ENDSH
```

```
# This program runs the whole simulation using different programs and
files
#!/bin/csh -f
set icount = 1
set iend = 7201
while ($icount != $iend)
sh cconp.sh cconp
 @ icount++
end
#f77 -o ave ave.f
#ave
f77 -o init init.f
init
#cat INITIAL.DAT yy2.out > yy1.out
#rm yy2.out
```

```
# This is an example of the input file.
# The first line indicates the pressure in atm and Temperature in kelvin.
# The following lines indicate the initial mole fraction of different
species
# Finally the line after the End statement refers to initial time, final
time
# the time interval and the number of run respectively.
      1.00000000000000        298.000000000000
      O2                      0.21
      O                       0.
      N                       0.
      N2                      0.79
      NO                      0.0001
      O3                      0.
      E                       O.1E-O9
      N02                     0.
      N03                     0.
      N20                     0.
      END
      O 1E-06 1E-07           1
```

Appendix B: Senior Honors Thesis - The Effects of Particles on Pulsed Streamer Corona Discharge Characteristics

THE EFFECTS OF PARTICLES ON PULSED STREAMER CORONA DISCHARGE CHARACTERISTICS

by

David R. Grymonpré

April 27, 1995

Department of Chemical Engineering
FAMU/FSU College of Engineering
Tallahassee, FL 32316-2175

Submitted in partial fulfillment of the requirements for the
Directed Individual Study in Chemical Engineering

Dr. Bruce R. Locke
Associate Professor and Directing Advisor

Dr. Pedro Arce
Director of DIS / HONORS Program in Chemical Engineering

Mr. Wright C. Feeney
Associate in Research

Table of Contents

Abstract

Pulsed streamer corona treatment is an advanced oxidation technology using a nonthermal plasma that produces hydroxyl radicals, hydrogen peroxide, and aqueous electrons, all of which react with water-borne organic contaminants in the removal process (Clements el. al., 1985). Pulsed streamer corona is an electrical discharge created by applying a continual series of sustainable, short lived, high voltage pulses to a small diameter metallic electrode. This discharge creates an electric field between a point-to-plane electrode geometry within a batch reactor containing organic contaminants in deionized water. A rotating spark gap power supply generates this pulsed corona, which has electrical characteristics of short (200 - 1000 ns) pulse width, fast (20 - 50 ns) rise time, and 60 Hz pulse frequency

Recent experimental results have shown that the addition of various types of solid particles to test solutions in the aqueous phase pulsed streamer corona reactor affects the physical nature of the corona discharge. The composition of these solutions included adding granular activated carbon, (2360 μm particle diameter), powdered activated carbon (75 - 300 μm average particle diameter), and small glass beads (of sizes: 110 - 180 μm, 53 - 78 μm, 30 - 64 μm, and 25 and finer particle diameters) to deionized water in a one liter volume reactor vessel. The discharge and ground electrodes are suspended within the solution. The addition of the powdered carbon to the aqueous system showed a change in characteristics of the corona discharge such as increased numbers of streamers, an increase in streamer length, and most notably, a large increase in the

maximum applied voltage achieved prior to sparkover. With the addition of the glass particles, the discharge characteristics of the corona remained the same, and the sparkover voltage increased with the addition of the two smaller dimensioned glass spheres.

Acknowledgments

I acknowledge the continuing support of this project by the Department of Chemical Engineering, FAMU/FSU College of Engineering. Additionally, I would like to thank the Department of Nuclear Services and the Department of Physics at Florida State University for providing experimental equipment and facilities to conduct all of our experimental corona runs.

I thank Mr. Wright C. Finney for all of the help and support he gave throughout the project and for also fixing the equipment during this project. I also thank Keri Campbell and Kalyana Swaminathan for assisting me in the experimental work.

I would like to acknowledge Mr. Marnix Tas from the Eindhoven University of Technology, Netherlands, for sharing his ideas on pulsed corona in aqueous solutions

Finally, I would like to thank Dr. Bruce R. Locke for serving as my project director on this senior Directed Individual Study project, and also the other member of my committee, Dr. Pedro Arce.

Introduction

Recently, there has been an increased interest in the efficient and cost effective removal of organic contaminants from groundwater and wastewater. Hazardous organic contaminants such as phenol, benzene, and PCBs are found in surface and subsoils and also in the treated sewage effluent contained in storage vessels. Several sources contribute to this problem including leaking petroleum tanks, landfill and cropland runoff, and illegal industrial waste dumping. Federal and state laws now mandate that these contaminants be removed and that clean water be returned to the environment.

Investigations in the field of removing organic contaminants from aqueous solutions have included using advanced oxidation technologies such as direct ozonation, electron beam bombardment, UV photolysis, ultrasonification, microwave plasma reduction, and gamma radiation treatment. Over the past decade, another technology involving the use of a pulsed streamer corona discharge in the liquid phase (Clements, et al., 1985) has been found to be an effective way to remove organics from aqueous solutions. This technique utilizes chemical radicals produced from a pulsed streamer corona discharge that is sustained in an aqueous phase medium. Preliminary studies at the FAMU/FSU College of Engineering have demonstrated the complete degradation of phenol in solution (Sharma, 1993), and the determination of the rates of formation of hydrogen peroxide, hydroxyl radicals, and aqueous electrons (Joshi, 1994).

Recently, it has been observed in our laboratory that the addition of particles to a test solution affects the physical characteristics (i.e., streamer length, intensity, number of streamers, and sparkover voltage) of the streamer corona discharge. The principal

objective of the present work is to document preliminary experimental results of the effects of the addition of several different types of particles to the aqueous phase pulsed streamer corona reactor. The particles used for this investigation included 1) 75 - 300μm diameter powdered activated carbon, 2) 1.40 - 3.35 mm diameter granular activated carbon, 3) 110 - 180 μm diameter glass beads, 4) 53 - 78 μm diameter glass beads, 5) 30 - 64 μm diameter glass beads, and 6) 25 μm and finer diameter glass beads. The experiments conducted in this work focus on determining how the physical nature of the corona discharge (size and number of streamers) is affected by the addition of these particles to the pulsed corona reactor, and how the maximum voltage before sparkover is changed when the particles are added.

In this report, a brief literature review in chapter II will give a background on the pulsed corona process. In chapter III, a simplified model of the process will be given. The experimental equipment and procedure will be discussed in chapter IV. The results of a number of experiments will be presented and discussed in chapter V. Chapter VI will discuss future experimental and theoretical work.

Literature Review

Pulsed corona technology has been employed in pollution migration for almost a decade and a half. The use of a pulsed streamer corona has proven to be an effective method of removing contaminants such as NOx and SOx from air streams (Masuda, 1990; Kamase, 1991). Clements et al. (1985) were the first to adapt a pulsed streamer corona to an aqueous phase system. This group also performed work on ozone formation, dye breakdown, and electrical discharge characteristics in an aqueous phase pulsed streamer corona system. The discharge consists of repetitive pulses with a short pulse width (200 ns) at an applied voltage of 20 - 45 kV. The advantage of using a pulsed power supply over continuous power (DC) is that the energy input to the system is used to produce reactive chemical radicals while minimizing the heating of the solution. The chemical radicals produced from the pulsed streamer corona discharge in the aqueous phase are given in Figure 1.

More recently, the aqueous phase pulsed streamer corona technology has been significantly extended, and experimental and modeling aspects of this work have been documented in several publications (Sharma et al., 1993; Joshi et al., 1994). Many of the chemical reactions involved in this process have been characterized (Clements et al.; 1985, Sharma et al., 1993; Joshi et al., 1994). These reactions include such species as hydroxyl radicals, hydrogen peroxide, and aqueous electrons. The reaction and removal rates of phenol have been reported for different experimental conditions (Sharma et al., 1993). Experiments were carried out using a point-to-plane electrode geometry within a batch reactor filled with deionized water and various additives. In all cases, at higher

applied electric fields the rate of phenol removal increased. The addition of iron to the reactor was found to increase the rate of phenol removal due to Fenton's reaction (Joshi, et al., 1994; Sharma, et al., 1993). Several other additives, such as bubbling oxygen through the discharge electrode, enhanced the rate of phenol removal.

The present work concerns the addition of coarse and fine particles to the aqueous phase reactor to ascertain the particles' effect on the sparkover voltage and the nature of the discharge. The addition of particles to the pulsed corona system has not been reported in the literature, however, the addition of particles can affect both the chemical and physical aspects of the discharge. The preliminary experiments presented in this report indicate that adding particles (powdered activated carbon, in particular) to the reactor greatly affects the properties of the corona discharge. To better understand this phenomenon, the corona discharge and the propagation of the streamers need to be analyzed.

Analysis of the voltage breakdown of a pulsed electrode system in aqueous solutions has been previously presented and modeled in several different ways. One method of analysis has been through an approximation of a shock wave (Klimkin et al., 1978). In this method, shock waves, similar to ultrasonic treatments, are used to estimate the basic energy relations for the beginning stage of breakdown in the aqueous phase. Another mechanism was proposed that, during pulse application, hydrogen atoms become excited in the gas phase, and lead to the formation of gas bubbles (Kuskova, 1983). This formation has been observed in previous work (Clements et al., 1985). These gas bubbles expand and have secondary reactions such as hydroxyl radicals and peroxides (Klimkin, 1990).

A method proposed and developed by Neimeyer et al. for modeling gas phase dielectric discharge has been introduced by studying computer simulations of stochastic Monte Carlo models (Niemeyer et al., 1984). To do this, they solved the following Laplace equation:

$$\nabla^2\phi=0 \tag{1}$$

over a circular lattice (matrix), the center potential (discharge needle point) being zero and the outer ring potential (ground plate) being one. Each time this equation is solved, a probability for the streamer propagation to an adjacent point in the grid is given to each of the corresponding points on the matrix. Propagation is then achieved using a random move for each step. The Laplace equation is solved for each iteration. Based upon this model, more complicated models have been developed to determine the effect of other variables on the nature of the breakdown (Niemeyer et al.; 1989, Kupershtok, 1992). The addition of particles and spatial discontinuities to the grid developed by Neimeyer et al. (1989) may allow for a qualitative analysis of the effect of various sizes, shapes, and material types of particles. Also note that the material type may also alter the dielectric constants.

Modeling

A simple model was derived from a charge balance to simulate the system used in the present work. Using Poisson's Equation, with the given boundary conditions,

$$\frac{d^2\phi}{dx^2} = -\rho \qquad \begin{matrix} x = 0,\ \phi = 1 \\ x = 1,\ \phi = 0 \end{matrix} \tag{2}$$

where ϕ is the electric potential, and ρ, assumed to be a constant, is the charge density of the solution, we can obtain a simple one-dimensional model for the electrical discharge in the system for this work. The solution of this equation is the following:

$$\phi = [(\rho/2)x + 1](1-x) \tag{3}$$

The graph of this solution is shown in Figure 2. In this figure, each line represents a constant charge density. From this figure, it is noticed that as ρ increases, the maximum electric potential, ϕ_m, increases. When the graph of maximum potential, ϕ_m, versus different values of the charge density, ρ, Figure 3 is obtained. This gives a relation between the charge density in the solution containing particles, and the maximum electric potential.

The maximum potential is expected to simulate the voltage at which sparkover occurs. The charge density can be related to the surface area of the particles in suspension and to the composition of the particles themselves. The following equations

for field charging will show how charge density is related to the surface area of the particle and the composition of the particle. When a single dielectric particle of radius R_p containing a charge q, is placed in an electric field, E_∞, in cylindrical coordinates, at any point outside the sphere is (Stratton, 1941, Flagan and Seinfeld, 1988):

$$V = \frac{q}{4\pi\epsilon_0\kappa_2 r} + \left[\frac{r}{R_p} + \frac{\kappa_1 - \kappa_2}{\kappa_1 + 2\kappa_1}\frac{R_p^2}{r}\right] E_\infty R_p \cos\theta \qquad (4)$$

where κ_1 is the dielectric constant of water, κ_2 is the dielectric constant of the particle added, and ϵ_0 is the permittivity of free space. The values for κ are 80 for water, 5.75 for carbon, and 4.42 for the glass beads. Differentiating this equation in the r-component:

$$E_e = -\frac{\partial V}{\partial r} = -E_\infty \cos\vartheta \left[1 + 2\frac{\kappa_1 - \kappa_2}{\kappa_1 + 2\kappa_2}\frac{r\, R_p^3}{r^3}\right] + \frac{q}{4\pi r^2 \epsilon_0 \kappa_2} \qquad (5)$$

The charge on the particle increases as more charge migrates to the particle. Under the conditions present in the pulsed corona reactor, the saturation charge is attained soon after initiation of the discharge. The final charge on the particle is represented by the following:

$$q_{fc} = \left[\frac{3\kappa_1}{\kappa_1 + 2\kappa_2} \right] \pi \epsilon_0 \kappa_2 E_\infty D_p^2 \qquad (6)$$

For the limiting case of equation (6), where $\kappa_1 >> \kappa_2$, such as the system in this project, the following equation arises:

$$q_{fc} = 3\pi \epsilon_0 \kappa_2 E_\infty D_p^2 \qquad (7)$$

which relates the field charge to κ_2, which is the dielectric constant of the particle. In equation (7), the given charge density is linearly proportional to the surface area through D_p^2, where D_p is the particle diameter. To determine the charge density from the field charge, multiply the particle charge by the total number of particles in the solution, and then divide this total by the volume of the solution. This gives a relationship between the charge density, surface area of the particle, and the composition of the particle. These charge densities can now be applied to the theoretical models from equation (3).

Experimental Equipment and Procedure

The experimental apparatus used in this study is shown in Figure 4. The apparatus consists of a 550 ml plexiglass vessel used as a reaction chamber. This vessel is closed at both ends and is submerged in an ice bath to approximate isothermal conditions. The region of electrical discharge is located at the tip of a hollow hypodermic needle, which is connected to a high voltage pulsed power supply. The corona extends from the needle upwards toward the stainless steel ground plate in a point-to-plane geometry. The separation distance between the needle tip and ground plate is set at 5 cm. A magnetic stirrer at the bottom of the vessel provides thorough mixing of the solution. Two nylon fittings on the side of the vessel are used to take samples for analysis.

The difference between this system and other corona discharges such as dc discharge, ac discharge, and long-pulse (μs - ms pulse width) treatments is that the electrical discharge in this reactor has a short pulse width and a fast rise time. Pulsed power is produced by a rotating spark gap high voltage pulsed power supply, capable of supplying the reactor discharge electrode with high voltage (20 - 45 kV), short duration, (200 - 1000 ns), fast rise time (20 - 50 ns), repetitive (60 Hz), electrical pulses. The pulsed power supply used for this project is shown in Figure 5. The source input is a high voltage transformer supplying a rectified AC power to the pulse forming circuit. This high voltage goes through a series of current-limiting resistors and a set of diodes that remove the negative part of the sine wave. The half-wave rectified voltage then charges an array of ceramic "doorknob" capacitors which discharge into the reactor load whenever the rotating spark gap closes.

For each set of experimental conditions, three or more trials were made to obtain appropriate statistical interpretations of the data. The initial experimental trials for this work consisted of control runs of 550 ml of deionized water only in the pulsed corona reactor. Two different controls were run, during which measurements of the voltage and current between the high voltage and ground electrodes were made and qualitative observations of the length and quantity of the streamers were made. The first control utilized a fully exposed discharge electrode needle, and the second employed a needle covered with a plastic covering along the needle shaft, leaving only the tip exposed in order to simulate a more true point-to-plane geometry.

The first set of experiments testing the effects of adding particles to the reactor solution were performed using powdered activated carbon (50 to 200 mesh, 300 - 75 μm particle size) at concentrations of 0.5 g, 1.0 g, 2.0 g, 3.0 g, and 5.0 g per 550 ml of deionized water. The carbon was added to the stirred water in the vessel before the trials began to obtain a well-mixed solution when the experiment started. The second set of experiments used a larger type of particle, granular activated carbon (6 to 14 mesh, 3.3 - 1.4 mm particle size). These experiments were run with concentrations of 1.0 g, 2.0 g, and 5.0 g of carbon per 550 ml of deionized water. Finally, the last set of experiments were performed with four different sizes of spherical silica glass beads, 110 - 180 μm diameter, 53 - 78 μm diameter, 30 - 60 μm diameter, and 25 μm and finer diameter glass beads. Again, each of the sizes were evaluated at concentrations of 1.0 g, and 2.0 g,(and 5.0 g at the 110 - 180 μm diameter and 53 - 78 μm diameter sizes only) per 550 ml deionized water.

Once these test solutions were made, samples were taken to measure the initial temperature, pH, and conductivity. To begin a trial, a test solution was introduced into the reactor, and the pulsed power supply was engaged at an initial applied voltage of 10 kV. The voltage was then increased at increments of 2.5 kV until sparkover was reached. Sparkover occurs when the applied voltage is high enough to cause a spark to bridge the two electrodes. At each voltage setting, the average peak current was read using an ammeter, and visual observations were made of the size, quality, and quantity of the streamers. Subsequent to sparkover, samples were again taken to test the temperature, pH, and conductivity of the solution.

Also, aqueous solutions of potassium iodide (KI) were made at concentrations of 0.0301 M. These solutions contained no particles but had high ionic content. These experiments were done to compare the affects of a solution with a higher conductivity due to a dissolved salt, to that of solid particles in suspension. Each of these solutions was tested before and after treatment for temperature, pH, and conductivity. The experiments with the KI started with an applied voltage of 10 kV and increased incrementally by 2.5 kV until approximately 80 kV.

Experimental Results and Discussion

Current vs. voltage plots for the two initial experiments with no particles in the system are shown in Figure 6. The streamers observed emanating from the discharge electrode appeared higher in number for the control run with the covered needle electrode when compared to the run with the uncovered needle. Sparkover was reached at 42.5 kV for the uncovered needle control and sparkover was at 40 kV for the covered needle control. These observations are consistent with those found in previous work (Sharma, et al., 1993). All further experiments were conducted with the covered needle, and these experiments were compared to the data and observations of the control run with the needle shaft covered in plastic. Once again, the covered needle gives the system a truer point-to-plane geometry than using the uncovered needle.

The first set of experiments testing particles in solution were performed by adding powdered activated carbon at concentrations of 0.5 g, 1.0 g, 2.0 g, 3.0 g, and 5.0 g to 550 ml of deionized water in the pulsed corona reactor. The current vs. applied voltage data are presented in Figure 7. In all five trials with the particles present, the current measurement at the corona onset voltage of 20 kV was higher than that for the no-particle control trial. All of the trials with particles produced a greater number of streamers and longer streamers at a given voltage when compared to the control with no particles. These determinations are qualitative by observation and no exact measurements were made. As the concentration of the powdered carbon increased from 0.5 g to 5.0 g,, the quantity and length of streamers also increased for equal voltage applied.

The most significant observations were the voltage differences at which sparkover occurred. Sparkover is very distinguishable in that there is a very bright streamer

connecting the two electrodes accompanied by a loud noise. Table 1 shows the voltage at sparkover for the six different powdered carbon particle concentrations.

Table 1. Carbon Particle Concentration With Sparkover Voltages

Concentration of Carbon Particles per 550 ml DI Wager (g)	0	0.5 g	1.0 g	2.0 g	3.0 g	5.0 g
Sparkover Voltage (kV)	40 kV	45 kV	57.5 kV	62.5 kV	82.5 kV	>100 kV

This table shows that as the concentration of the carbon particles is increased, the applied voltage at which the system achieves sparkover also increases. This phenomena is significant because the higher the electric field (i.e. applied voltage) the more chemical radicals produced and therefore a higher contaminant removal. Treatment at or above sparkover essentially short circuits the system therefore not producing as many of the chemical radicals that the pulsed streamer corona creates.

These results show a large increase in the maximum applied voltage achieved before sparkover as the concentration of the powdered activated carbon is raised. The results also give a graph (Figure 7) that shows a linear increase in the applied voltage at sparkover as the amount of carbon increases. In previous work in this laboratory using only deionized water in the reactor, the maximum voltage prior to sparkover was 40 kV for the same electrode geometry without particles. With the addition of the carbon particles, higher voltages can be achieved, which may lead to higher conversion rates and faster degradation of organic contaminants in the reactor. The solution with the 5 g of carbon never reached sparkover because the upper voltage limit of the power supply is

100 kV. On Figure 7, the graphs show a clear picture of two different slopes for each of the lines representing current, a small slope initially, and then at a given point, a larger slope occurs.

The experimental results for the sparkover voltage vs. the total particle surface area are shown in Figure 8. A best fit of these points gives a straight line. This linear trend corresponds with that predicted from the theoretical background for large ρ shown in Figure 3. For these quantities of carbon particles, the total surface area of the particle samples are very high and therefore the range of the charge density corresponds with the straight portion of the slope in Figure 3. There is a need to relate the concentrations of the carbon particles to the charge density.

The second type of particle tested in the corona reactor was the granular activated carbon. These experiments used samples of 550 ml deionized water containing concentrations of 1.0 g, 2.0 g, and 5.0 g of granular activated carbon. Figure 9 shows the relationship between the current and voltage for these four granular carbon concentration experiments. There were no significant differences between the granular activated carbon runs and the control except for the 5 g concentration experiments. At 5 g of carbon, the measured current was slightly higher and the sparkover increased to 42.5 kV from 40 kV at all other concentrations. There were no observed differences in streamer quantity or length between any of the granular carbon runs. A possible reason for the lack of change in the properties of the corona might be that the granular activated carbon particles were difficult to suspend in solution, and vigorous stirring caused most of the particles to be accelerated outward to the reactor margin, away from the middle of the solution where the high voltage discharge needle is located.

The next set of experiments were done with two different sizes of glass beads, 110 - 180 μm diameter and 53 - 78 μm diameter. Again, each of the sizes was evaluated at concentrations of 1.0 g, 2.0 g, and 5.0 g per 550 ml deionized water in the pulsed corona reactor. The effects of the particles on the current vs. voltage characteristics are shown in Figures 10 and 11. For fixed voltages, there was an increase in current for experiments with the smaller sized glass beads and less of a change for the experiments with larger sized glass beads when compared to the no-particle control. The sparkover voltage was 37.5 kV for all six of the concentrations and sizes of glass beads. The most notable observation for all of these trials was that the streamer size decreased, but the number of streamers increased and they seemed to be much more intense and brighter. At these concentrations, the current varied for each of the runs. This is why the statistical analysis is not shown on any of the graphs. A reason for this problem is that the ammeter might have been damaged from overuse and this could be the reason why the results were sporadic.

Also, the smaller glass particles that were looked at were the 30 - 64 μm diameter glass beads and the 25 μm diameter and finer glass beads. The results for the current vs. voltage graphs is shown in Figures 12 - 15. These figures show the same trend as the previous glass beads in that the current increases as the voltage increases. The 25 μm and finer diameter glass beads showed the closest resemblance to the powdered activated carbon in that the sparkover voltage increased with increasing concentrations of the glass beads. When the glass beads of this diameter are suspended by the stirring bar, the solution becomes very cloudy therefore visual observations of the corona discharge were not made.

Sparkover voltage plotted against the surface area for all of the glass particles is given in Figure 16. The glass particles had very little total surface area when compared to the carbon particles due to the carbon particles being very porous and the glass is non-porous. Due to this small surface area, this graph may correspond to the section of the graph of charge density vs. surface area in the theoretical background (Figure 3). The graph in Figure 3 first shows a flat section and then an increase in the maximum electrical potential at small values of the charge density.

An analysis of the charge density is shown in Figure 17. This is shown by plotting the sparkover voltage vs. the charge density of the various concentrations of glass beads in solution. Charge density was found by first finding the charge density on each particle using the field charging theory in equation (6), multiplying this number by the total number of particles, and then dividing by the volume of the reactor. The result of this analysis is a slope that is similar to that of the predicted theoretical graph of the maximum electric potential versus the charge density as shown in Figure 3. The graphs look similar over the initial regions where the slope is flat and then starts to increase corresponding to small values in ρ. The solutions for the carbon were not analyzed in this manner because the field charging equation is modeled for a system for solid spherical particles in an electric field. The carbon particles are not spherical and were very porous. The actual total surface area is 10^6 times greater than the outer surface area. An equation needs to be devised that will account for this great surface area.

Finally, the results of the trials with the potassium iodide solutions, the current vs. voltage plots are given in Figure 18. These experiments were done to compare the affects of solution with a higher conductivity due to a dissolved salt to that of solid particles in

suspension. The graph in Figure 18 shows an increase in current with an increase in applied voltage. This system did not achieve sparkover even when the applied voltage reached 80 kV. The conductivity of this solution was 10^4 times greater than the solutions with the carbon and the glass particles. The streamers in this solution were much smaller than DI water alone, but the streamers were much more intense.

The current to voltage relationships for all of the particles had different slopes. The KI solutions had the smallest slopes, the glass beads had a slightly higher slope, DI water was greater than the glass beads, and the powdered activated carbon particles had the highest slope. These carbon particles were also the only solution that had two different slopes. The slope of the current for these carbon particles started at one slope and then suddenly increased the slope of the current. The cause of these slopes is unknown at this time. The conductivity of the solution might have a function in the different slopes of the solutions.

From these results, the particle type having the greatest effect on the sparkover voltage in the reactor was the powdered activated carbon. Addition of powdered carbon to the aqueous solution produced more streamers, longer streamers, and increased sparkover voltage. With these characteristics, it is possible that the removal of organics such as phenols would be accelerated greatly since the production of hydroxyl radicals, aqueous electrons, and hydrogen peroxide increases with increases in the applied discharge voltage. This would lead to decreased exposure time and therefore increased efficiency.

Future Work

These results bring up many new questions on the addition of particles to deionized water in the pulsed streamer corona reaction vessel. More investigation of the physical aspects of the process as well as the chemical aspects of the process should be investigated.

Further development of the model presented in this work is needed. The least understood part of this model is the definition of the maximum electric potential. It is predicted that the maximum potential is related to the point at which sparkover is achieved, but the relation is not well understood. Also, other kinds of particles such as copper or photocatalysts should be looked at to aid in this prediction. The copper will give a non-porous conducting particle and the photocatalysts could promote surface reactions.

To this point, chemical aspects of the effect of adding particles, such as the rates of formation of the reactive species, and the rate of phenol breakdown, has not been investigated. Pulsed corona treatments of contaminated water containing particles should be fully analyzed. Carbon is known to adsorb small aromatic organics and carbon has shown to promote surface reactions (Vidic, Suldan, and Brenner, 1993. Abuzald and Nakhla, 1994.) The kinetics of the formation of the different reactive species should be reanalyzed for the addition of the carbon and glass particles. Also, the adsorption of the contaminants and subsequent surface reactions should also be noted.

Literature Cited

1. Abuzald, N. S. and Nakhla, G. F. 1994: Dissolved Oxygen Effects on Equilibrium and Kinetics of Phenolics Adsorption by Activated Carbon. Environ. Sci. Technol. p. 216.

2. Clements, J.S., Sato, M., and Davis, R.H., 1985: Preliminary Investigation of Prebreakdown Phenomena and Chemical Reactions Using a Pulsed High Voltage Discharge in Water. IEEE Trans. Ind Appl. IA-23, 1372.

3. Flagan, R. C., and Seinfeld, J. H., 1988, Fundamentals of Air Pollution Engineering, Pretince Hall, Englewood Cliffs, New Jersey.

4. Jones, H. M., and Kundhardt, E. E., 1995, Development of Pulsed Dielectric Breakdown in Liquids. Journal of Physics D: Applied Physics V.28, p.178-188.

5. Joshi, A.A., 1994: Formation of Hydroxyl Radicals, Hydrogen Peroxide, and Aqueous Electrons by Pulsed Streamer Corona Discharge in Aqueous Solutions, M.S. Thesis FAMU/FSU College of Engineering, Tallahassee, FL.

6. Kamase, Y., and Mizuno, A.,: Removal of Ethylene by Streamer Corona Discharge.

7. Klimkin, V. F., and Ponomarenko, A. G., 1979: Interferometric Study of Pulsed Breakdown in a Liquid. Sov. Psys. Tech. Phys. 24(9), 1067.

8. Klimkin, V. F., 1990: Mechanisms of Electric Breakdo~vn of Water from Pointed Anode in the Nanosecond Range. Sov. Psys. Tech. Phys. 16(2), 146.

9. Klimkin, V. F., 1991: A Multitrame Ultrafast Laser Schlieren S;stem for the Observation of Pre-breakdown Phenomena in Liquids in the Nanosecond Range. Sov. Psys. Tech. Phys. 36(9), 375.

10. Kupershtok, A. L., 1992: Fluctuation Model of the Breakdown of Liquid Dielectrics. Sov. Tech. Phys. Lett. 18(10), 647.

11. Kuskova, N. I., 1983: Mechanism of Leader Propagation in Water. Sov. Psys. Tech. Phys. 28(5), 591.

12. Masuda, S., and Nakao, H.: Control of NOx by Positive and Negative Pulsed Corona Discharges. IEEE Trans. Ind. App. 26(2) 974.

13. McAllister, D., Smith, J. R., and Diserens, N. J., 1985, Computer Modeling in Electrostatics Research Studies Press LTD, Letchworth, England.

14. Niemeyer, l, Pietronero, L, and Weisman, H.J., 1984: Fractal Dimension of Dielectric Breakdown. Physical Review Letters, 52(12), 1033.

15. Niemeyer, L., Ullrich, L., and Wiegart, N., 1989: The Mechanism of Leader Breakdown in Electronegative Gases. IEEE Trans. Elec. Insul., 24(2), 309.

16. Scaife, B. K. P., 1989, Principles of Dielectrics, Clarendon Press, Oxford.

17.. Sharma, A. K., 1993: High Voltage Pulsed Streamer Corona Discharges for the Removal of Organic Contaminants From Aqueous Solutions, M.S.. Thesis, FAMU/FSU College of Engineering, Tallahassee.

18. Sharma, A. K., Locke, B. R., Arce, P., Finney, W. C., 1993, A Preliminary Study of Pulsed Streamer Corona Discharge for the Degradation of Phenol in Aqueous Solutions. Hazardous Waste & Hazardous Materials, 10 (2), p. 209.

19. Stratton, J. A., 1941, Electromagnetic Theory, McGraw-Hill Book Company, New York.

20. Vidic, R. D., Suldan, M. T., and Brenner, R. T., 1993: Oxidative Coupling of Phenols on Activated Carbon: Impact on Adsorption Equilibrium. Environ. Sci. Technol. 27, p. 2085.

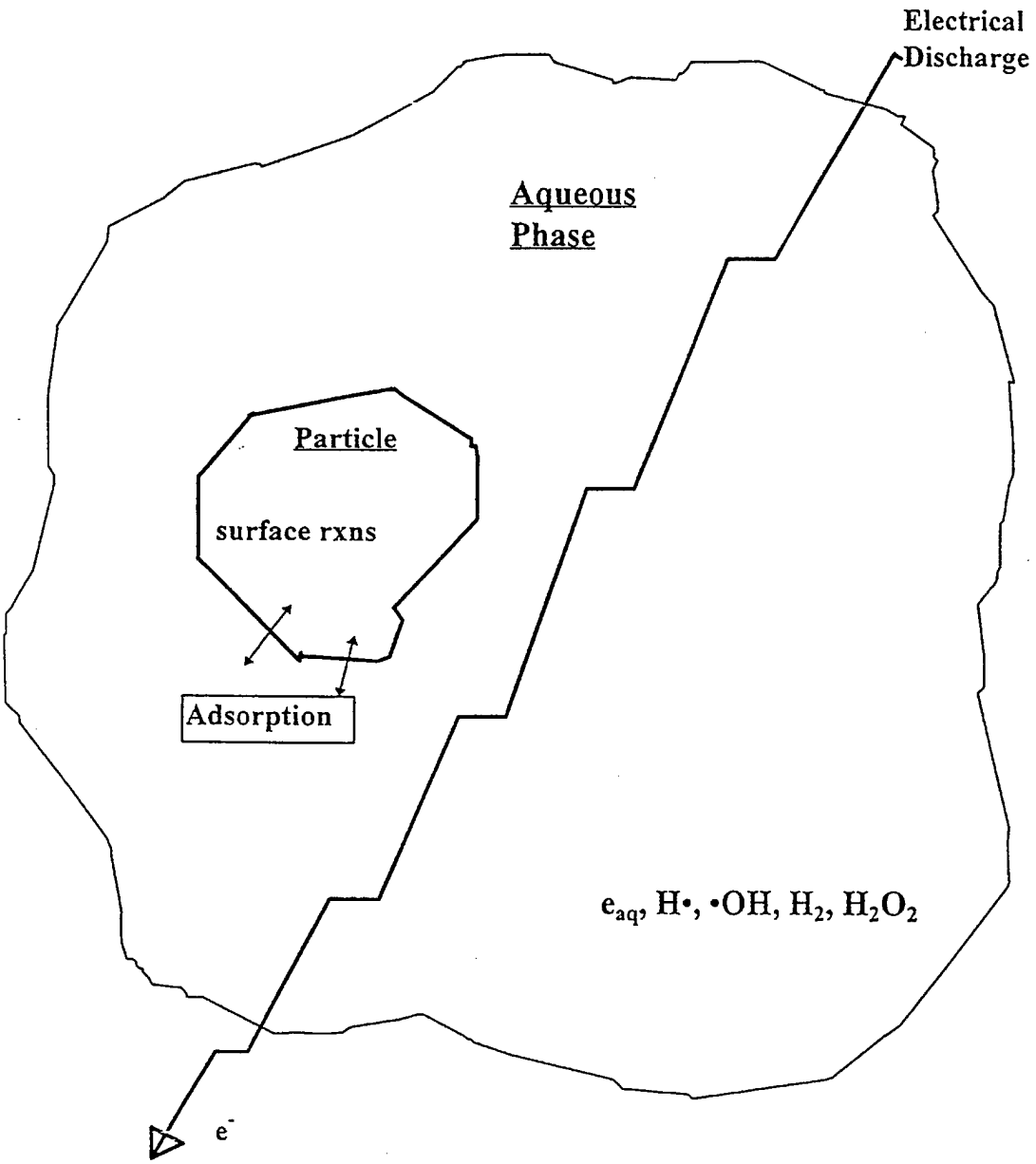
Chemical Processes:
Electrical
Discharge
Aqueous
Phase
Particle
surface rxns
Adsorption
e_{aq}, H•, •OH, H_2, H_2O_2
e^-

Figure 1

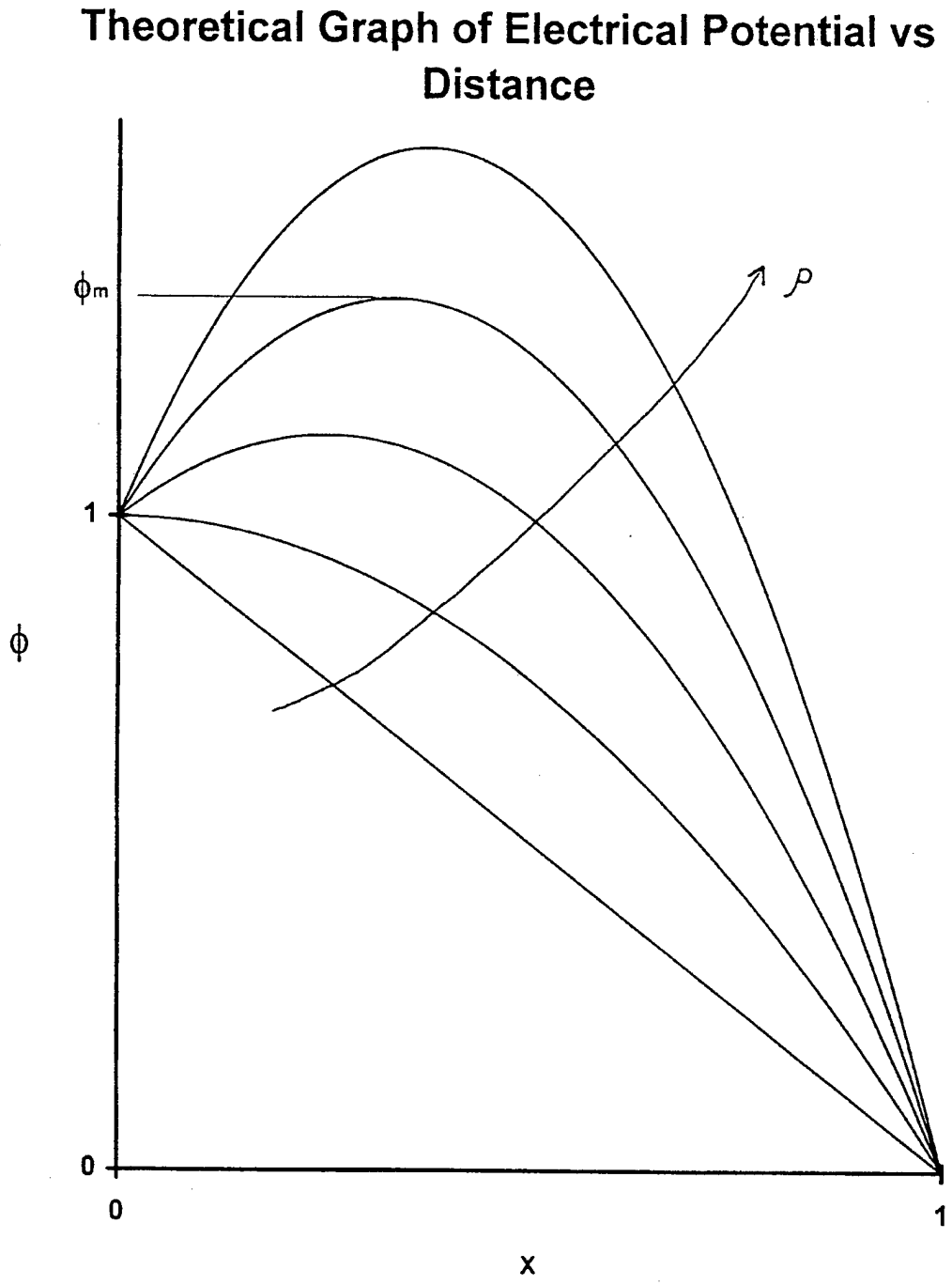
Theoretical Graph of Electrical Potential vs Distance
ϕ_m
1
ϕ
0
0
1
X
ρ

Figure 2

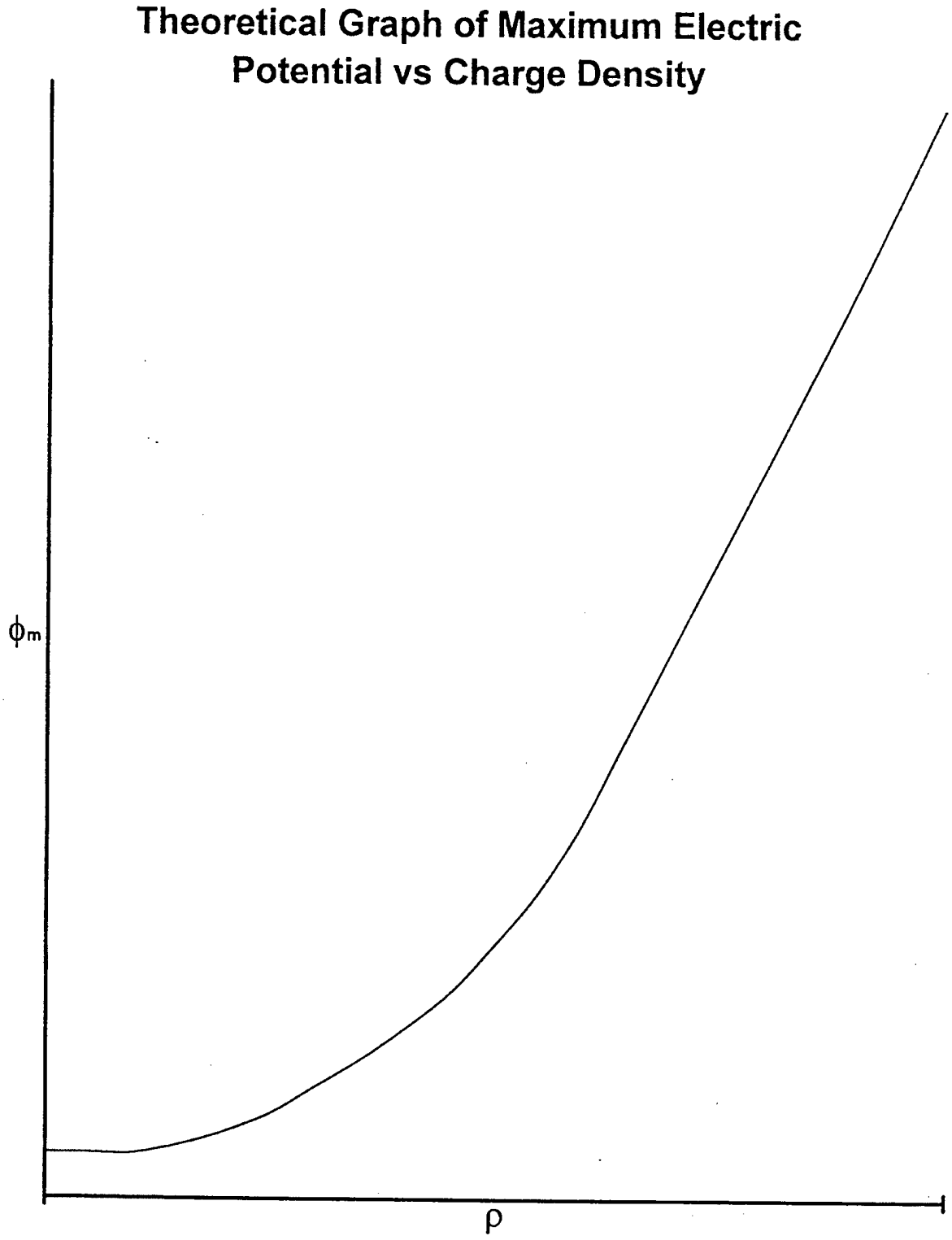
Theoretical Graph of Maximum Electric Potential vs Charge Density
ϕ_m
ρ

Figure 3

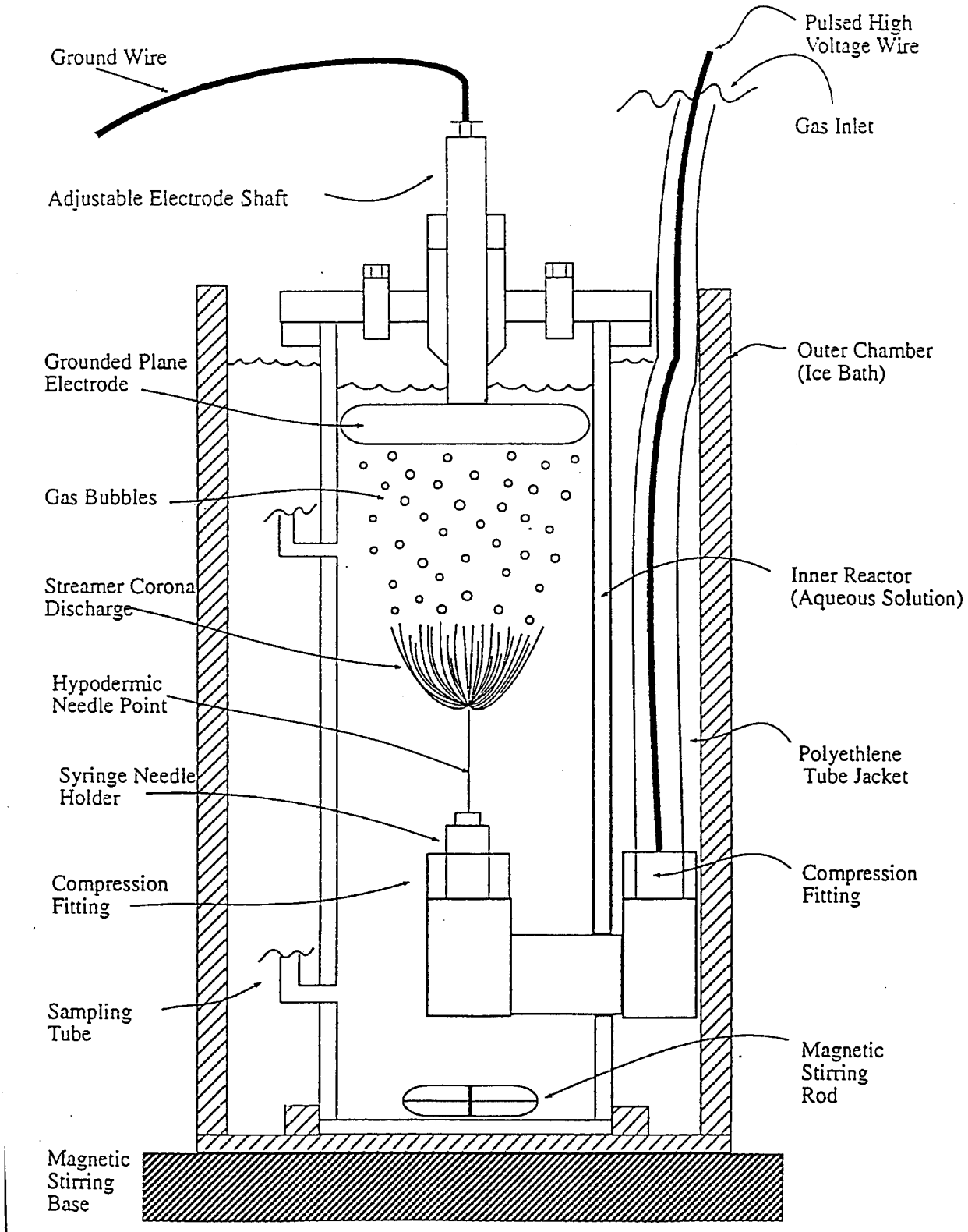
Ground Wire
Pulsed High Voltage Wire
Gas Inlet
Adjustable Electrode Shaft
Grounded Plane Electrode
Outer Chamber (Ice Bath)
Gas Bubbles
Inner Reactor (Aqueous Solution)
Streamer Corona Discharge
Hypodermic Needle Point
Polyethlene Tube Jacket
Syringe Needle Holder
Compression Fitting
Compression Fitting
Sampling Tube
Magnetic Stirring Rod
Magnetic Stirring Base

Figure 4

Pulsed Power Supply

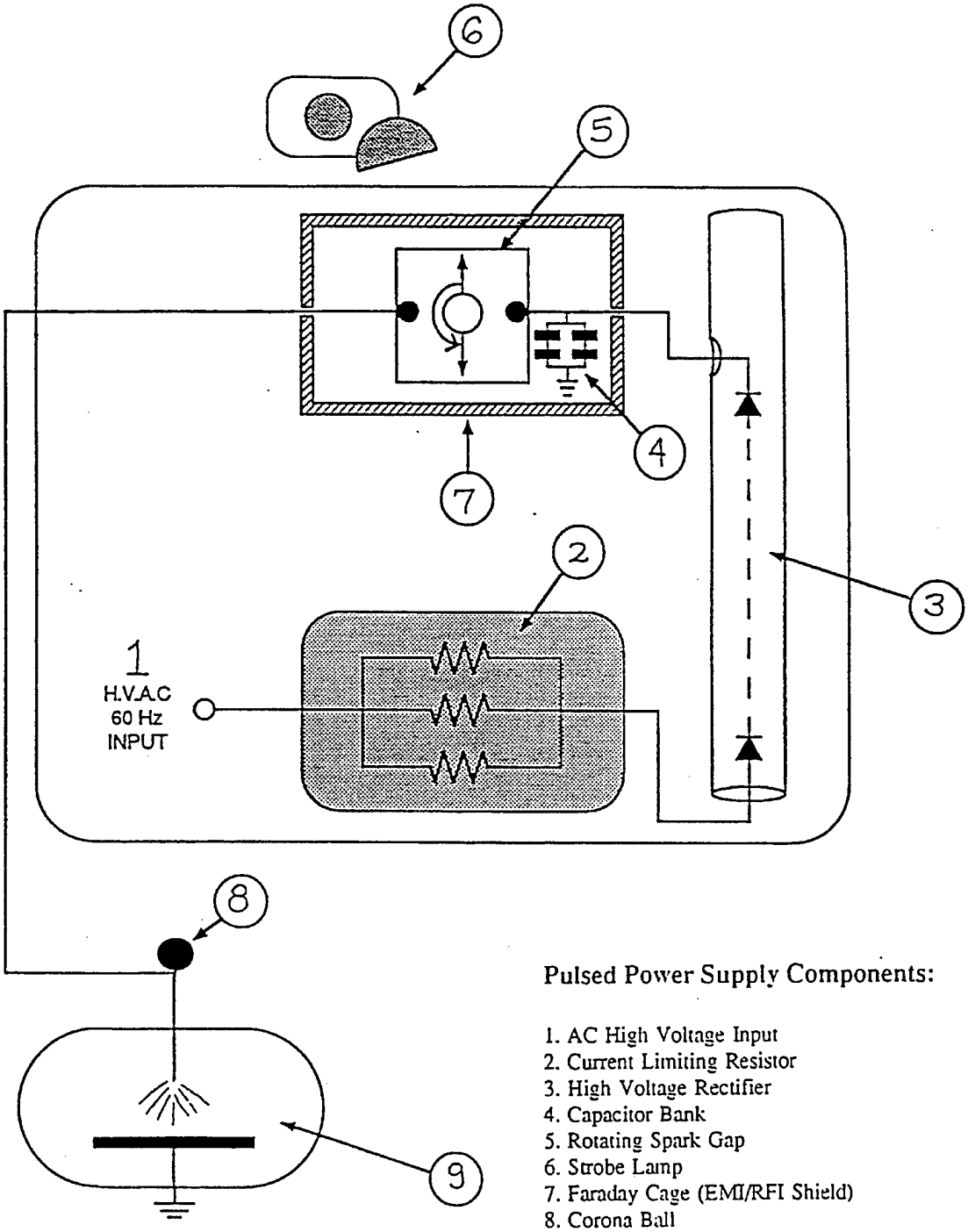

Pulsed Power Supply Components:

1. AC High Voltage Input
2. Current Limiting Resistor
3. High Voltage Rectifier
4. Capacitor Bank
5. Rotating Spark Gap
6. Strobe Lamp
7. Faraday Cage (EMI/RFI Shield)
8. Corona Ball
9. Reactor Vessel & Electrodes

Figure 5

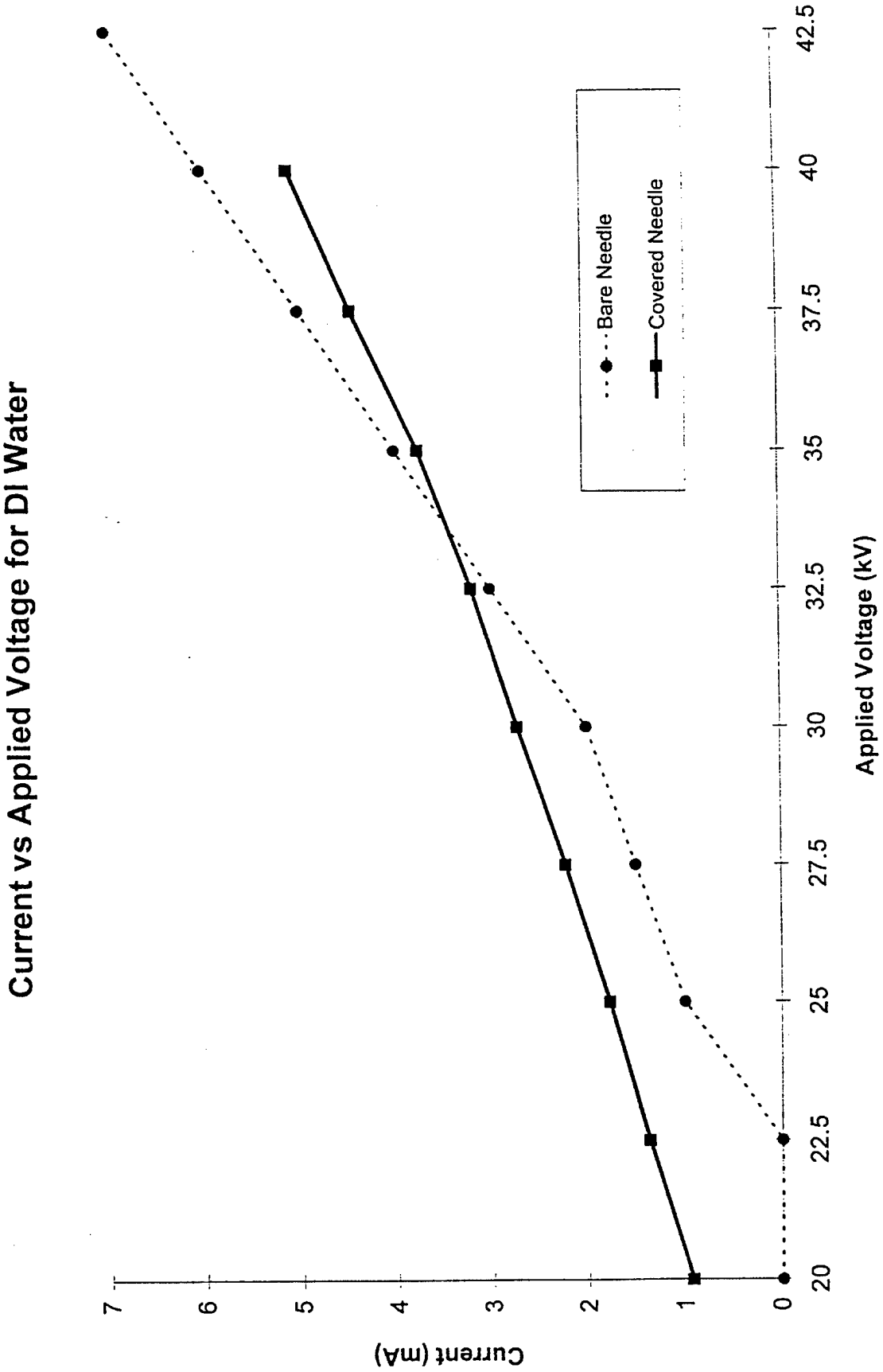
Current vs Applied Voltage for DI Water
Current (mA)
0
1
2
3
4
5
6
7
20
22.5
25
27.5
30
32.5
35
37.5
40
42.5
Applied Voltage (kV)
Bare Needle
Covered Needle

Figure 6

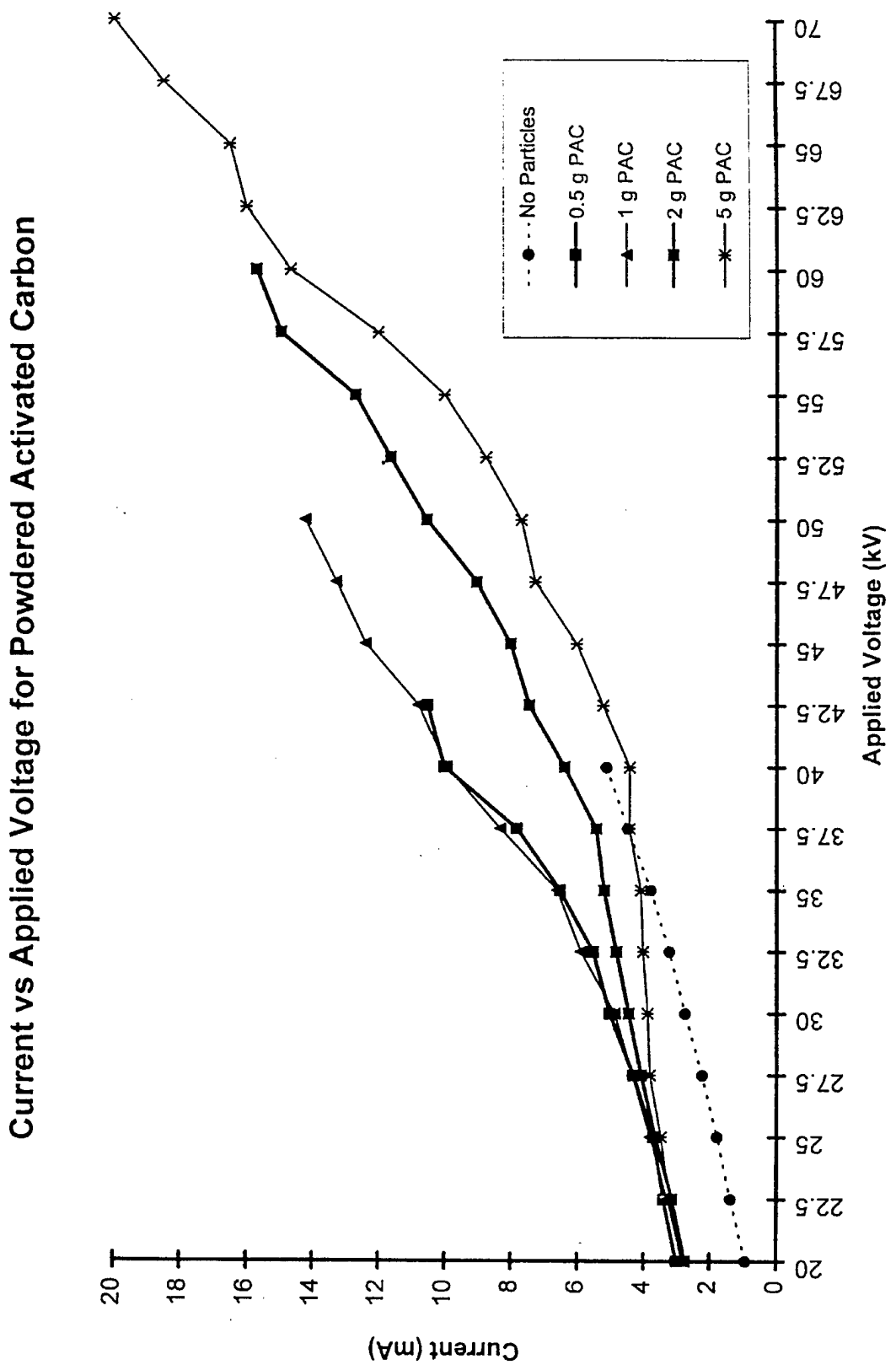
Current vs Applied Voltage for Powdered Activated Carbon
Current (mA)
Applied Voltage (kV)
No Particles
0.5 g PAC
1 g PAC
2 g PAC
5 g PAC
0
2
4
6
8
10
12
14
16
18
20
22.5
25
27.5
30
32.5
35
37.5
40
42.5
45
47.5
50
52.5
55
57.5
60
62.5
65
67.5
70

Figure 7

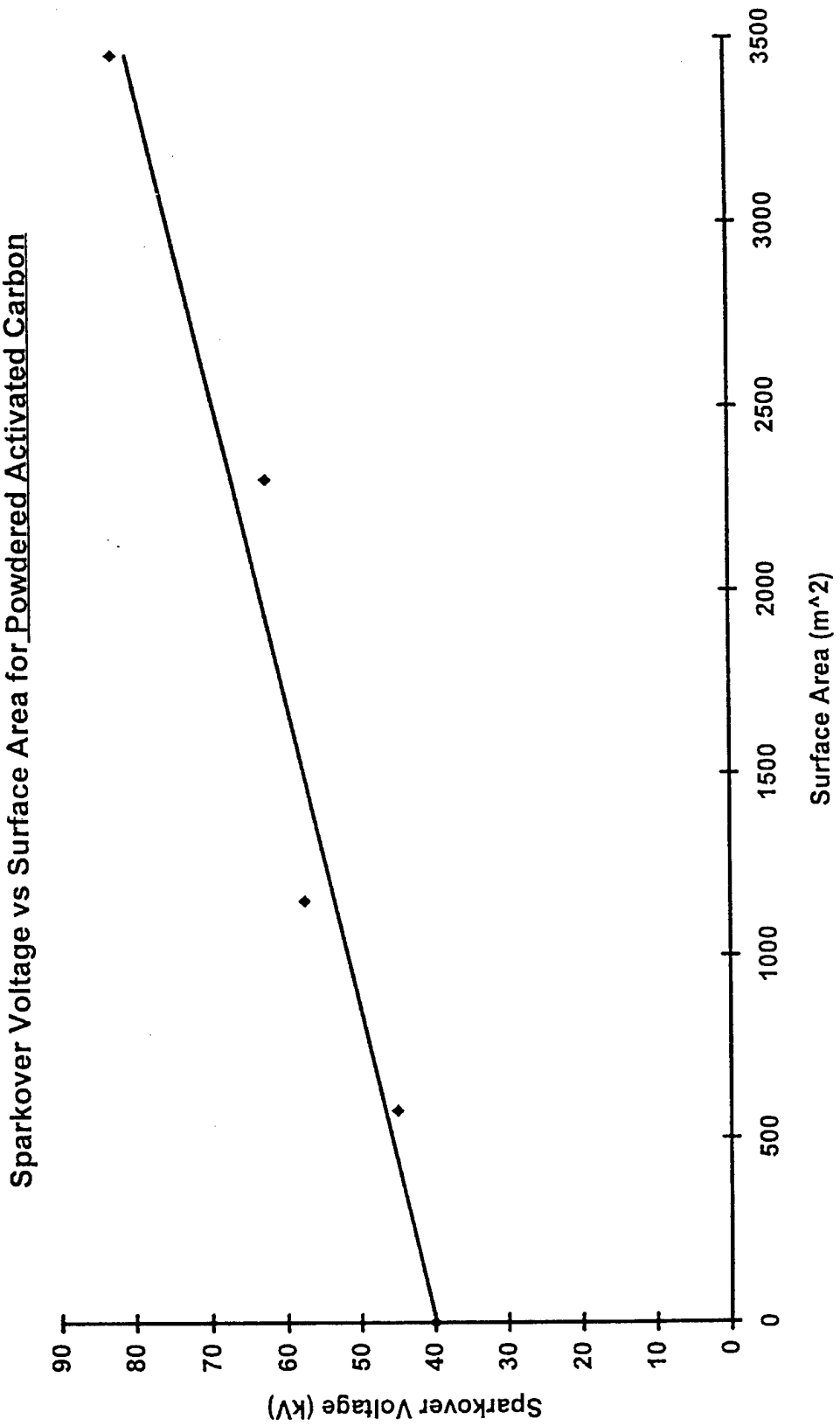
Sparkover Voltage vs Surface Area for Powdered Activated Carbon
Sparkover Voltage (kV)
90
80
70
60
50
40
30
20
10
0
0
500
1000
1500
2000
2500
3000
3500
Surface Area (m^2)

Figure 8

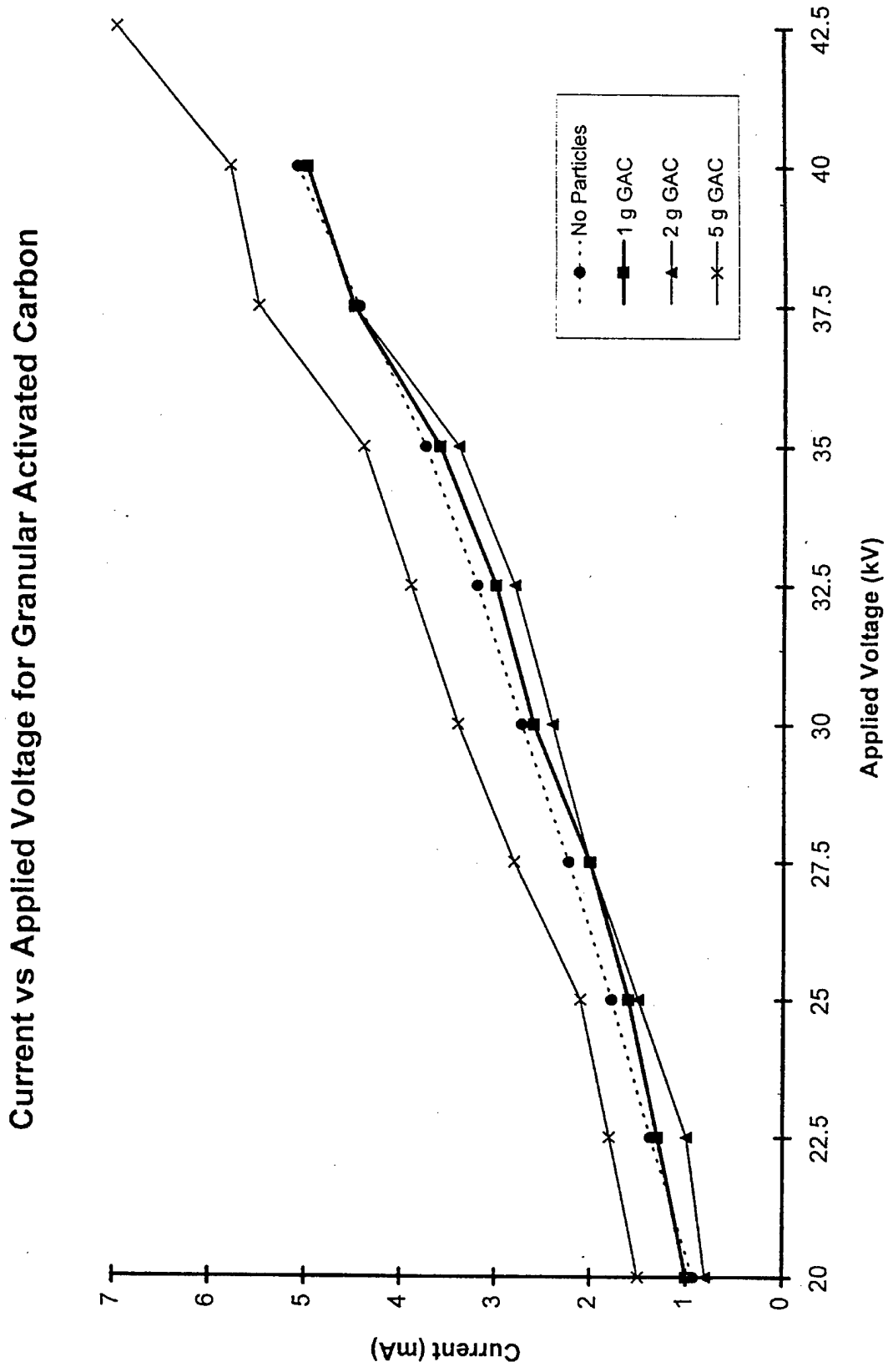
Current vs Applied Voltage for Granular Activated Carbon
Current (mA)
Applied Voltage (kV)
No Particles
1 g GAC
2 g GAC
5 g GAC
0
1
2
3
4
5
6
7
20
22.5
25
27.5
30
32.5
35
37.5
40
42.5

Figure 9

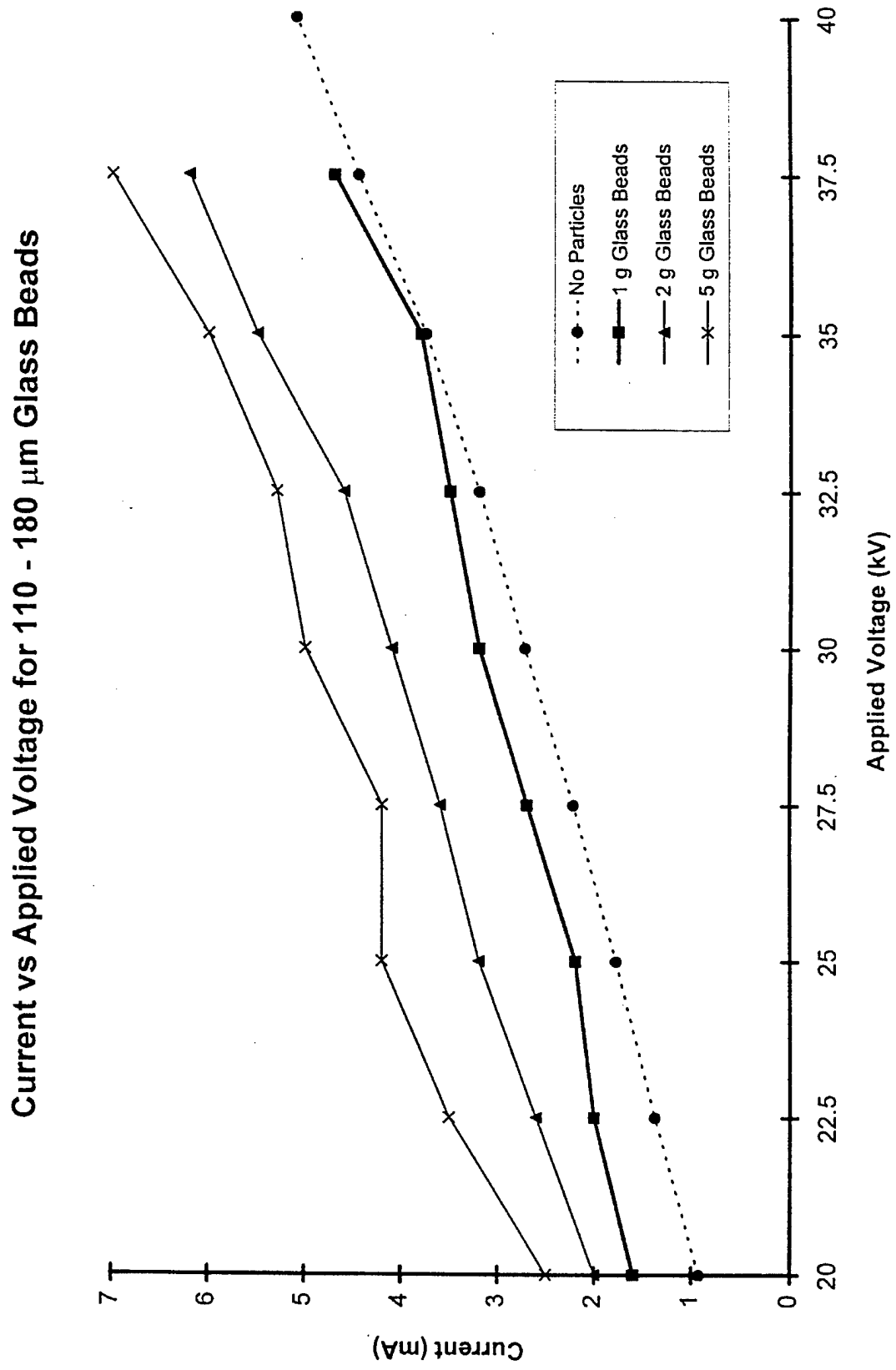
Current vs Applied Voltage for 110 - 180 μm Glass Beads
Current (mA)
Applied Voltage (kV)
No Particles
1 g Glass Beads
2 g Glass Beads
5 g Glass Beads
0
1
2
3
4
5
6
7
20
22.5
25
27.5
30
32.5
35
37.5
40

Figure 10

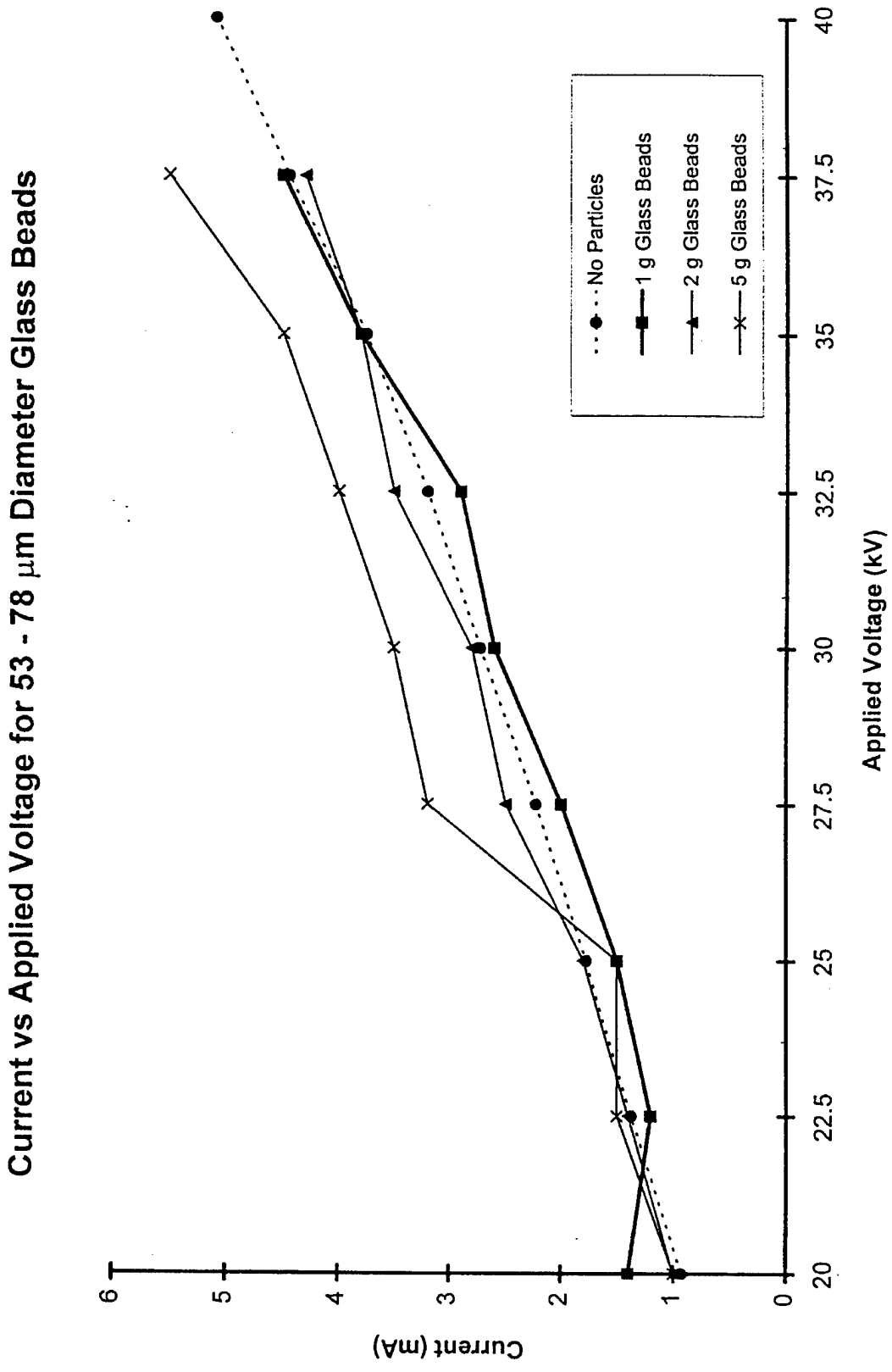
Current vs Applied Voltage for 53 - 78 μm Diameter Glass Beads
Current (mA)
Applied Voltage (kV)
No Particles
1 g Glass Beads
2 g Glass Beads
5 g Glass Beads
0
1
2
3
4
5
6
20
22.5
25
27.5
30
32.5
35
37.5
40

Figure 11

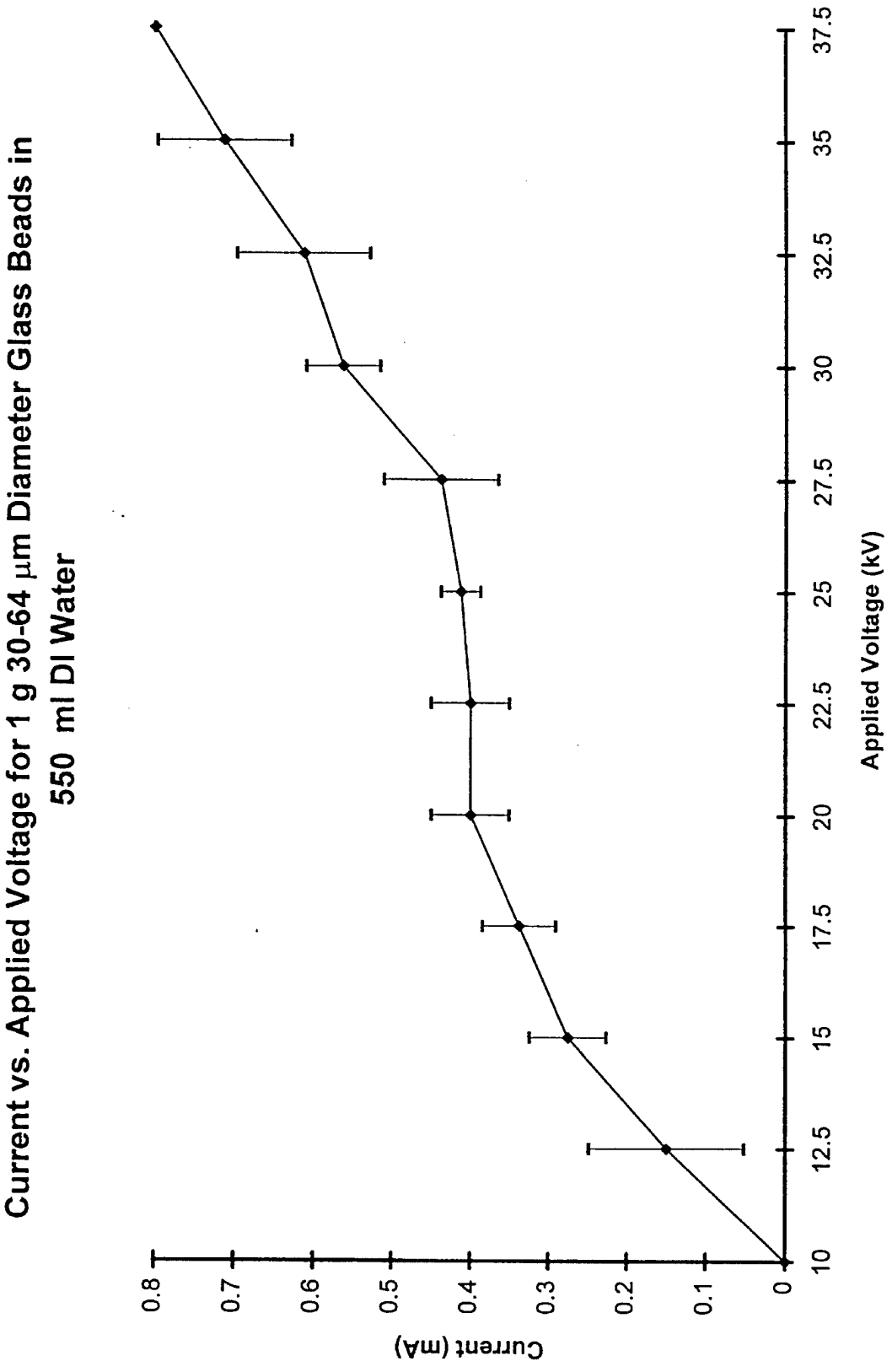
Current vs. Applied Voltage for 1 g 30-64 μm Diameter Glass Beads in 550 ml DI Water
Current (mA)
0.8
0.7
0.6
0.5
0.4
0.3
0.2
0.1
0
10
12.5
15
17.5
20
22.5
25
27.5
30
32.5
35
37.5
Applied Voltage (kV)

Figure 12

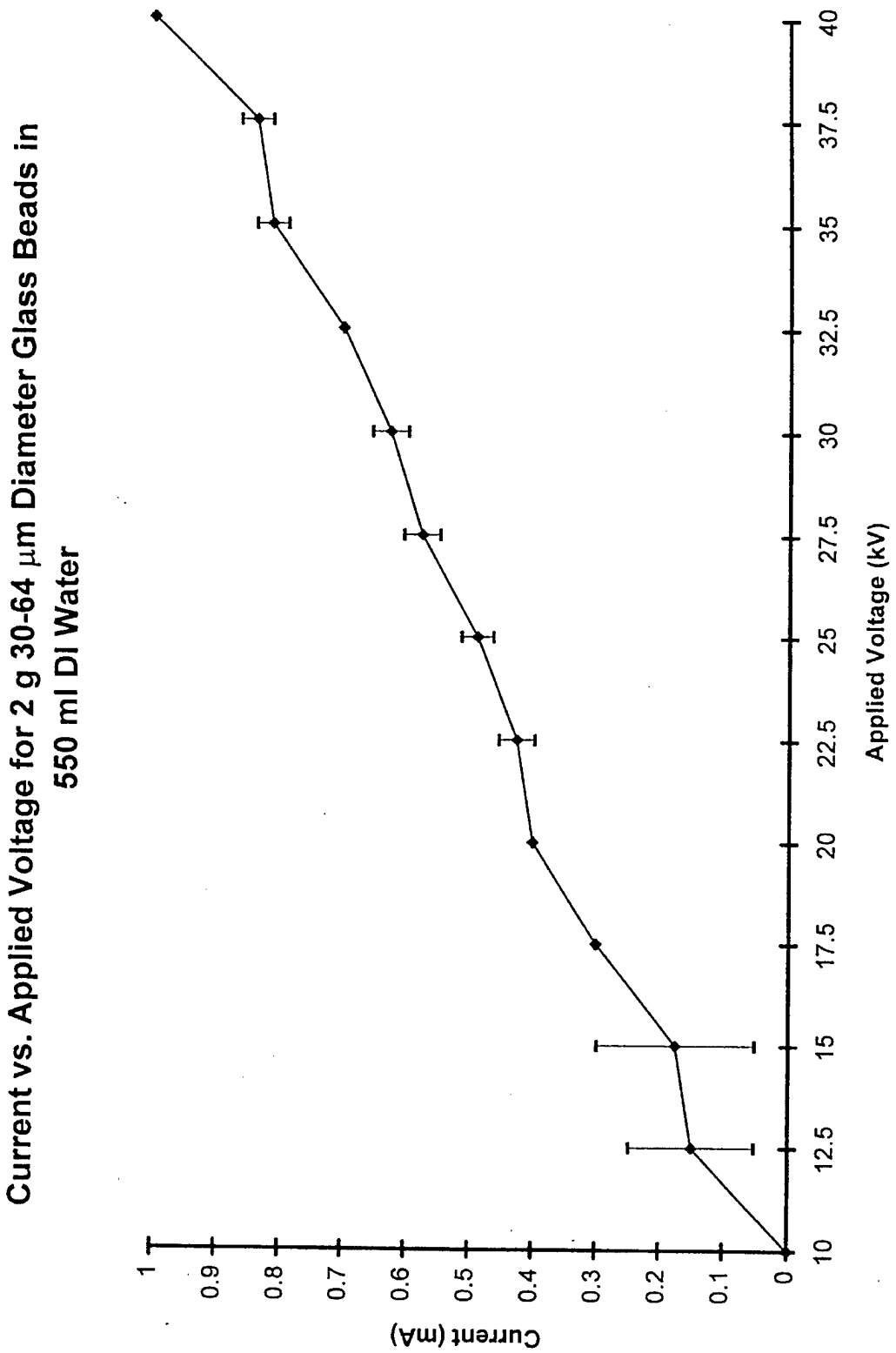
Current vs. Applied Voltage for 2 g 30-64 μm Diameter Glass Beads in 550 ml DI Water
Current (mA)
1
0.9
0.8
0.7
0.6
0.5
0.4
0.3
0.2
0.1
0
10
12.5
15
17.5
20
22.5
25
27.5
30
32.5
35
37.5
40
Applied Voltage (kV)

Figure 13

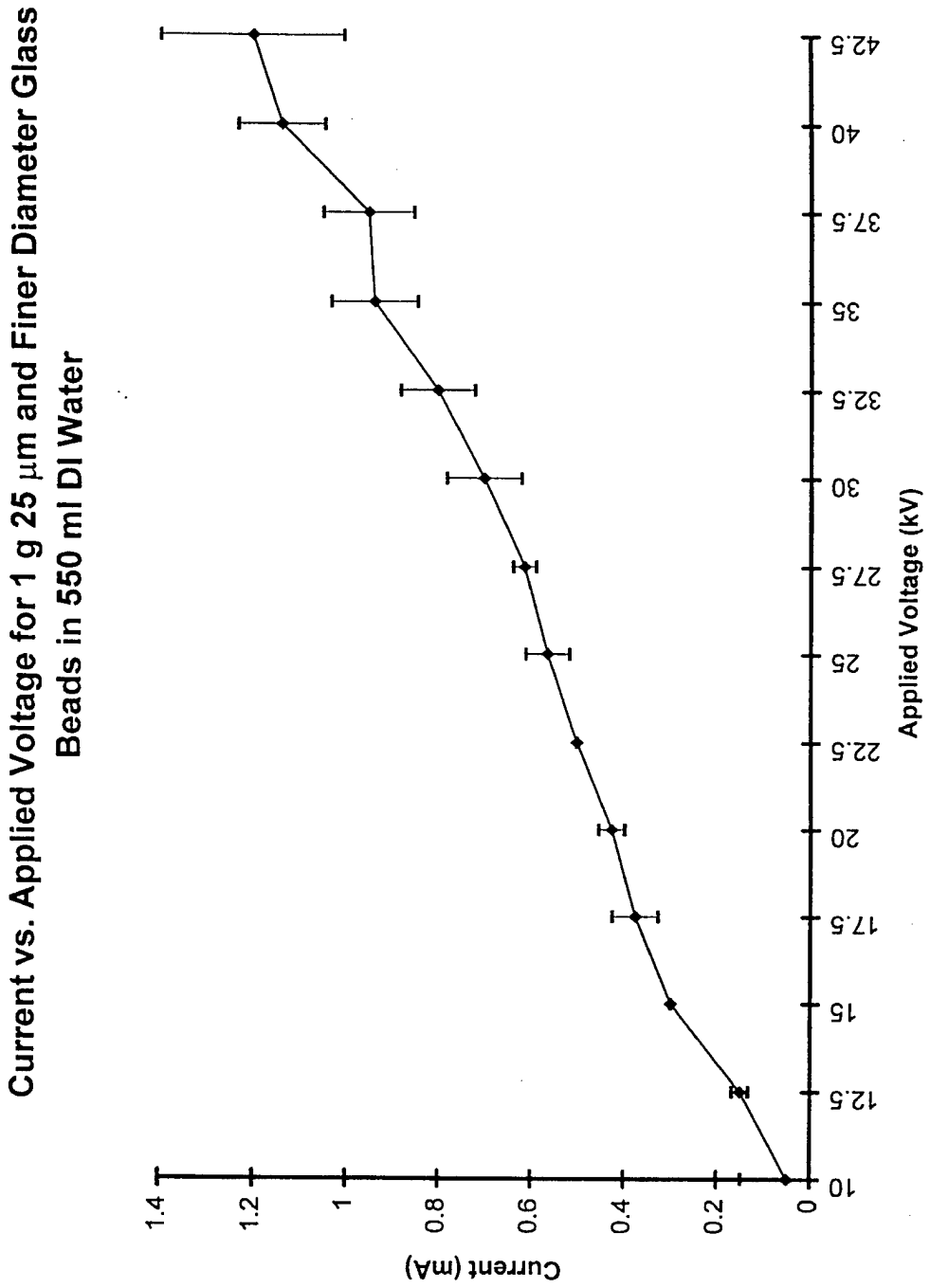
Current vs. Applied Voltage for 1 g 25 μm and Finer Diameter Glass Beads in 550 ml DI Water
Current (mA)
1.4
1.2
1
0.8
0.6
0.4
0.2
0
Applied Voltage (kV)
10
12.5
15
17.5
20
22.5
25
27.5
30
32.5
35
37.5
40
42.5

Figure 14

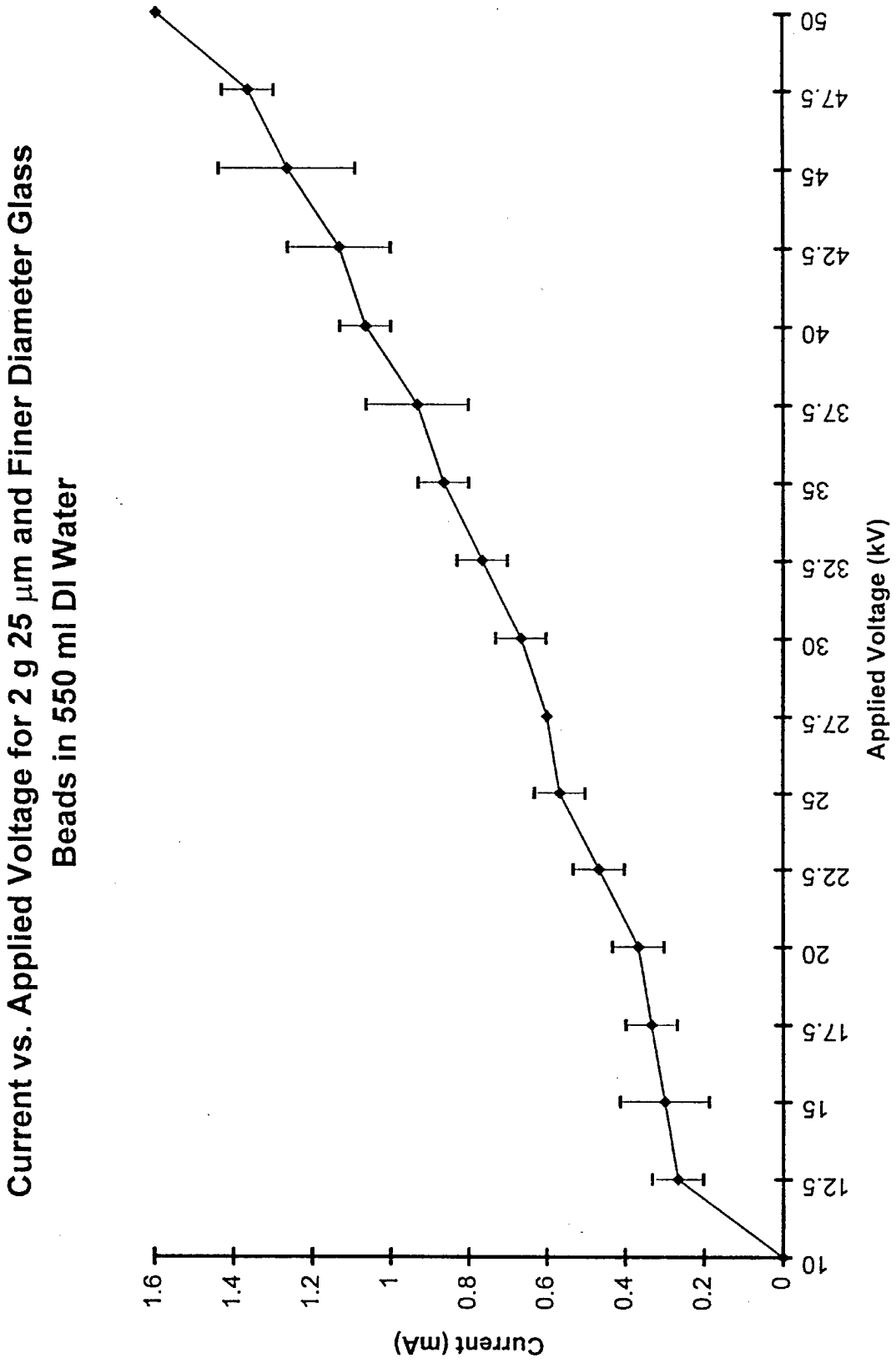
Current vs. Applied Voltage for 2 g 25 μm and Finer Diameter Glass Beads in 550 ml DI Water
Current (mA)
0
0.2
0.4
0.6
0.8
1
1.2
1.4
1.6
Applied Voltage (kV)
10
12.5
15
17.5
20
22.5
25
27.5
30
32.5
35
37.5
40
42.5
45
47.5
50

Figure 15

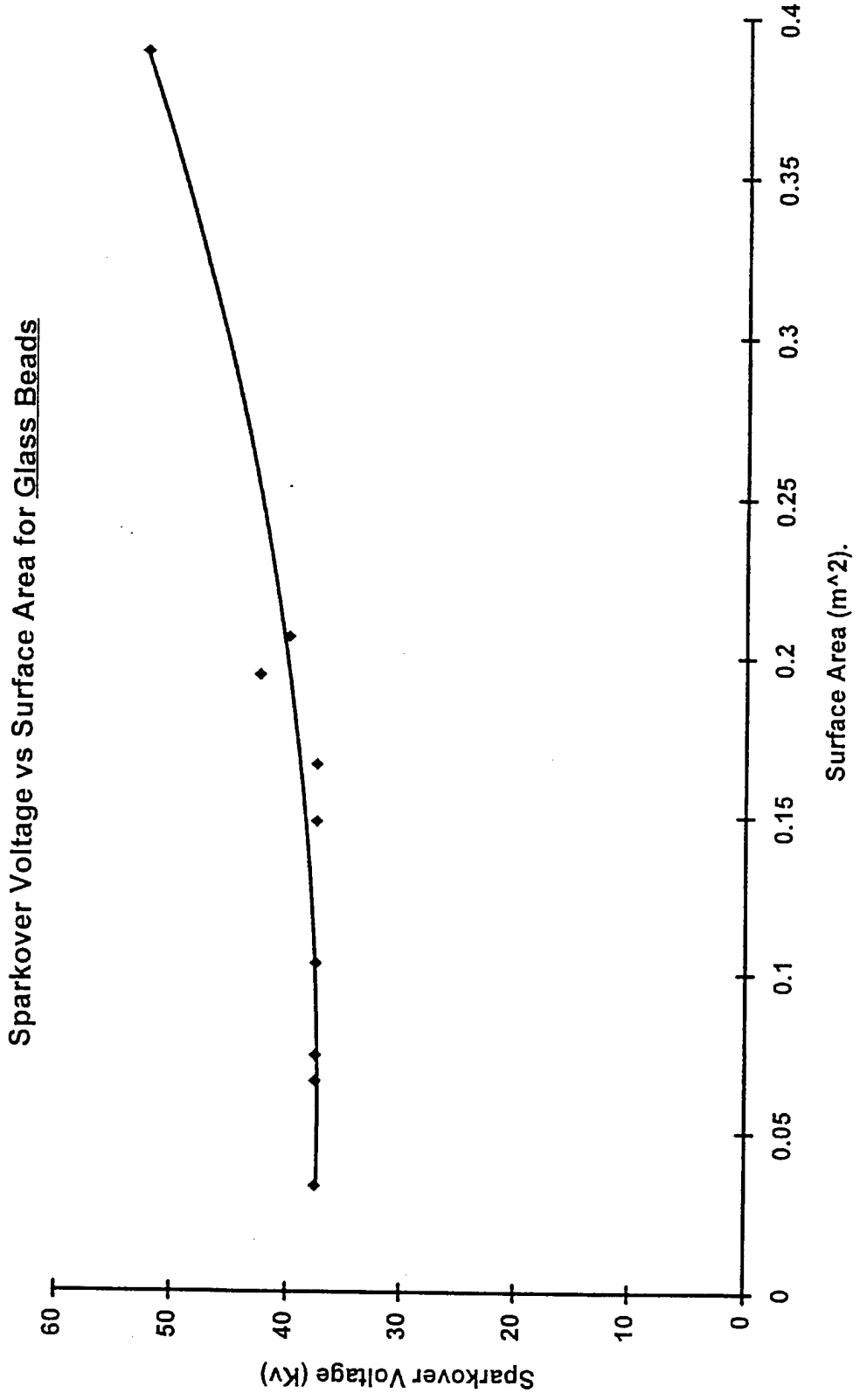
Sparkover Voltage vs Surface Area for Glass Beads
Sparkover Voltage (kV)
60
50
40
30
20
10
0
0
0.05
0.1
0.15
0.2
0.25
0.3
0.35
0.4
Surface Area (m^2).

Figure 16

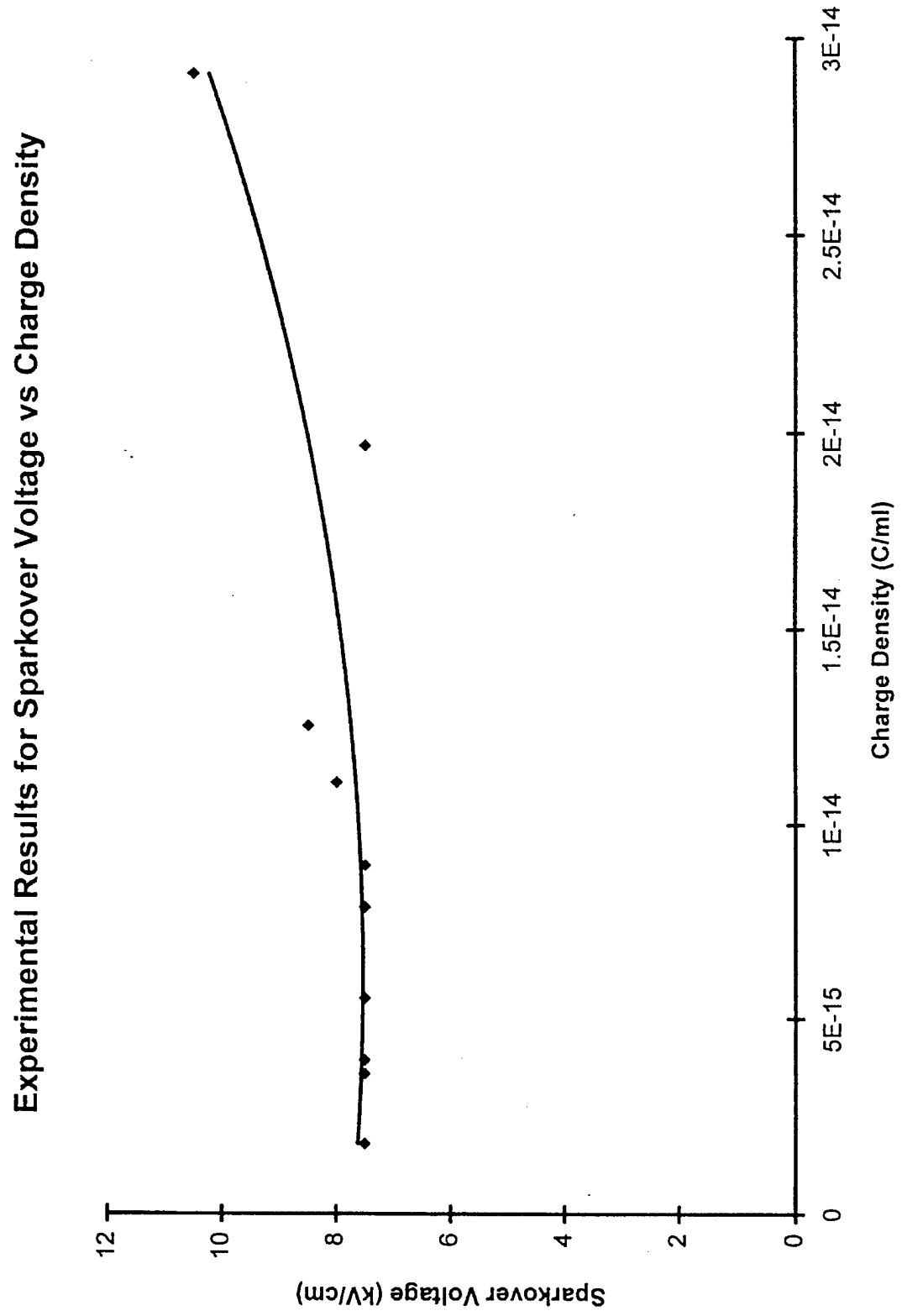
Experimental Results for Sparkover Voltage vs Charge Density
Sparkover Voltage (kV/cm)
12
10
8
6
4
2
0
0
5E-15
1E-14
1.5E-14
2E-14
2.5E-14
3E-14
Charge Density (C/ml)

Figure 17

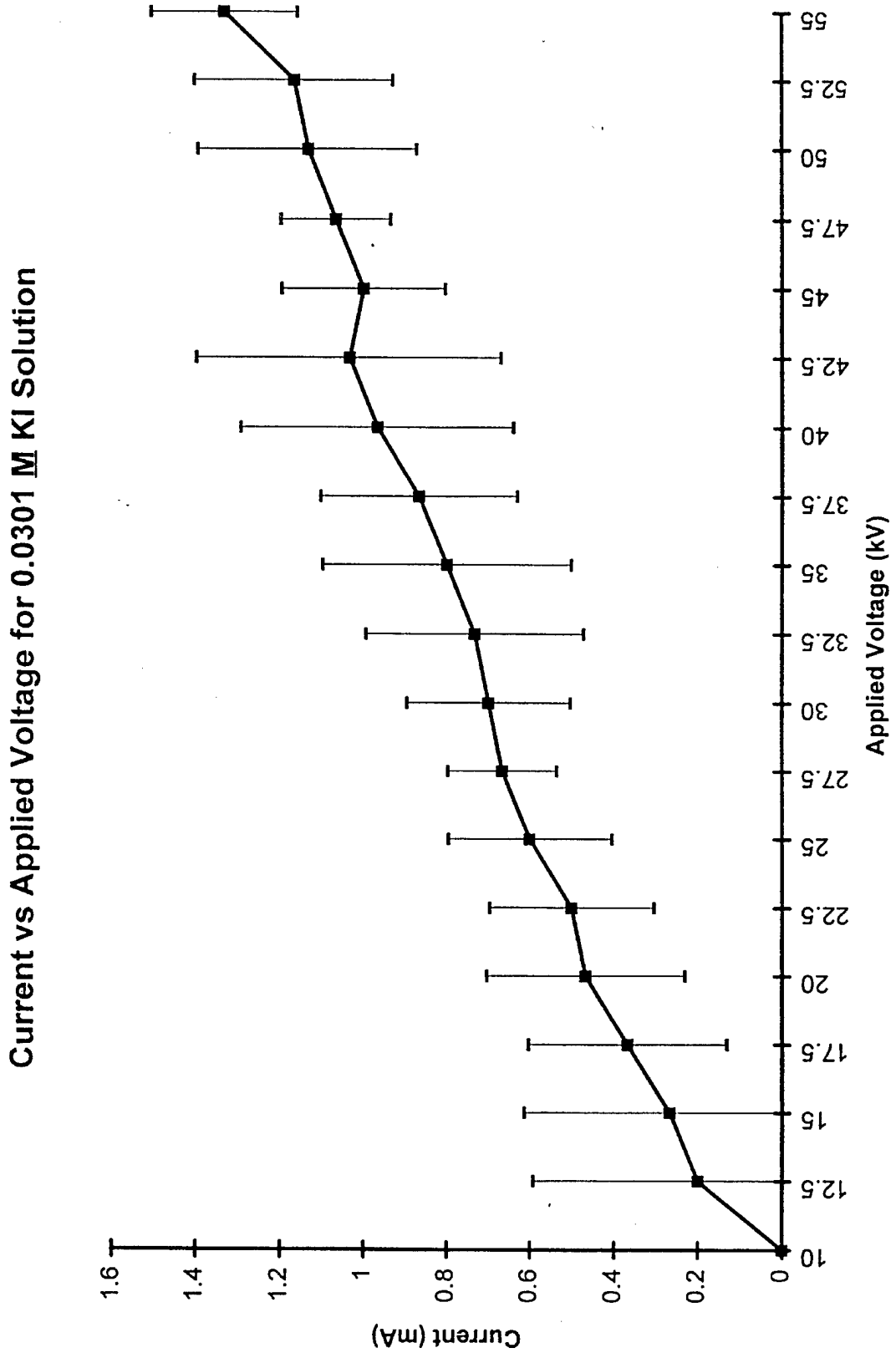
Current vs Applied Voltage for 0.0301 M KI Solution
Current (mA)
1.6
1.4
1.2
1
0.8
0.6
0.4
0.2
0
Applied Voltage (kV)
10
12.5
15
17.5
20
22.5
25
27.5
30
32.5
35
37.5
40
42.5
45
47.5
50
52.5
55

Figure 18